Structure-Property Relationship of Bacterial Cellulose Nanofiber Networks Leading to Precise Material Design

高山, 剛

Structure–Property Relationship of Bacterial Cellulose Nanofiber Networks Leading to Precise Material Design

Go Takayama

Kyushu University

2023

Contents

List of Abbreviations

AFM	Atomic force microscopy
BC	Bacterial cellulose
CLSM	Confocal laser scanning microscopy
DTAP	Dichlorotriazinyl propargylamine
E	Elastic modulus
$E(t)$	Relaxation modulus
FB28	Fluorescent Brightener 28
$H(\tau)$	Relaxation spectrum
LAS X	Leica application suite X
$l_{end\text{-}to\text{-}end}$	End-to-end distance
$l_{contour}$	Contour length
NC	Nanocellulose
OD_{600}	Optical density at wavelength of 600 nm
PDMS	Polydimethylsiloxane
PTFE	Polytetrafluoroethylene
R^2	Coefficient of determination
SEM	Scanning electron microscopy
SD	Standard deviation
SE	Standard error
TC	Terminal complex

α	Scaling exponent
ε	Tensile strain
σ	Tensile stress
6FAM	6-Carboxyfluorescein

General Introduction

Towards realization of a circular society

Promoting the use of bio-based materials is one of the solutions to realize a circular society. To date, the use of synthetic materials has established the present basis of human life. However, it has also caused problems including the depletion of petroleum resources, the increasing emission of greenhouse gases, and the environmental discharge of waste to our surrounding environment. These environmental issues urgently require a comprehensive reassessment of the entire material lifecycle including the production of raw materials, processing, utilization, recovery, and disposal.

Utilization of bio-based materials is considered as a key issue to solve these problems, and to advance realization of a sustainable society, as they possess biodegradability accompanied with low-energy production processes under ambient temperature and low pressure.

Utilization of cellulosic material

Cellulose, a polysaccharide derived from plants, is a prominent representative among biobased materials that has been utilized for various purposes throughout history. It has been playing a vital role in daily life as an essential material in the form of wood, paper, and cotton. In the last two decades, nanocellulose (NC), obtained by defibrillating plant cell walls, has attracted an increasing attention as a novel nano-sized fiber material (Dhali et al., 2021; Isogai, 2021;

Klemm et al., 2018; Kondo, 2022; Moon et al., 2011). Nanocellulose owns a highly crystalline fiber structure composed of extended chains of β-1,4-linked glucopyranose units, which are tightly packed by intra- and inter-molecular hydrogen bonds (Atalla & Vanderhart, 1984; Nishiyama, 2018; Nishiyama et al., 2002, 2003). It exhibits high stiffness and chemical stability, which makes it one of the most rigid and chemically stable materials among various bio-based structural materials. Nanocellulose is insoluble in most organic solvents and has a low linear thermal expansion of < 6 ppm/K in the molecular chain direction (Guan et al., 2020; Hori & Wada, 2005). Throughout the extensive evolutionary history, living organisms have developed mechanisms to produce two major categories of biopolymers: protein polymers composed of amino acid monomers and polysaccharides composed of sugar monomers. Structural polysaccharides such as cellulose and chitin, and structural proteins, including silkworm silk, spider silk, collagen, elastin, and keratin, have evolved. Among these structural biopolymers, cellulose, known for its densely crystallized structure, exhibits the exceptional mechanical properties. This is reflected in the fact that the true density of native cellulosic material is ~1.6 g/cm^3 (Ek et al., 1998; Hervy et al., 2017; Nishiyama, 2018; Sun, 2005), which is significantly higher than that of other biopolymers, and nanocellulose has the highest elastic modulus among biopolymers made from light elements (Ling et al., 2018; Wegst et al., 2015) (Fig. G-1).

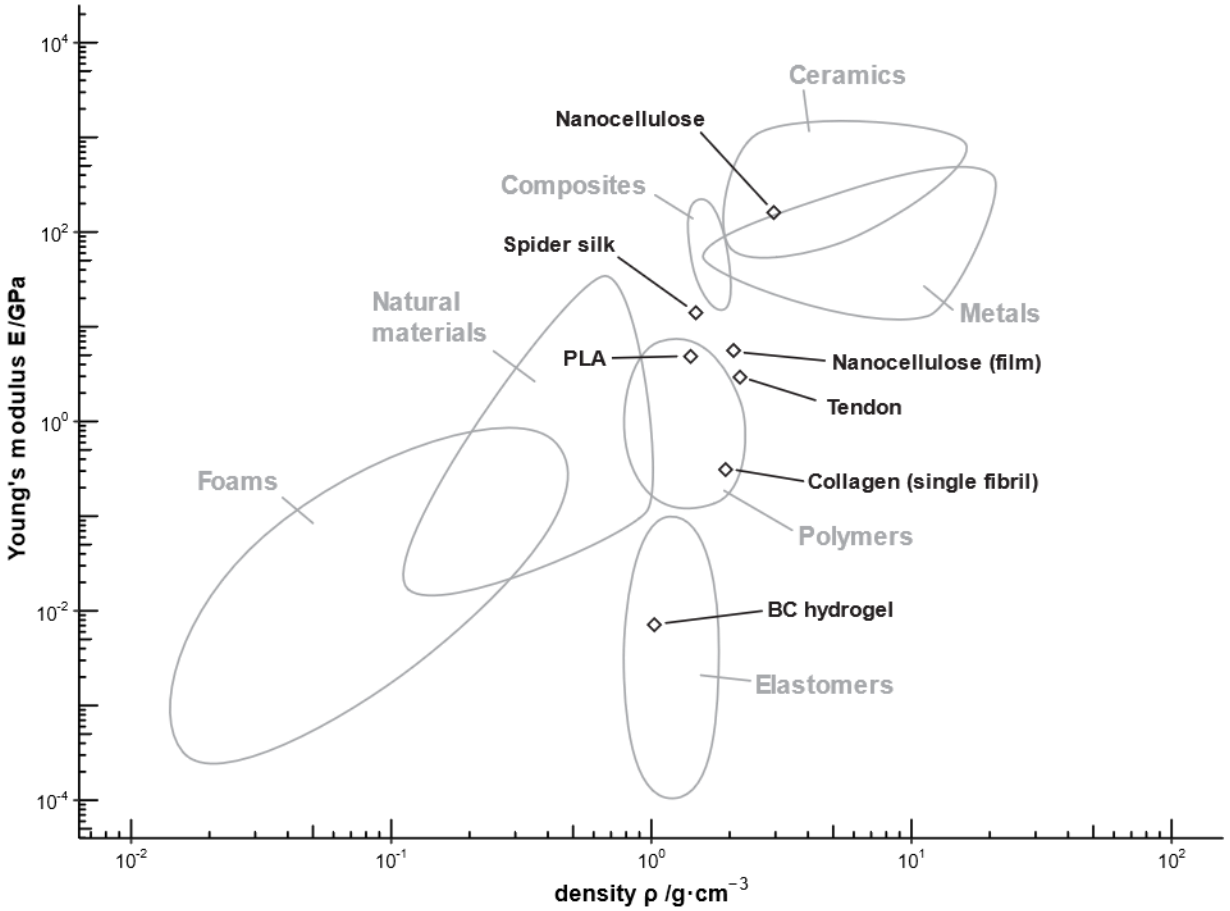

Fig. G-1 Ashby plot of various materials (based on Wegst & Ashby, 2004). Specific density and Young's modulus of materials are plotted in logarithmic scale.

The outstanding mechanical properties and stability of nanocellulose are balanced by its inherent challenges in terms of moldability and processability. Due to the crystal structure stabilized by inter- and intramolecular hydrogen bonds and van der Waals force, cellulose has a thermal decomposition point (320°C) (D. Y. Kim et al., 2001; U. J. Kim et al., 2010) that is lower than its estimated melting point, resulting in the absence of thermoplastic behavior. Similarly, cellulose is insoluble in most solvents, posing challenges in its formability and processability akin to plastics. Currently, nanocellulose is commonly utilized as a film or as a composite material with thermoplastic resin. It is crucial for the constituent fibers to establish a

percolation network to ensure maximum mechanical properties. In nature, the secretion and deposition of cellulose microfibrils undergo precise spatiotemporal control guided by genetic information, resulting in the formation of cell wall structures (Allen et al., 2021; Polko & Kieber, 2019; Song et al., 2020). The hierarchical organization thus created plays a significant role in determining the mechanical properties of wood materials (Fratzl & Weinkamer, 2007). However, the reconstruction of an ordered hierarchical structure from disassembled nanocellulose is hindered by entropic disadvantages, which limits the realization of the maximum potential of nanocellulose. Consequently, the assembly of nanocellulose building blocks and the construction of three-dimensional materials pose significant challenges in the utilization of nanocellulose materials.

Bacterial cellulose: biosynthesis, structure, property, and applications

Bioassmebled cellulosic material

In addition to plants, microorganisms of the genus *Komagataeibacter* are also recognized for their ability to produce cellulose nanofibers (= bacterial cellulose, BC). This process results in the formation of a membranous cellulose hydrogel at the surface of a liquid medium, known as BC pellicle, which is composed of a network of nanocellulose (A. J. Brown, 1886; Hibbert, 1930; Kaushal & Walker, 1947). Unlike plant-derived cellulose, BC is secreted extracellularly in the form of nanofibers and is intrinsically pure, which has the advantage that it can be obtained without complicated purification and extraction processes such as those for plant cell walls.

When classifying biobased materials based on their production methods and forms, the BC pellicle is classified as a bioassembled material, i.e., a material with macroscopic structures directly produced by living organisms (Fig. G-2). This is in contrast to biofabricated ingredients like nanocellulose, spider silk, and polyhydroxyalkanoates, which necessitate secondary

processing to form macroscale structures after the biological fabrication process. Consequently, BC pellicles, which are bioassembled materials, have an advantage over plant-derived nanocellulose in that they can directly produce macroscale cellulosic materials without additional processing steps.

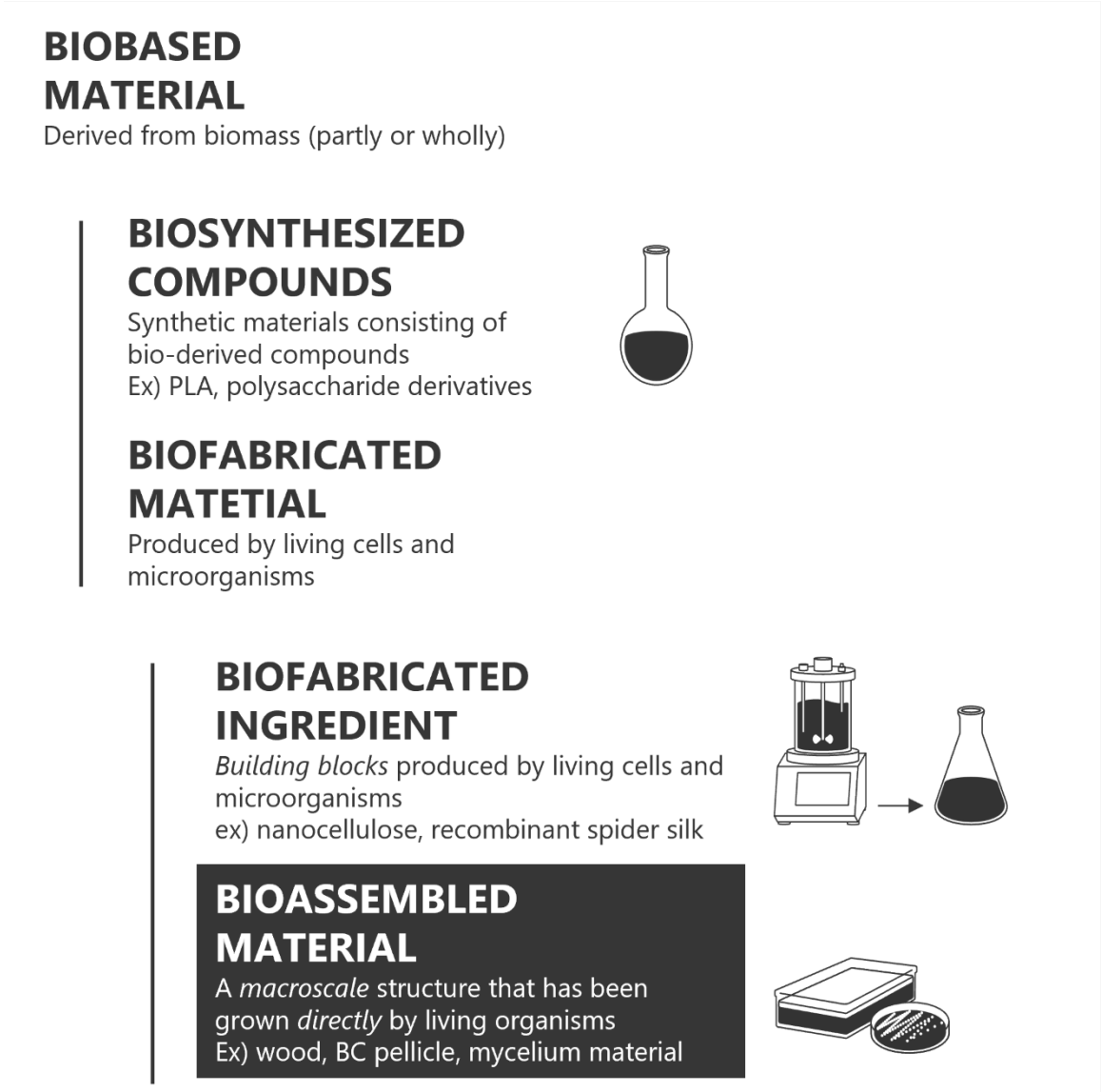

Fig. G-2 Classification of biobased materials in their production method and morphology

Biosynthesis and structure of BC

The physical properties of BC pellicles, classified as bioassembled materials, are determined by the secretion process of nanocellulose network by bacteria. Therefore, understanding the process of structural formation in BC pellicles is crucial. As mentioned earlier, BC pellicles are formed by inoculating microorganisms into a liquid medium and allowing them to incubate aerobically. This process results in formation of a centimeter-thick gel-like membrane (= pellicle) on the surface of the medium (Fig. G-3a). Through the purification of this membrane, a sheet material consisting of highly pure cellulose (with a cellulose content of approximately 1%) can be obtained. The process can be divided into two parts: (1) biofabrication, which involves the enzymatic synthesis of cellulose molecules accompanied with their self-assembly, and (2) bioassembly, which involves the formation of a fiber network through collective behaviors of cellulose fiber-secreting bacteria.

First, *Komagataeibacter* bacteria carry out cellulose biosynthesis through a gigantic enzyme complex called Terminal Complexes (TCs) located on the cell surface (Abidi et al., 2022; R. M. Brown et al., 1976; Nicolas et al., 2020; Zaar, 1979). The TCs have a linear alignment consisting of several dozen complex units composed of multiple enzymes, including BcsA, B, C, and D (Du et al., 2016; Tajima et al., 2022). The individual enzyme units within the TCs synthesize molecular chains, which immediately self-assemble with neighboring molecular chains to form elementary fibrils with a diameter of 1.5−3 nm (Fig. G-3b) (R. M. Brown et al., 1976; Nicolas et al., 2020). The elementary fibrils further assemble to form ribbon-like nanofibers (BC ribbons) with a cross-sectional shape of a few nm in thickness and 20−50 nm in width (Yamanaka & Sugiyama, 2000). In this manner, a highly crystalline (>80% crystallinity, rich in Cellulose I_{α} crystal (Atalla & Vanderhart, 1984; Baker et al., 2000; Martínez-Sanz,

Gidley, et al., 2016; Martínez-Sanz, Mikkelsen, et al., 2016; Persson et al., 1991) cellulose nanofibril is secreted from a single bacterium.

Then, the secreted BC ribbons interact with each other, leading to formation of a fiber network structure (Fig. G-3b). This bioassembly process is closely related to the motility of the bacteria. Unlike bacteria such as *Escherichia coli* that swim using flagella, the cellulose-producing bacteria utilize the BC ribbons they secrete as a scaffold for their movement (moving rate: approximately 5 μm/min) (R. M. Brown et al., 1976; Hesse & Kondo, 2005; Tomita & Kondo, 2009). In addition to secreting BC ribbons and moving in one direction, they were observed to secrete new BC ribbons while tracing over a single fiber and to transfer from one BC ribbon to another (Fig. G-3c). Based on these observations, it is hypothesized that the bundling of fibers and the formation of branching and merging points through the transit behavior of cellulose-producing bacteria contribute to formation of interconnected fiber networks. However, the detailed mechanisms and processes underlying the bioassembly of BC pellicles are still not fully understood, and further research is needed to gain a comprehensive understanding of their structural formation.

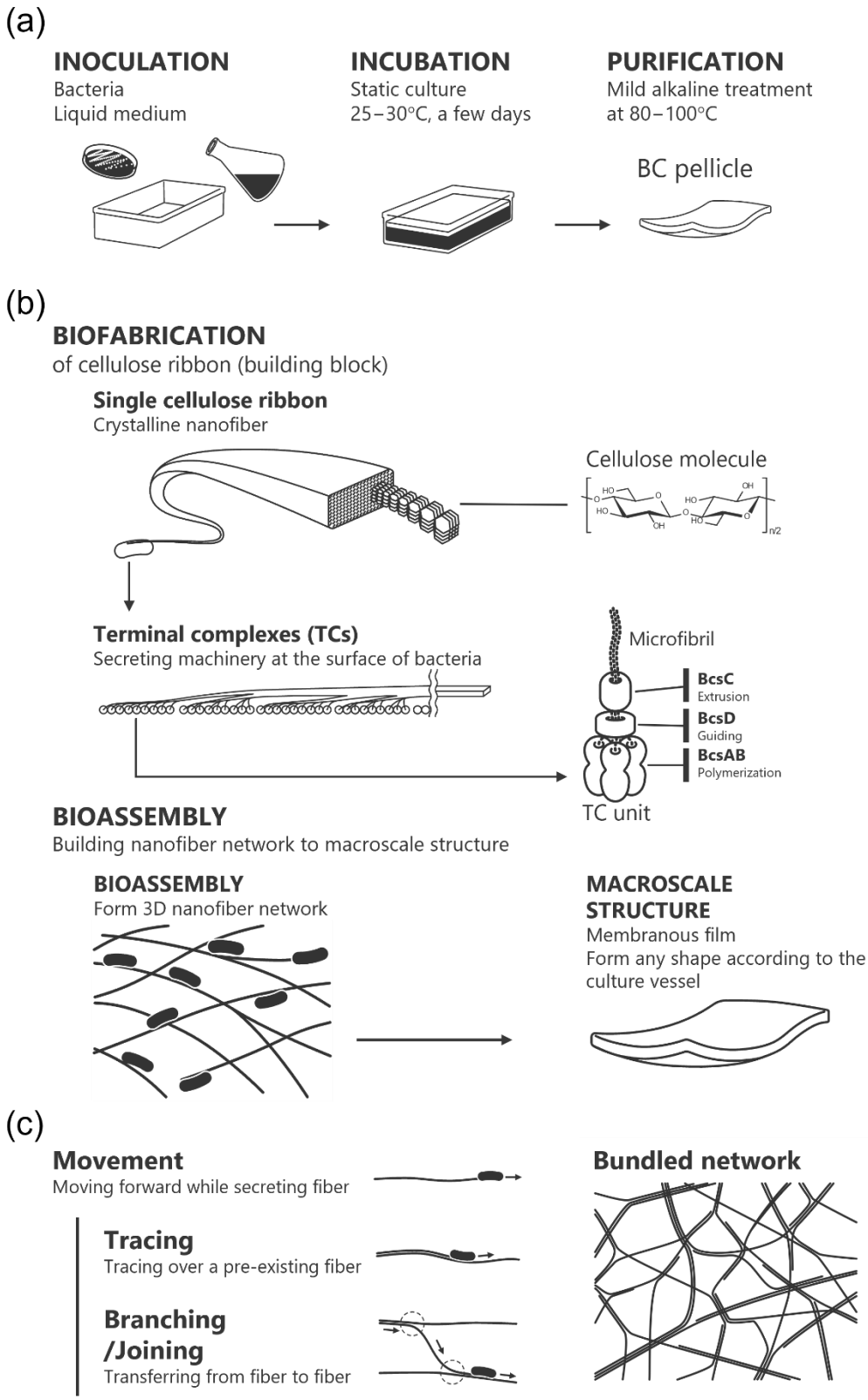

Fig. G-3 Overview of BC pellicle production by static culture of bacteria (a), Schematic diagram of biofabrication/bioassembly of BC (b) and formation of fiber network (c)

Properties of BC

In general, BC pellicles are characterized by biodegradability (Hu & Catchmark, 2011; Park et al., 2004), biocompatibility (Helenius et al., 2006), high purity, porosity (W. Tang et al., 2010), and water holding capacity (Ul-Islam et al., 2012), but their mechanical properties are particularly important for BCs that are expected to be used as structural materials. The BC pellicles composed of nanofiber networks exhibit unique and non-linear mechanical properties that are different from those of typical polymer hydrogels. Fibrous materials can be classified according to whether or not the constituent elements are subject to thermal fluctuations (Broedersz & Mackintosh, 2014; Picu, 2020). Fiber networks with a high flexibility are subject to thermal fluctuations and are classified as thermal networks, displaying entropic elasticity (James & Guth, 1943; Kuhn, 1936). Nanocellulose has often been analyzed using concepts from the field of polymer rubber elasticity, owing to its historical background in polymer chemistry research. On the other hand, rigid fiber networks like non-woven fabrics are not affected by thermal fluctuations and is classified as athermal networks, exhibiting energetic (enthalpic) elasticity arising from fiber stiffness. The BC pellicle, a network of semiflexible nanofibers, is expected to be in its transitional region, but has not been studied in detail. The mechanical properties of BC ribbons have been measured directly using atomic force microscopy (AFM) and indirectly assessed through Raman scattering, indicating a uniaxial tensile Young's modulus of approximately 80 GPa (Guhados et al., 2005; Hsieh et al., 2008; Tanpichai et al., 2012). However, macroscopic properties of BC pellicles are not determined solely by the properties of the individual fiber but are determined by the overall fiber network structure. Therefore, even though they are composed of the same cellulose type I BC ribbons, there is a large variation in their mechanical properties; the tensile strengths range from 0.15 to 0.95 MPa (E. E. Brown et al.,

2012; Chen et al., 2018; McKenna et al., 2009) in the hydrated state and 16 to 145 MPa in the dried state (Kaczmarek et al., 2022; Semjonovs et al., 2017). As mentioned earlier, the fiber network is constructed by a complex bacterial bioassembly process, making difficulty in evaluating its inherent effects. Although the significance of the influence of the fiber network structure on the physical properties is generally recognized, detailed investigations in this regard have not been fully conducted.

Application of BC

Current Status of BC Applications

Research and development toward the utilization of BC have been conducted, and some of them have been commercialized. Production forms of BC can be classified into four types: hydrogel, film, sheet, and aqueous dispersion (Fig. G-4). The use of BC as a hydrogel is for application exploiting the mechanical properties and water retention properties derived from its unique network structure. In particular, BC hydrogel has been applied in medical fields, and research and development in applications such as wound dressing, artificial blood vessels, drug delivery, and cell culture substrates are being conducted (Abeer et al., 2014; Almeida et al., 2014; Bäckdahl et al., 2006, 2008; Helenius et al., 2006; Klemm et al., 2001; Picheth et al., 2017; Ullah et al., 2016). Particularly, the use of BC hydrogel as a wound dressing material is one of the applications that have been commercialized in actual products (Ahmed et al., 2020; Czaja et al., 2007; Gama & Dourado, 2018; Gregory et al., 2021; Schönfelder et al., 2005). BC produced as a membrane can be processed into thin films and sheets, and is expected to be used as packaging films for food products and fabrics for clothing (Azeredo et al., 2019; da Silva et al., 2021; Domskiene et al., 2019; Ludwicka et al., 2020; Melton, 2022). BC can be pulverized into nanofibers (Bacterial nanocellulose, BNC) or colloidal dispersions and used as a viscosity

modifier in the food and cosmetics industries, and as a reinforcing material for composite materials (El-Gendi et al., 2022; Kose et al., 2013). Considering that the use of BC as a nanocellulose dispersion competes with plant-derived nanocellulose, the use of BC with its advantageous network structure is one of the strategies to maximize the value of BC. However, it should be noted that the current production cost of BCs is higher than that of plant-derived nanocellulose (Dourado et al., 2016). Therefore, it is also important to seek high added value applications to overcome this cost difference.

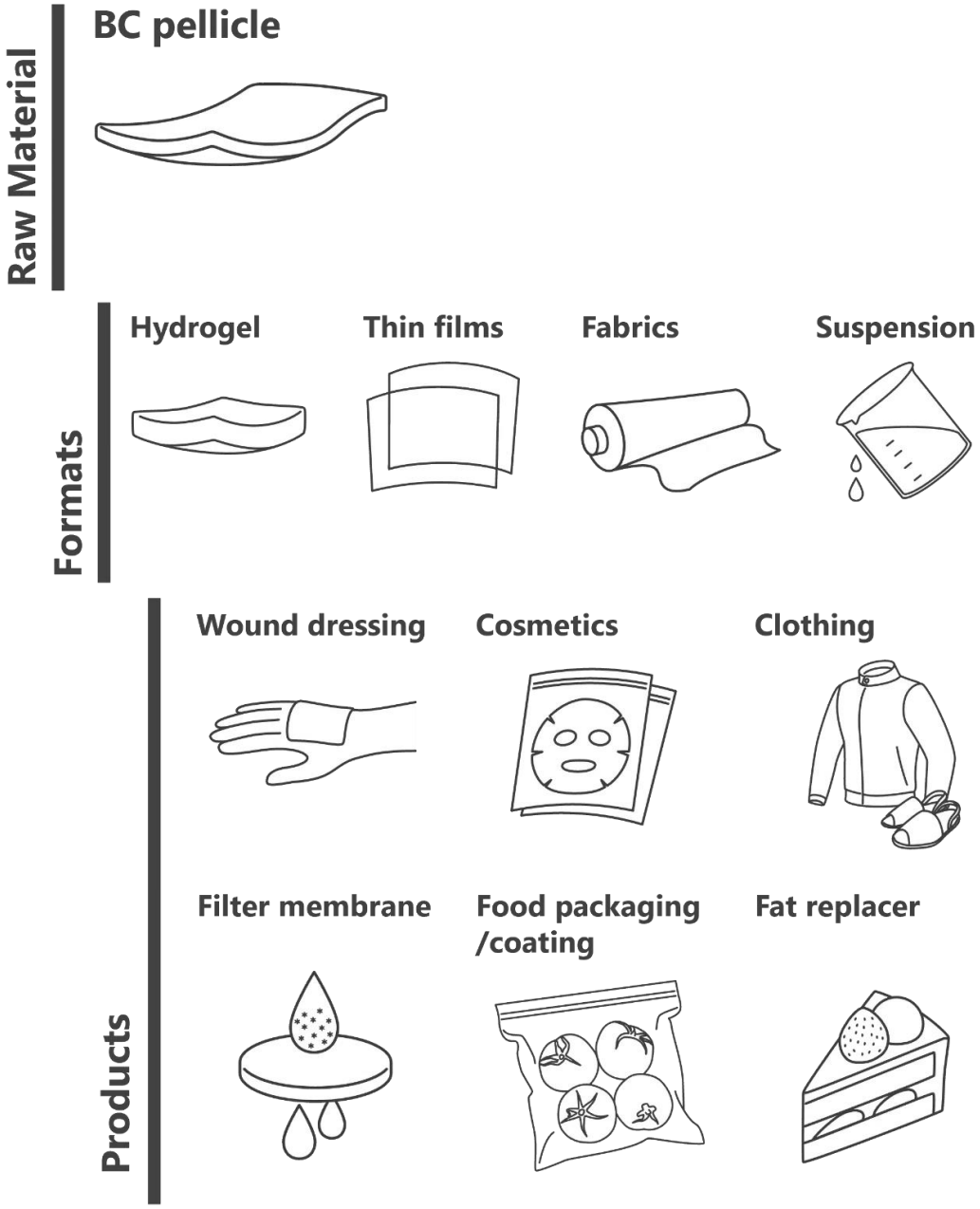

Fig. G-4 Overview of production forms of bacterial cellulose and its application fields

One approach to maximize the potential of BC pellicles is to utilize their network structure as a fiber framework in composite materials, rather than simply as a filler. Composite materials with various resins and polysaccharides have been studied, and improvements in the physical properties of BC have been reported (Ashori et al., 2012; Chakrabarty & Teramoto,

2018; Dufresne, 2017; Liu et al., 2020; Quero et al., 2010; Shah et al., 2013; Whitney et al., 1999; Yano et al., 2005). These improvements in physical properties are due to the nanocellulose fiber network embedded in the base material. To achieve further enhancement of physical properties, it is essential to focus on intrinsic improvements through the control of the network structure itself. BC pellicles, being sheet-like materials, hold promise not only in structural applications like composite materials but also in the textile field (da Silva et al., 2021; Domskiene et al., 2019; Fernandes et al., 2019; Melton, 2022). Such utilization also requires the control of multifaceted physical properties such as high elasticity, breathability, and light weight in addition to high strength and stiffness. Therefore, the precise control of physical properties through the manipulation of the network structure of BC hydrogel opens a possibility for its applications.

For practical applications, it is necessary to address the issue of production costs as well, as mentioned above. In laboratory-scale settings, the production of membranous BC pellicles is commonly achieved by inoculating bacteria into a cultivation vessel containing a liquid medium and under static cultivation for several days. However, this production method is not sufficient in terms of scalability and the production rate. Optimization of the culture medium in terms of production costs and yields is also insufficient. For these reasons, extensive research has been conducted on BC production systems and media composition, yielding significant progress (Dourado et al., 2016; Islam et al., 2017; Y. J. Kim et al., 2007; Lee et al., 2014). For instance, manufacturing methods such as the Horizontal bioreactor (Kralisch et al., 2010), which enables continuous cultivation of BC sheets as rolls to impart scalability to the pellicle size, and the Aerosol bioreactor (Hornung et al., 2007), which allows continuous growth of pellicles in the thickness direction, have been reported. It should be noted that utilizing agricultural and

industrial waste materials for the cultivation medium and carbon source can potentially lead to a reduction in production costs. (Carreira et al., 2011; Lu et al., 2011; Rani et al., 2011; Skiba et al., 2020; Vazquez et al., 2013). The advancement of such studies holds promise to extend the utilization of this material with the excellent properties.

A new direction: material design by synthetic biology

In addition to the aforementioned applications, recent advancements in synthetic biology have brought BC back into the spotlight. Synthetic biology is a rapidly growing field that involves designing biological systems or modules with user-defined functions, and it has experienced significant growth in recent years (Gallup et al., 2021). In the past, synthetic biology primarily focused on the production of useful substances such as biomedicines (Paddon & Keasling, 2014; Yue et al., 2023). However, in recent years, there has been a growing interest in the application of synthetic biology to the design of materials with macroscopic structures, known as material design by synthetic biology (Gilbert et al., 2021; T. C. Tang et al., 2021).

Material design by synthetic biology aims to produce a new type of material with responsive and adaptive functionalities and properties using biological systems such as microorganisms. For instance, research is underway to develop functional materials like biosensors and biotherapeutics by incorporating microorganisms with programmable genetic circuits into the internal structure of materials (Goodchild-Michelman et al., 2023; Moradali & Rehm, 2020; Srubar, 2021). This approach enables the production of materials with unique functionalities and properties. Concerning this, *Komagataeibacter* bacteria, which possess the ability to secrete cellulose nanofibers and form macroscopic scaffolds, have garnered attention as promising candidates for the substrate of living materials, which are defined as engineered materials composed of living cells that form or assemble the material itself and modulate the

functional performance of the material postproduction (Gilbert et al., 2021; Jin et al., 2022; Moradali & Rehm, 2020; Nguyen et al., 2018; Walker et al., 2019). This trend is expected to accelerate in combination with the in vivo composite material method using *Komagataeibacter* bacteria based on genetic engineering conducted so far (Fang et al., 2015; Takahama et al., 2021, 2022). The application of synthetic biology tools and techniques to *Komagataeibacter* bacteria, which exhibit biocompatibility, high mechanical strength, and the ability to construct macroscopic scaffolds, opens exciting possibilities for the development of new BC-based materials with tailored functionality (Fig. G-5). This convergence of synthetic biology and *Komagataeibacter* bacteria will spark new interest in the utilization of BC, leading to groundbreaking research and applications across diverse fields.

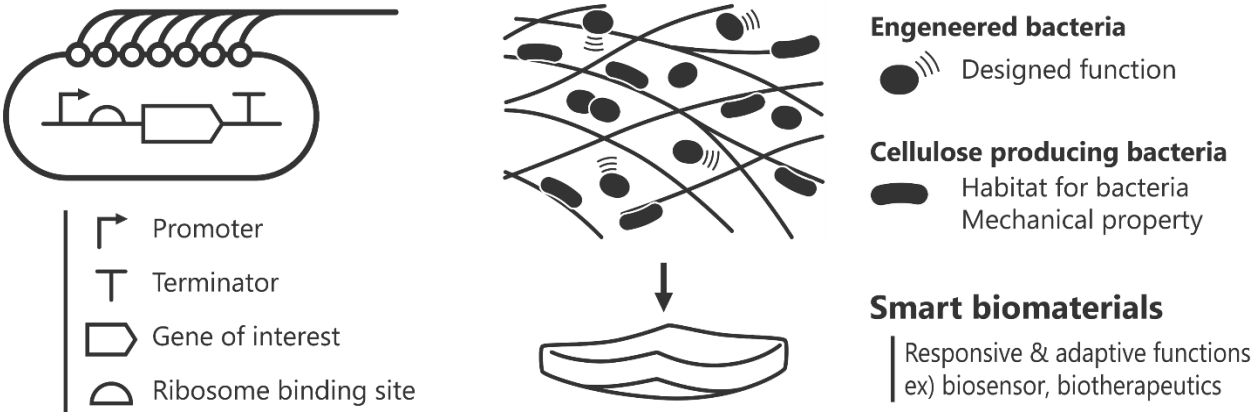

Fig. G-5 Schematic images of living materials utilizing BC pellicle.

Outlook for further Material Applications of BC

Despite the promising potential of BC pellicles in various applications, the lack of understanding of their physical property manifestation mechanisms has hindered their true utilization. While progress has been made in the areas of composite formation, functionalization, and manufacturing process optimization, the fundamental problem of how the network structure

formed by microorganisms and its subsequent property expression remain unresolved. The fibrous nature of BC pellicles exhibits non-linear and complex properties inherently. Furthermore, BC produced by microorganisms shows a significant variability in its properties. The combination of the factors makes a difficulty in a comprehensive understanding of the structure–property relationship. BC pellicles are a unique biomaterial that yields a network structure of cellulose nanofibers with exceptional mechanical characteristics simply by culturing them in a liquid medium. However, without advancing the foundational understanding of physical property manifestation, their latent potential cannot be fully realized. Returning to the basics, unraveling the microbial-driven structural formation process and the mechanisms behind physical property manifestation is the key to unlocking the path toward material applications.

Objectives of this dissertation

BC is believed as a natural resource with promising applications as a next-generation biomaterial. Although enormous efforts have been devoted to the research on composite material development and process improvement, the fundamental understanding in relationship between the fibrous network structure and properties of BC pellicles is still insufficient. Limited understanding of the complex structures produced by microorganisms and the difficulty in controlling them have become bottlenecks in promoting the utilization of BC materials. To fully harness the potential of BC as a bio-based material, developing novel material design strategies that control the higher-order structure of BC hydrogels, as well as establishing simplified prediction methods and stable quality management techniques for the properties that vary significantly with manufacturing conditions and bacterial strains. This dissertation aims to

establish a foundation for precise control of BC material properties by elucidating the network structure–property relationship.

In Chapter 1, the tensile deformation mechanism of BC hydrogels, where the characteristics of fibrous network materials are pronounced, is precisely modeled based on the visualization of the microscopic behavior of nanofiber networks. Chapter 2 focuses on establishing quantitative evaluation methods for the fibrous network structures and experimentally demonstrating the correlation with tensile properties. In Chapter 3, the structural formation process of BC hydrogels by *Komagataeibacter* bacteria is analyzed in detail to provide clues towards the novel material design.

References

Abeer, M. M., Cairul, M., Amin, I. M., Martin, C., Kebangsaan Malaysia, U., Raja, J., Aziz, M. A., & Lumpur, K. (2014). *A review of bacterial cellulose-based drug delivery systems: their biochemistry, current approaches and future prospects*. https://doi.org/10.1111/jphp.12234

Abidi, W., Decossas, M., Torres-Sánchez, L., Puygrenier, L., Létoffé, S., Ghigo, J. M., & Krasteva, P. V. (2022). Bacterial crystalline cellulose secretion via a supramolecular BcsHD scaffold. *Science Advances*, *8*(50). https://doi.org/10.1126/sciadv.add1170

Ahmed, J., Gultekinoglu, M., & Edirisinghe, M. (2020). Bacterial cellulose micro-nano fibres for wound healing applications. *Biotechnology Advances*, *41*(February), 107549. https://doi.org/10.1016/j.biotechadv.2020.107549

Allen, H., Wei, D., Gu, Y., & Li, S. (2021). A historical perspective on the regulation of cellulose biosynthesis. *Carbohydrate Polymers*, *252*. https://doi.org/10.1016/j.carbpol.2020.117022

Almeida, I. F., Pereira, T., Silva, N. H. C. S., Gomes, F. P., Silvestre, A. J. D., Freire, C. S. R., Sousa Lobo, J. M., & Costa, P. C. (2014). Bacterial cellulose membranes as drug delivery systems: An in vivo skin compatibility study. *European Journal of Pharmaceutics and Biopharmaceutics*, *86*(3), 332–336. https://doi.org/10.1016/j.ejpb.2013.08.008

Ashori, A., Sheykhnazari, S., Tabarsa, T., Shakeri, A., & Golalipour, M. (2012). Bacterial cellulose/silica nanocomposites: Preparation and characterization. *Carbohydrate Polymers*, *90*(1), 413–418. https://doi.org/10.1016/j.carbpol.2012.05.060

Atalla, R. H., & Vanderhart, D. L. (1984). Native Cellulose: A Composite of Two Distinct-Crystalline Forms. *Science*, *223*(4633), 283–285. https://doi.org/10.1126/science.223.4633.283

Azeredo, H. M. C., Barud, H., Farinas, C. S., Vasconcellos, V. M., & Claro, A. M. (2019). Bacterial Cellulose as a Raw Material for Food and Food Packaging Applications. *Frontiers in Sustainable Food Systems*, *3*(February). https://doi.org/10.3389/fsufs.2019.00007

Bäckdahl, H., Esguerra, M., Delbro, D., Risberg, B., & Gatenholm, P. (2008). Engineering microporosity in bacterial cellulose scaffolds. *Journal of Tissue Engineering and Regenerative Medicine*, *2*(6), 320–330. https://doi.org/10.1002/term.97

Bäckdahl, H., Helenius, G., Bodin, A., Nannmark, U., Johansson, B. R., Risberg, B., & Gatenholm, P. (2006). Mechanical properties of bacterial cellulose and interactions with smooth muscle cells. *Biomaterials*, *27*(9), 2141–2149. https://doi.org/10.1016/j.biomaterials.2005.10.026

Baker, A. A., Helbert, W., Sugiyama, J., & Miles, M. J. (2000). New insight into cellulose structure by atomic force microscopy shows the I(α) crystal phase at near-atomic resolution. *Biophysical Journal*, *79*(2), 1139–1145. https://doi.org/10.1016/S0006-3495(00)76367-3

Broedersz, C. P., & Mackintosh, F. C. (2014). Modeling semiflexible polymer networks. *Reviews of Modern Physics*, *86*(3), 995–1036. https://doi.org/10.1103/RevModPhys.86.995

Brown, A. J. (1886). XLIII. On an acetic ferment which forms cellulose. *Journal of the Chemical Society, Transactions*, *49*(0), 432–439. https://doi.org/10.1039/CT8864900432

Brown, E. E., Laborie, M. P. G., & Zhang, J. (2012). Glutaraldehyde treatment of bacterial cellulose/fibrin composites: Impact on morphology, tensile and viscoelastic properties. *Cellulose*, *19*(1), 127–137. https://doi.org/10.1007/s10570-011-9617-9

Brown, R. M., Willison, J. H., & Richardson, C. L. (1976). Cellulose biosynthesis in Acetobacter xylinum: visualization of the site of synthesis and direct measurement of the in vivo process. *Proceedings of the National Academy of Sciences*, *73*(12), 4565–4569.

https://doi.org/10.1073/pnas.73.12.4565

Carreira, P., Mendes, J. A. S., Trovatti, E., Serafim, L. S., Freire, C. S. R., Silvestre, A. J. D., & Neto, C. P. (2011). Utilization of residues from agro-forest industries in the production of high value bacterial cellulose. *Bioresource Technology*, *102*(15), 7354–7360. https://doi.org/10.1016/j.biortech.2011.04.081

Chakrabarty, A., & Teramoto, Y. (2018). Recent advances in nanocellulose composites with polymers: A guide for choosing partners and how to incorporate them. *Polymers*, *10*(5). https://doi.org/10.3390/polym10050517

Chen, S. Q., Lopez-Sanchez, P., Wang, D., Mikkelsen, D., & Gidley, M. J. (2018). Mechanical properties of bacterial cellulose synthesised by diverse strains of the genus Komagataeibacter. *Food Hydrocolloids*, *81*, 87–95. https://doi.org/10.1016/j.foodhyd.2018.02.031

Czaja, W. K., Young, D. J., Kawecki, M., & Brown, R. M. (2007). The future prospects of microbial cellulose in biomedical applications. *Biomacromolecules*, *8*(1), 1–12. https://doi.org/10.1021/bm060620d

da Silva, C. J. G., de Medeiros, A. D. M., de Amorim, J. D. P., do Nascimento, H. A., Converti, A., Costa, A. F. S., & Sarubbo, L. A. (2021). Bacterial cellulose biotextiles for the future of sustainable fashion: a review. *Environmental Chemistry Letters*, *19*(4), 2967–2980. https://doi.org/10.1007/s10311-021-01214-x

Dhali, K., Ghasemlou, M., Daver, F., Cass, P., & Adhikari, B. (2021). A review of nanocellulose as a new material towards environmental sustainability. *Science of the Total Environment*, *775*(145871). https://doi.org/10.1016/j.scitotenv.2021.145871

Domskiene, J., Sederaviciute, F., & Simonaityte, J. (2019). Kombucha bacterial cellulose for

sustainable fashion. *International Journal of Clothing Science and Technology*, *31*(5), 644–652. https://doi.org/10.1108/IJCST-02-2019-0010

Dourado, F., Fontão, A., Leal, M., Cristina Rodrigues, A., & Gama, M. (2016). Chapter 12 - Process Modeling and Techno-Economic Evaluation of an Industrial Bacterial NanoCellulose Fermentation Process. In M. Gama, F. Dourado, & S. Bielecki (Eds.), *Bacterial Nanocellulose* (pp. 199–214). Elsevier. https://doi.org/https://doi.org/10.1016/B978-0-444-63458-0.00012-3

Du, J., Vepachedu, V., Cho, S. H., Kumar, M., & Nixon, B. T. (2016). Structure of the cellulose synthase complex of Gluconacetobacter hansenii at 23.4 Å resolution. *PLoS ONE*, *11*(5). https://doi.org/10.1371/journal.pone.0155886

Dufresne, A. (2017). Cellulose nanomaterial reinforced polymer nanocomposites. *Current Opinion in Colloid and Interface Science*, *29*, 1–8. https://doi.org/10.1016/j.cocis.2017.01.004

Ek, R., Gustafsson, C., Nutt, A., Iversen, T., & Nyström, C. (1998). Cellulose powder from Cladophora sp. algae. *Journal of Molecular Recognition*, *11*(1–6), 263–265. https://doi.org/10.1002/(SICI)1099-1352(199812)11:1/6<263::AID-JMR437>3.0.CO;2-G

El-Gendi, H., Taha, T. H., Ray, J. B., & Saleh, A. K. (2022). Recent advances in bacterial cellulose: a low-cost effective production media, optimization strategies and applications. *Cellulose*, *29*(14), 7495–7533. https://doi.org/10.1007/s10570-022-04697-1

Fang, J., Kawano, S., Tajima, K., & Kondo, T. (2015). In Vivo Curdlan/Cellulose Bionanocomposite Synthesis by Genetically Modified Gluconacetobacter xylinus. *Biomacromolecules*, *16*(10), 3154–3160. https://doi.org/10.1021/acs.biomac.5b01075

Fernandes, M., Gama, M., Dourado, F., & Souto, A. P. (2019). Development of novel bacterial

cellulose composites for the textile and shoe industry. *Microbial Biotechnology*, *12*(4), 650–661. https://doi.org/10.1111/1751-7915.13387

Fratzl, P., & Weinkamer, R. (2007). Nature's hierarchical materials. *Progress in Materials Science*, *52*(8), 1263–1334. https://doi.org/10.1016/j.pmatsci.2007.06.001

Gallup, O., Ming, H., & Ellis, T. (2021). Ten future challenges for synthetic biology. *Engineering Biology*, *5*(3), 51–59. https://doi.org/10.1049/enb2.12011

Gama, M., & Dourado, F. (2018). Bacterial NanoCellulose: What future? *BioImpacts*, *8*(1), 1–3. https://doi.org/10.15171/bi.2018.01

Gilbert, C., Tang, T. C., Ott, W., Dorr, B. A., Shaw, W. M., Sun, G. L., Lu, T. K., & Ellis, T. (2021). Living materials with programmable functionalities grown from engineered microbial co-cultures. *Nature Materials*, *20*(5), 691–700. https://doi.org/10.1038/s41563-020-00857-5

Goodchild-Michelman, I. M., Church, G. M., Schubert, M. G., & Tang, T. C. (2023). Light and carbon: Synthetic biology toward new cyanobacteria-based living biomaterials. *Materials Today Bio*, *19*. https://doi.org/10.1016/j.mtbio.2023.100583

Gregory, D. A., Tripathi, L., Fricker, A. T. R., Asare, E., Orlando, I., Raghavendran, V., & Roy, I. (2021). Bacterial cellulose: A smart biomaterial with diverse applications. *Materials Science and Engineering R: Reports*, *145*. https://doi.org/10.1016/j.mser.2021.100623

Guan, Q. F., Yang, H. Bin, Han, Z. M., Zhou, L. C., Zhu, Y. B., Ling, Z. C., Jiang, H. Bin, Wang, P. F., Ma, T., Wu, H. A., & Yu, S. H. (2020). Lightweight, tough, and sustainable cellulose nanofiber-derived bulk structural materials with low thermal expansion coefficient. *Science Advances*, *6*(18), 1–9. https://doi.org/10.1126/sciadv.aaz1114

Guhados, G., Wan, W., & Hutter, J. L. (2005). Measurement of the elastic modulus of single

bacterial cellulose fibers using atomic force microscopy. *Langmuir*, *21*(14), 6642–6646. https://doi.org/10.1021/la0504311

Helenius, G., Bäckdahl, H., Bodin, A., Nannmark, U., Gatenholm, P., & Risberg, B. (2006). In vivo biocompatibility of bacterial cellulose. *Journal of Biomedical Materials Research - Part A*, *76*(2), 431–438. https://doi.org/10.1002/jbm.a.30570

Hervy, M., Santmarti, A., Lahtinen, P., Tammelin, T., & Lee, K. Y. (2017). Sample geometry dependency on the measured tensile properties of cellulose nanopapers. *Materials and Design*, *121*, 421–429. https://doi.org/10.1016/j.matdes.2017.02.081

Hesse, S., & Kondo, T. (2005). Behavior of cellulose production of Acetobacter xylinum in 13C-enriched cultivation media including movements on nematic ordered cellulose templates. *Carbohydrate Polymers*, *60*(4), 457–465. https://doi.org/10.1016/j.carbpol.2005.02.018

Hibbert, H. (1930). Action of Bacteria and Enzymes on Carbohydrates and Their Bearing on Plant Synthesis. *Science*, *71*(1842), 419.

Hori, R., & Wada, M. (2005). The thermal expansion of wood cellulose crystals. *Cellulose*, *12*(5), 479–484. https://doi.org/10.1007/s10570-005-5967-5

Hornung, M., Ludwig, M., & Schmauder, H. P. (2007). Optimizing the production of bacterial cellulose in surface culture: A novel aerosol bioreactor working on a fed batch principle (Part 3). *Engineering in Life Sciences*, *7*(1), 35–41. https://doi.org/10.1002/elsc.200620164

Hsieh, Y. C., Yano, H., Nogi, M., & Eichhorn, S. J. (2008). An estimation of the Young's modulus of bacterial cellulose filaments. *Cellulose*, *15*(4), 507–513. https://doi.org/10.1007/s10570-008-9206-8

Hu, Y., & Catchmark, J. M. (2011). In vitro biodegradability and mechanical properties of bioabsorbable bacterial cellulose incorporating cellulases. *Acta Biomaterialia*, *7*(7), 2835–

2845. https://doi.org/10.1016/j.actbio.2011.03.028

Islam, M. U., Ullah, M. W., Khan, S., Shah, N., & Park, J. K. (2017). Strategies for cost-effective and enhanced production of bacterial cellulose. *International Journal of Biological Macromolecules, 102*, 1166–1173. https://doi.org/10.1016/j.ijbiomac.2017.04.110

Isogai, A. (2021). Emerging Nanocellulose Technologies: Recent Developments. *Advanced Materials, 33*(28), 1–10. https://doi.org/10.1002/adma.202000630

James, H. M., & Guth, E. (1943). Theory of the elastic properties of rubber. *The Journal of Chemical Physics, 11*(10), 455–481. https://doi.org/10.1063/1.1723785

Jin, K., Jin, C., & Wu, Y. (2022). Synthetic biology-powered microbial co-culture strategy and application of bacterial cellulose-based composite materials. *Carbohydrate Polymers*, *283*, 119171. https://doi.org/10.1016/j.carbpol.2022.119171

Kaczmarek, M., Jędrzejczak-Krzepkowska, M., & Ludwicka, K. (2022). Comparative Analysis of Bacterial Cellulose Membranes Synthesized by Chosen Komagataeibacter Strains and Their Application Potential. *International Journal of Molecular Sciences*, *23*(6). https://doi.org/10.3390/ijms23063391

Kaushal, R., & Walker, T. K. (1947). Formation of cellulose by Acetobacter acetigenum. *Nature*, *160*(4069), 572–573. https://doi.org/10.1038/160572b0

Kim, D. Y., Nishiyama, Y., Wada, M., Kuga, S., & Okano, T. (2001). Thermal decomposition of cellulose crystallites in wood. *Holzforschung*, *55*(5), 521–524. https://doi.org/10.1515/HF.2001.084

Kim, U. J., Eom, S. H., & Wada, M. (2010). Thermal decomposition of native cellulose: Influence on crystallite size. *Polymer Degradation and Stability*, *95*(5), 778–781. https://doi.org/10.1016/j.polymdegradstab.2010.02.009

Kim, Y. J., Kim, J. N., Wee, Y. J., Park, D. H., & Ryu, H. W. (2007). Bacterial cellulose production by Gluconacetobacter sp. PKY5 in a rotary biofilm contactor. *Applied Biochemistry and Biotechnology*, *137–140*(1–12), 529–537. https://doi.org/10.1007/s12010-007-9077-8

Klemm, D., Cranston, E. D., Fischer, D., Gama, M., Kedzior, S. A., Kralisch, D., Kramer, F., Kondo, T., Lindström, T., Nietzsche, S., Petzold-Welcke, K., & Rauchfuß, F. (2018). Nanocellulose as a natural source for groundbreaking applications in materials science: Today's state. *Materials Today*, *21*(7), 720–748. https://doi.org/10.1016/j.mattod.2018.02.001

Klemm, D., Schumann, D., Udhardt, U., & Marsch, S. (2001). Bacterial synthesized cellulose - Artificial blood vessels for microsurgery. *Progress in Polymer Science (Oxford)*, *26*(9), 1561–1603. https://doi.org/10.1016/S0079-6700(01)00021-1

Kondo, T. (2022). Cellulose Nanofibrils Pulverized from Biomass Resources: Past, Present, and Future Perspectives. *KONA Powder and Particle Journal*. https://doi.org/10.14356/kona.2023003

Kose, R., Sunagawa, N., Yoshida, M., & Tajima, K. (2013). One-step production of nanofibrillated bacterial cellulose (NFBC) from waste glycerol using Gluconacetobacter intermedius NEDO-01. *Cellulose*, *20*(6), 2971–2979. https://doi.org/10.1007/s10570-013-0050-0

Kralisch, D., Hessler, N., Klemm, D., Erdmann, R., & Schmidt, W. (2010). White biotechnology for cellulose manufacturing - The HoLiR concept. *Biotechnology and Bioengineering*, *105*(4), 740–747. https://doi.org/10.1002/bit.22579

Kuhn, W. (1936). Beziehungen zwischen Molekülgröße, statistischer Molekülgestalt und

elastischen Eigenschaften hochpolymerer Stoffe. *Kolloid-Zeitschrift*, *76*(3), 258–271. https://doi.org/10.1007/BF01451143

Lee, K. Y., Buldum, G., Mantalaris, A., & Bismarck, A. (2014). More than meets the eye in bacterial cellulose: Biosynthesis, bioprocessing, and applications in advanced fiber composites. *Macromolecular Bioscience*, *14*(1), 10–32. https://doi.org/10.1002/mabi.201300298

Ling, S., Chen, W., Fan, Y., Zheng, K., Jin, K., Yu, H., Buehler, M. J., & Kaplan, D. L. (2018). Biopolymer nanofibrils: Structure, modeling, preparation, and applications. *Progress in Polymer Science*, *85*, 1–56. https://doi.org/10.1016/j.progpolymsci.2018.06.004

Liu, W., Du, H., Zhang, M., Liu, K., Liu, H., Xie, H., Zhang, X., & Si, C. (2020). Bacterial Cellulose-Based Composite Scaffolds for Biomedical Applications: A Review. *ACS Sustainable Chemistry and Engineering*, *8*(20), 7536–7562. https://doi.org/10.1021/acssuschemeng.0c00125

Lu, Z., Zhang, Y., Chi, Y., Xu, N., Yao, W., & Sun, B. (2011). Effects of alcohols on bacterial cellulose production by Acetobacter xylinum 186. *World Journal of Microbiology and Biotechnology*, *27*(10), 2281–2285. https://doi.org/10.1007/s11274-011-0692-8

Ludwicka, K., Kaczmarek, M., & Białkowska, A. (2020). Bacterial nanocellulose—a biobased polymer for active and intelligent food packaging applications: Recent advances and developments. *Polymers*, *12*(10), 1–23. https://doi.org/10.3390/polym12102209

Martínez-Sanz, M., Gidley, M. J., & Gilbert, E. P. (2016). Hierarchical architecture of bacterial cellulose and composite plant cell wall polysaccharide hydrogels using small angle neutron scattering. *Soft Matter*, *12*(5), 1534–1549. https://doi.org/10.1039/c5sm02085a

Martínez-Sanz, M., Mikkelsen, D., Flanagan, B., Gidley, M. J., & Gilbert, E. P. (2016). Multi-

scale model for the hierarchical architecture of native cellulose hydrogels. *Carbohydrate Polymers*, *147*, 542–555. https://doi.org/10.1016/j.carbpol.2016.03.098

McKenna, B. A., Mikkelsen, D., Wehr, J. B., Gidley, M. J., & Menzies, N. W. (2009). Mechanical and structural properties of native and alkali-treated bacterial cellulose produced by Gluconacetobacter xylinus strain ATCC 53524. *Cellulose*, *16*(6), 1047–1055. https://doi.org/10.1007/s10570-009-9340-y

Melton, L. (2022). Cellulose shoes made by bacteria. *Nature Biotechnology*, *40*(8), 1163. https://doi.org/10.1038/s41587-022-01431-x

Moon, R. J., Martini, A., Nairn, J., Simonsen, J., & Youngblood, J. (2011). Cellulose nanomaterials review: Structure, properties and nanocomposites. *Chemical Society Reviews*, *40*(7), 3941–3994. https://doi.org/10.1039/c0cs00108b

Moradali, M. F., & Rehm, B. H. A. (2020). Bacterial biopolymers: from pathogenesis to advanced materials. *Nature Reviews Microbiology*, *18*(4), 195–210. https://doi.org/10.1038/s41579-019-0313-3

Nguyen, P. Q., Courchesne, N. M. D., Duraj-Thatte, A., Praveschotinunt, P., & Joshi, N. S. (2018). Engineered Living Materials: Prospects and Challenges for Using Biological Systems to Direct the Assembly of Smart Materials. *Advanced Materials*, *30*(19), 1–34. https://doi.org/10.1002/adma.201704847

Nicolas, W. J., Ghosal, D., Tocheva, E. I., Meyerowitz, E. M., & Jensen, G. J. (2020). Structure of the bacterial cellulose ribbon and its assembly-guiding cytoskeleton by electron cryotomography. *Journal of Bacteriology*, *203*(3), 1–13. https://doi.org/10.1128/jb.00371-20

Nishiyama, Y. (2018). Molecular interactions in nanocellulose assembly. In *Philosophical*

Transactions of the Royal Society A: Mathematical, Physical and Engineering Sciences (Vol. 376, Issue 2112). https://doi.org/10.1098/rsta.2017.0047

Nishiyama, Y., Langan, P., & Chanzy, H. (2002). Crystal structure and hydrogen-bonding system in cellulose Iβ from synchrotron X-ray and neutron fiber diffraction. *Journal of the American Chemical Society*, *124*(31), 9074–9082. https://doi.org/10.1021/ja0257319

Nishiyama, Y., Sugiyama, J., Chanzy, H., & Langan, P. (2003). Crystal Structure and Hydrogen Bonding System in Cellulose Iα from Synchrotron X-ray and Neutron Fiber Diffraction. *Journal of the American Chemical Society*, *125*(47), 14300–14306. https://doi.org/10.1021/ja037055w

Paddon, C. J., & Keasling, J. D. (2014). Semi-synthetic artemisinin: A model for the use of synthetic biology in pharmaceutical development. *Nature Reviews Microbiology*, *12*(5), 355–367. https://doi.org/10.1038/nrmicro3240

Park, C. H., Kang, Y. K., & Im, S. S. (2004). Biodegradability of cellulose fabrics. *Journal of Applied Polymer Science*, *94*(1), 248–253. https://doi.org/10.1002/app.20879

Persson, J., Chanzy, H., & Sugiyama, J. (1991). Combined Infrared and Electron Diffraction Study of the Polymorphism of Native Celluloses. *Macromolecules*, *24*(9), 2461–2466. https://doi.org/10.1021/ma00009a050

Picheth, G. F., Pirich, C. L., Sierakowski, M. R., Woehl, M. A., Sakakibara, C. N., de Souza, C. F., Martin, A. A., da Silva, R., & de Freitas, R. A. (2017). Bacterial cellulose in biomedical applications: A review. *International Journal of Biological Macromolecules*, *104*, 97–106. https://doi.org/10.1016/j.ijbiomac.2017.05.171

Picu, C. R. (2020). Mechanics of Random Fiber Networks: Structure–Properties Relation. In *Mechanics ofFibrous Materials and Applications* (pp. 1–61). Springer International

Publishing. https://doi.org/10.1007/978-3-030-23846-9_1

Polko, J. K., & Kieber, J. J. (2019). The regulation of cellulose biosynthesis in plants. *Plant Cell*, *31*(2), 282–296. https://doi.org/10.1105/tpc.18.00760

Quero, F., Nogi, M., Yano, H., Abdulsalami, K., Holmes, S. M., Sakakini, B. H., & Eichhorn, S. J. (2010). Optimization of the mechanical performance of bacterial cellulose/poly(L-lactic) acid composites. *ACS Applied Materials and Interfaces*, *2*(1), 321–330. https://doi.org/10.1021/AM900817F/ASSET/IMAGES/LARGE/AM-2009-00817F_0009.JPEG

Rani, M. U., Rastogi, N. K., & Anu Appaiah, K. A. (2011). Statistical optimization of medium composition for bacterial cellulose production by Gluconacetobacter hansenii UAC09 using coffee cherry husk extract - an agro-industry waste. *Journal of Microbiology and Biotechnology*, *21*(7), 739–745. https://doi.org/10.4014/jmb.1012.12026

Schönfelder, U., Abel, M., Wiegand, C., Klemm, D., Elsner, P., & Hipler, U. C. (2005). Influence of selected wound dressings on PMN elastase in chronic wound fluid and their antioxidative potential in vitro. *Biomaterials*, *26*(33), 6664–6673. https://doi.org/10.1016/j.biomaterials.2005.04.030

Semjonovs, P., Ruklisha, M., Paegle, L., Saka, M., Treimane, R., Skute, M., Rozenberga, L., Vikele, L., Sabovics, M., & Cleenwerck, I. (2017). Cellulose synthesis by Komagataeibacter rhaeticus strain P 1463 isolated from Kombucha. *Applied Microbiology and Biotechnology*, *101*(3), 1003–1012. https://doi.org/10.1007/s00253-016-7761-8

Shah, N., Ul-Islam, M., Khattak, W. A., & Park, J. K. (2013). Overview of bacterial cellulose composites: A multipurpose advanced material. *Carbohydrate Polymers*, *98*(2), 1585–1598. https://doi.org/10.1016/j.carbpol.2013.08.018

Skiba, E. A., Budaeva, V. V, Ovchinnikova, E. V, Gladysheva, E. K., Kashcheyeva, E. I., Pavlov, I. N., & Sakovich, G. V. (2020). A technology for pilot production of bacterial cellulose from oat hulls. *Chemical Engineering Journal*, *383*, 1385–8947. https://doi.org/10.1016/j.cej.2019.123128

Song, B., Zhao, S., Shen, W., Collings, C., & Ding, S. Y. (2020). Direct Measurement of Plant Cellulose Microfibril and Bundles in Native Cell Walls. *Frontiers in Plant Science*, *11*(April), 1–11. https://doi.org/10.3389/fpls.2020.00479

Srubar, W. V. (2021). Engineered Living Materials: Taxonomies and Emerging Trends. *Trends in Biotechnology*, *39*(6), 574–583. https://doi.org/10.1016/j.tibtech.2020.10.009

Sun, C. (2005). True Density of Microcrystalline Cellulose. *Journal of Pharmaceutical Sciences*, *94*(10), 2132–2134. https://doi.org/10.1002/JPS.20459

Tajima, K., Imai, T., Yui, T., Yao, M., & Saxena, I. (2022). Cellulose-synthesizing machinery in bacteria. In *Cellulose* (Vol. 29, Issue 5, pp. 2755–2777). Springer Netherlands. https://doi.org/10.1007/s10570-021-04225-7

Takahama, R., Kato, H., Tajima, K., Tagawa, S., & Kondo, T. (2021). Biofabrication of a Hyaluronan/Bacterial Cellulose Composite Nanofibril by Secretion from Engineered Gluconacetobacter. *Biomacromolecules*, *22*(11), 4709–4719. https://doi.org/10.1021/acs.biomac.1c00987

Takahama, R., Kato, H., Takayama, G., Tajima, K., & Kondo, T. (2022). Physical characteristics and cell-adhesive properties of in vivo fabricated bacterial cellulose/hyaluronan nanocomposites. *Cellulose*, *29*(6), 3239–3251. https://doi.org/10.1007/s10570-022-04480-2

Tang, T. C., An, B., Huang, Y., Vasikaran, S., Wang, Y., Jiang, X., Lu, T. K., & Zhong, C. (2021). Materials design by synthetic biology. *Nature Reviews Materials*, *6*(4), 332–350.

https://doi.org/10.1038/s41578-020-00265-w

Tang, W., Jia, S., Jia, Y., & Yang, H. (2010). The influence of fermentation conditions and post-treatment methods on porosity of bacterial cellulose membrane. *World Journal of Microbiology and Biotechnology*, *26*(1), 125–131. https://doi.org/10.1007/s11274-009-0151-y

Tanpichai, S., Quero, F., Nogi, M., Yano, H., Young, R. J., Lindström, T., Sampson, W. W., & Eichhorn, S. J. (2012). Effective young's modulus of bacterial and microfibrillated cellulose fibrils in fibrous networks. *Biomacromolecules*, *13*(5), 1340–1349. https://doi.org/10.1021/bm300042t

Tomita, Y., & Kondo, T. (2009). Influential factors to enhance the moving rate of Acetobacter xylinum due to its nanofiber secretion on oriented templates. *Carbohydrate Polymers*, *77*(4), 754–759. https://doi.org/10.1016/j.carbpol.2009.02.022

Ul-Islam, M., Khan, T., & Park, J. K. (2012). Water holding and release properties of bacterial cellulose obtained by in situ and ex situ modification. *Carbohydrate Polymers*, *88*(2), 596–603. https://doi.org/10.1016/j.carbpol.2012.01.006

Ullah, H., Santos, H. A., & Khan, T. (2016). Applications of bacterial cellulose in food, cosmetics and drug delivery. In *Cellulose* (Vol. 23, Issue 4, pp. 2291–2314). https://doi.org/10.1007/s10570-016-0986-y

Vazquez, A., Foresti, M. L., Cerrutti, P., & Galvagno, M. (2013). Bacterial Cellulose from Simple and Low Cost Production Media by Gluconacetobacter xylinus. *Journal of Polymers and the Environment*, *21*(2), 545–554. https://doi.org/10.1007/s10924-012-0541-3

Walker, K. T., Goosens, V. J., Das, A., Graham, A. E., & Ellis, T. (2019). Engineered cell-to-cell signalling within growing bacterial cellulose pellicles. *Microbial Biotechnology*, *12*(4),

611–619. https://doi.org/10.1111/1751-7915.13340

Wegst, U. G. K., & Ashby, M. F. (2004). The mechanical efficiency of natural materials. *Philosophical Magazine*, *84*(21), 2167–2186. https://doi.org/10.1080/14786430410001680935

Wegst, U. G. K., Bai, H., Saiz, E., Tomsia, A. P., & Ritchie, R. O. (2015). Bioinspired structural materials. *Nature Materials*, *14*(1), 23–36. https://doi.org/10.1038/nmat4089

Whitney, S. E. C., Gothard, M. G. E., Mitchell, J. T., & Gidley, M. J. (1999). Roles of cellulose and xyloglucan in determining the mechanical properties of primary plant cell walls. *Plant Physiology*, *121*(2), 657–663. https://doi.org/10.1104/pp.121.2.657

Yamanaka, S., & Sugiyama, J. (2000). Structural modification of bacterial cellulose. *Cellulose*, *7*(3), 213–225. https://doi.org/10.1023/A:1009208022957

Yano, H., Sugiyama, J., Nakagaito, A. N., Nogi, M., Matsuura, T., Hikita, M., & Handa, K. (2005). Optically transparent composites reinforced with networks of bacterial nanofibers. *Advanced Materials*, *17*(2), 153–155. https://doi.org/10.1002/adma.200400597

Yue, K., Chen, J., Li, Y., & Kai, L. (2023). Advancing synthetic biology through cell-free protein synthesis. *Computational and Structural Biotechnology Journal*, *21*, 2899–2908. https://doi.org/10.1016/j.csbj.2023.05.003

Zaar, K. (1979). Visualization of pores (export sites) correlated with cellulose production in the envelop of the gram-negative bacterium Acetobacter xylinum. *Journal of Cell Biology*, *80*(March), 773–777. https://doi.org/10.1083/jcb.80.3.773

Chapter 1

In situ Visualization of the Tensile Deformation Mechanism in Bacterial Cellulose Network

Introduction

BC pellicle, a nanofibrous material, exhibits nontrivial mechanical properties and distinct characteristics compared to polymer hydrogels. The mechanical properties of a single cellulose fiber can be explained in terms of the crystalline modulus (Nishino et al., 1995). The mechanical properties of a single BC ribbon have been directly measured (Guhados et al., 2005), and the elastic modulus has been determined using Raman spectroscopy (Hsieh et al., 2008; Tanpichai et al., 2012). However, BC pellicles composed of these cellulose nanofibers are capable of greater deformation than their constituent nanofibers and exhibit complex nonlinear mechanical responses that involve viscoelasticity and plasticity due to their fiber network structure. Frensemeier et al. analyzed the tensile deformation of BC pellicle using a simple Maxwell model and clarified the dependence of the elastic modulus and viscosity on the amount of strain and water in the network (Frensemeier et al., 2010). Furthermore, Gao et al. used a fraction-exponential model to analyze uniaxial tensile creep measurements and determine the time-dependent rheological behavior of BC pellicle (Gao et al., 2016).

To tailor the mechanical properties of BC pellicles as described above, it is necessary to elucidate the structure–property relationship of the fiber network. In this regard, Astley et al. used X-ray scattering to reveal the strain-dependent reorientation of fiber networks of water-containing BC pellicles (Astley et al., 2003). In addition, McKenna et al. analyzed fractured surfaces and found that rearrangement and pullout of fiber segments occur during uniaxial deformation (McKenna et al., 2009). Moreover, Gao et al. proposed a mesh deformation model based on the results of cyclic (loading, unloading, and reloading) tests in which water-containing pellicles are subjected to uniaxial tensile deformation at various stresses (Gao et al., 2015). These studies provide important insights into the deformation behavior of the fiber network. However, the response of the microscopic fiber network in tensile deformation is still a matter of speculation. There has been no study on the direct visualization of the processes occurring on the microscopic scale during tensile deformation. Therefore, real-time observation of the microscopic fiber network in water-containing pellicles under tensile deformation is expected to provide key insights into factors that control material properties.

To determine the response of the fiber network to tensile deformation, BC pellicles under tensile deformation were visualized in situ using a device for simultaneous confocal laser scanning microscopy (CLSM) and uniaxial tensile deformation. Furthermore, tensile tests and stress relaxation measurements under various conditions were conducted to investigate the tensile properties of BC pellicles in detail. The obtained microscopic images combined with the stress–strain curves and relaxation spectra were analyzed to propose a tensile deformation model, which was subsequently validated. Finally, the possibilities and challenges of engineering BC pellicles are discussed.

Materials and methods

Materials

Komagataeibacter hansenii (ATCC23769) (= formerly *Gluconacetobacter hansenii*) was purchased from the American Type Culture Collection (VA, USA). Bacto peptone and Bacto yeast extract were purchased from Difco Laboratories Inc. (NJ, USA). Glucose and cellulase (Celluclast 1.5 L) were purchased from Sigma–Aldrich (MO, USA). Disodium hydrogen phosphate heptahydrate ($Na_2HPO_4 \cdot 7H_2O$) was purchased from Nacalai Tesque Inc. (Kyoto, Japan). Citric acid and sodium hydroxide were purchased from Wako Pure Chemical Inc. (Osaka, Japan). Trichloro triazine, propargylamine, and triethylamine were purchased from Tokyo Chemical Industry (Tokyo, Japan). 6-Fluorescein azide (6-FAM azide) was purchased from AAT Bioquest (CA, USA).

Preparation of BC pellicles

Komagataeibacter hansenii (ATCC23769) was inoculated into a liquid medium and incubated statically. Generally, changes in the nutrient environment during incubation often produce pellicles with a heterogeneous structure. Considering this effect, pellicles with high uniformity were prepared by increasing the inoculum density and shortening the incubation time stipulated in the usual culture method. Specifically, bacteria were inoculated into baffled flasks containing Hestrin and Schramm (HS) medium (Hestrin & Schramm, 1954) and cultured at 30 °C with shaking at 125 rpm to prepare the bacteria for pellicle production. Culturing was continued until the turbidity of the cell suspension (optical density at 600 nm, OD_{600}) reached 2.4, and bacteria were collected as pellets by centrifugation (3600×g, 5 min). The harvested bacteria were resuspended in fresh HS medium to a final turbidity of OD_{600} = 0.6, and 20 mL of the cell

suspension was transferred to a petri dish (inner diameter of 86 mm) and statically incubated at 30 °C. After 24 h, the pellicle formed on the surface of the culture medium was harvested. The harvested pellicles were rinsed with water, immersed in 0.1 M NaOH, and heat-treated at 90 °C for 3 h. The purified pellicles were substituted with pure water and stored in a refrigerator. Dumbbell-shaped specimens for tensile tests were cut from BC pellicles using a dumbbell cutter (Super-Dumbbell, Saitama, Japan). Post-treatment of squeezing/freeze-drying/oven-drying was performed on the dumbbell-shaped specimens to prepare the BC pellicles with different hydration states. The squeezed BC pellicles were prepared by sandwiching the hydrated pellicles between filter papers and removing most of the water. The aerogel-like samples were prepared by freeze-drying the hydrated samples. To prepare the film samples, hydrated samples were mounted on polytetrafluoroethylene substrates and then dried in an oven at 50 °C for 3 h. The weight of the sample in its initial hydrated state, weight after squeezing, and weight after oven-drying were measured, and the cellulose content and water holding capacity of the sample were calculated according to the following equations.

$$Cellulose\ content\ (\mathrm{wt\%}) = \frac{dry\ weight\ (\mathrm{g})}{wet\ weigt\ (\mathrm{g})} \times 100$$

$$Water\ holding\ capacity\ (\mathrm{wt\%}) = \frac{wet\ weight\ (\mathrm{g}) - dry\ weight\ (\mathrm{g})}{dry\ weight\ (\mathrm{g})} \times 100$$

The results from three samples were averaged for each condition. All the specimens used in the experiments were prepared from the same batch.

Tensile testing

To determine the tensile mechanical properties of BC pellicles, tensile tests were conducted under various conditions. Uniaxial tensile tests of the prepared specimens (hydrated/squeezed/freeze-dried/oven-dried) were conducted using a tensile testing machine (STA-1250, A&D, Tokyo, Japan) equipped with a 50-N load cell at a crosshead speed of 10 mm/min (strain rate of 1.4 %/s). Ten measurements were performed under all test conditions. The thickness of the specimens, measured with a digital micrometer (OMV-25MX, Mitutoyo, Kanagawa, Japan), was used to calculate the stress (σ). Stress (σ)–strain (ε) curves were plotted from the obtained data, and the tangent modulus ($d\sigma/d\varepsilon$, the slope of the stress−strain curve) were calculated.

Fluorescent labeling of BC pellicles

To visualize the fiber network of BC pellicles, fluorescent labeling of cellulose nanofibers was performed following a previously reported method (Babi et al., 2021). Dichlorotriazinyl propargylamine (DTAP) was synthesized and introduced to the hydroxyl groups on the surface of the cellulose nanofiber. Specifically, the BC pellicle, DTAP, and NaOH were added to a 3:1 water/acetone mixture at final concentrations of 0.1 wt%, 10 mM, and 0.05 M, respectively. After the reaction proceeded at room temperature for 24 h, unreacted DTAP was removed by replacing the reaction mixture with water, phosphate-buffered saline (PBS), and water, three times. Then, fluorescent 6-FAM azide was introduced into the DTAP linkers by click chemistry. CuAAC (Cu(I)-catalyzed azide–alkyne cycloaddition) click reaction was initiated by adding the BC pellicle, 6-FAM azide, ascorbic acid, and $CuSO_4$ to a 1:1 water/methanol mixture at final concentrations of 0.1 wt%, 100 μM, 5 mM, and 0.3 mM,

respectively. The reaction was carried out with stirring at room temperature in the dark for 2 h. Washing followed the same procedure as that for DTAP.

In situ observation of tensile deformation

In situ observation of fluorescently labeled BC pellicles under tensile deformation was performed to determine the response of the fiber network to tensile deformation. A special tensile device for simultaneous fluorescence microscopy and uniaxial tensile deformation was fabricated by 3D printing. A dumbbell-shaped specimen labeled with 6-FAM was placed in the tensile device and observed with a confocal laser scanning microscope (TCS SP8, Leica Microsystems, Wetzlar, Germany). A 100× lens was used for observation, and the wavelengths of excitation and fluorescence detection were 488 and 493–650 nm, respectively. The confocal pinhole size and voxel size were set to 0.6 Airy unit (calculated at the wavelength of 525 nm) and 56 × 56 × 200 nm, respectively. After focusing the sample, uniaxial tensile strain (0%/5%/10%/15%/20%/25%) was applied stepwise to the sample, and after 5 min of standing, 3D images (29 × 29 × 5 μm) were acquired. The data were acquired at five different points in each strain stage. In addition, dynamic changes in the fiber network were observed immediately after the strain was applied. The video observations were conducted for a total of three replicates. The acquired 3D data were deconvoluted using Huygens Professional (Scientific Volume Imaging, Hilversum, Nederland) and contrast-adjusted using ImageJ (Schindelin et al., 2012). Fiber segmentation analysis using an open-source software, SOAX (Xu et al., 2015), was performed to quantitatively evaluate the fiber network. After converting the 3D data of 6 slices into Z-projection images, the fiber structures were extracted using SOAX, and the orientation and curvature of the extracted fiber segments were analyzed.

Stress relaxation test

Stress relaxation measurements were conducted to clarify the behavior of BC pellicles as viscoelastic solids in various strain regimes. Dumbbell-shaped specimens were immersed in a customized chamber filled with water. An initial strain of 5%, 10%, 15%, 20%, or 25% was applied to the specimens at a strain rate of 20 mm/min. The strain was maintained for up to 24 h, and the time-course of stress was recorded. From the obtained stress–time data, the relaxation modulus $E(t)$ (= *stress*/*initial strain*) was calculated. Assuming a generalized Maxwell model with one spring and multiple Maxwell elements connected in parallel, a continuous relaxation spectrum was calculated from the relationship between the measured relaxation modulus $E(t)$ and time t. The calculation was performed using pyReSpect, an open-source software package for the determination of relaxation spectra based on nonlinear Tikhonov regularization (Shanbhag, 2019).

Measurements of the recovery ratio of elongational strain

The elasticity and plasticity of the BC pellicle were investigated by measuring the recovery ratio of elongational strain. BC pellicles were subjected to 5%, 10%, 15%, 20%, or 25% elongational strain. After 3 min, the strain was released, and the pellicle was immersed in water and allowed to stand. After 6 h, the length of the specimen was measured. The elongation recovery ratio was calculated using the following equation: *Elongation recovery ratio* (%) = (*length after recovery* − *initial length*) / (*length after elongation* – *initial length*) × 100. Three samples were measured for each strain condition.

Results

Tensile mechanical properties of BC pellicles

The average values of the strength, and elongation at break obtained from tensile tests were 0.43 MPa, and 29.3%, respectively (Table 1-1). These values were within the range of previously reported values (Bäckdahl et al., 2006; Brown et al., 2012; Chen et al., 2018; McKenna et al., 2009). The stress (σ)–strain (ε) curve obtained at a strain rate of 10 mm/min (Fig. 1-1a) revealed the occurrence of strain hardening, which was further investigated by plotting the tangent modulus ($d\sigma/d\varepsilon$) versus strain (Fig. 1-1d). From the difference in the tangent modulus, the tensile deformation was classified into four strain regions: (i) 0%–2%, (ii) 2%–12%, (iii) 12%–25%, and (iv) 25%–30%. Initially, in strain region (i), the tangent modulus is relatively small and constant for a given strain. In strain region (ii), the modulus increases in proportion to the given strain, reaching a plateau in strain region (iii) and finally decreasing in region (iv). Thus, the pellicle undergoes multiple modes of tensile deformation depending on the magnitude of the strain.

Table 1-1. Tensile properties of BC pellicles under various conditions. Data are shown as the mean value ± standard error.

Condition	**Water holding capacity /wt%**	**Strength /MPa**	**Elongation at break /%**
Hydrated	360 ± 15	0.43 ± 0.02	29.3 ± 1.3
Squeezed	17 ± 0.6	0.53 ± 0.01	27.7 ± 1.1
Freeze dried	–	0.28 ± 0.03	3.2 ± 0.3
Oven dried	–	0.96 ± 0.14 (75.7 ± 11.0*)	5.7 ± 0.8

* True strength calculated from the thickness of the dried film.

To investigate the effect of incorporated water on the tensile mechanical properties of BC pellicles, tensile tests were conducted using pellicles with different water contents (hydrated, squeezed, freeze-dried and oven-dried samples). The initial cellulose content of BC pellicles was 0.45 ± 0.02 wt% and 95 wt% of water is drained out after squeezing. Water holding capacity is 360 ± 15 wt% for hydrated samples and 17 ± 0.6 wt% for squeezed samples (Table 1-1). Although the actual thickness of the samples changed due to the post-treatments (e.g., in the case of oven-drying, the thickness changed from 630 μm to 8 μm), the stress σ values were calculated using the thickness of the hydrated pellicle for all conditions. This allows comparison of tensile properties for each sample with the same fiber content. The tangent modulus of the squeezed sample indicated strain softening in the range of 2%–12%, in contrast to the hydrated sample (Fig. 1-1b, e). Specifically, the tangent modulus of the squeezed sample was the greatest at 0% and decreased with increasing strain. Above 12% strain, the flat region with a constant tangent modulus and the decreasing region before fracture were observed. In the region above 12% strain, the constant tangent modulus decreased before fracture. This trend was similar to that of the hydrated sample. In contrast, the stress–strain curves of the freeze-dried samples and the oven-dried sample revealed the occurrence of strain hardening (Fig. 1-1c, f). Additionally, the oven-dried sample had 2-times higher tensile strength, and 1/5-times smaller elongation at break than the hydrated sample (Table 1-1).

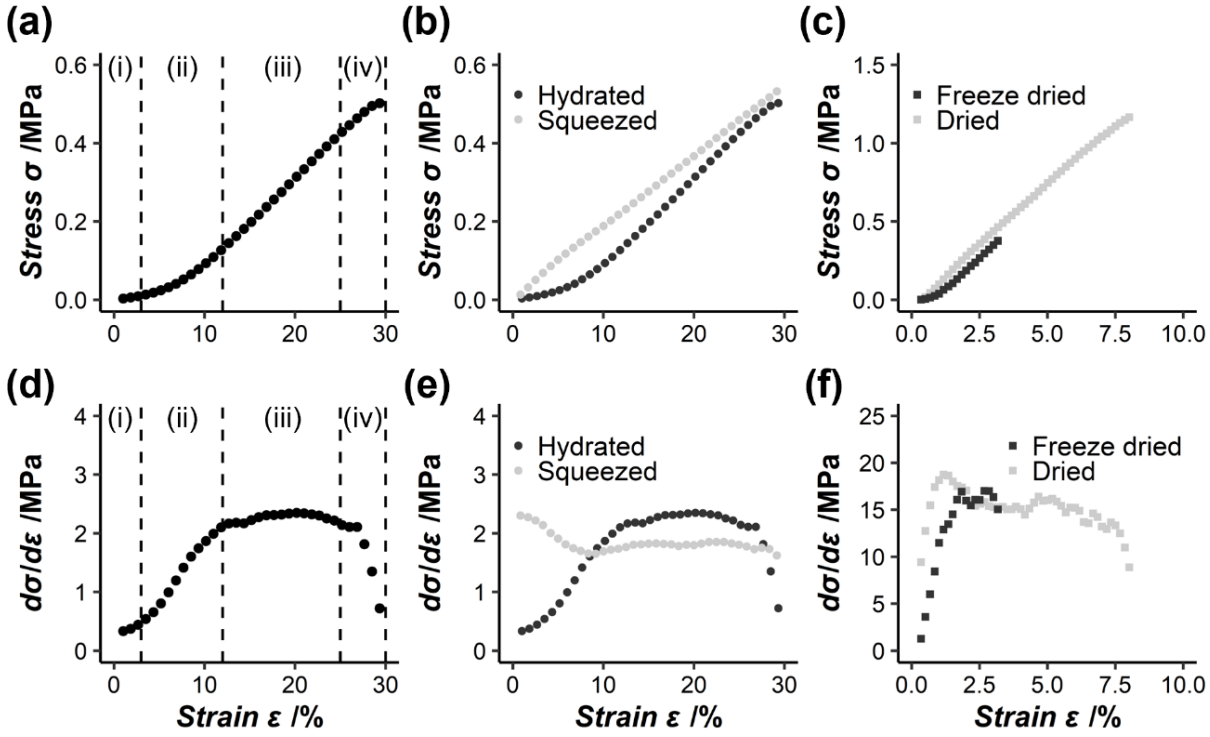

Fig. 1-1 (a–c) Representative stress–strain curves and (d–f) tangent moduli $d\sigma/d\varepsilon$ of BC pellicles obtained under various conditions.

In situ CLSM of the fiber network under deformation

In situ CLSM of the BC pellicle under tensile deformation was carried out to visualize microstructural changes in the fiber network. Because it was difficult to obtain data while applying strain owing to the vibration of the stage, the relaxation behavior of the network after applying the strain and the structure of the network after relaxation were investigated. Specifically, observations were made after applying constant strains of 0%, 5%, 10%, 15%, 20%, and 25% to the pellicle. Microscopic changes in the fiber network immediately after applying the strain was qualitatively observed. Shortly after the strain was applied, fiber segments stretched along the tensile direction (stress paths) appeared (Fig. 1-2a). The number of stress paths increased significantly after 10% strain. Thereafter, the overall network drifted along the tensile

direction for tens of seconds and then reached an equilibrium state. Therefore, in response to the strain, the stress is momentarily concentrated on some fiber segments to develop stress paths, although this may be relaxed by subsequent rearrangements of the fiber network.

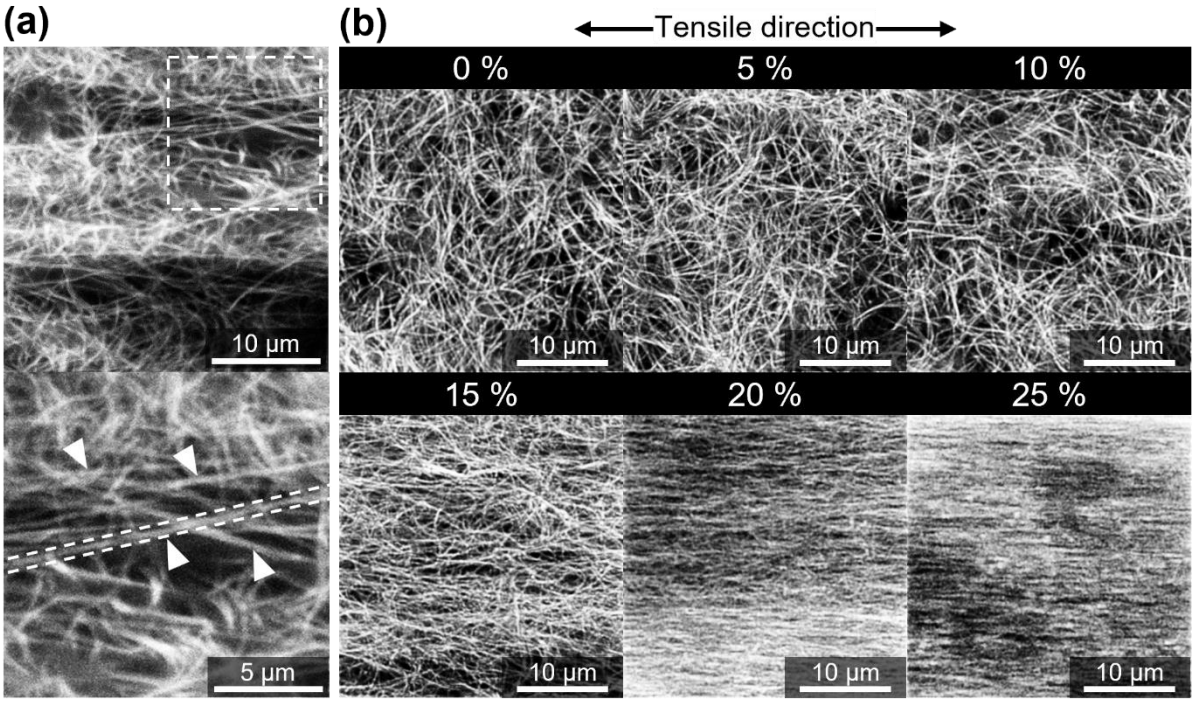

Fig. 1-2 (a) CLSM image of the fiber network in hydrated BC pellicles during deformation (strain = 12.5%). The lower image is an enlarged image of the area enclosed by the dashed line in the upper image. Stretched and strained fibers (stress paths) in the relaxed fiber network are indicated by dashed lines and arrowheads. (b) Microscopic images of the fiber network at each stage of tensile deformation visualized with in situ confocal laser scanning microscopy. The tensile direction is horizontal in all images.

The fiber network changed 5 min after applying the strain, and this change depended on the magnitude of the strain, as shown in Fig. 1-2b. Fibers were randomly oriented at 0% strain and started to orient along the tensile direction at 15% strain. At 20% and 25% strain, oriented fibers (along the tensile direction) became dominant over the entire network. Fiber segmentation

analysis was performed on the acquired images of the fiber network. The extracted fiber segments showed no orientation in the range of 0%−10% strain (Fig. 1-3a). The fiber segments were oriented along the tensile direction at 15% strain and highly oriented at 20% and 25% strain. Astley et al. analyzed the orientation of cellulose fibers under tensile deformation using small-angle X-ray measurements (Astley et al., 2003), revealing that the degree of orientation increases rapidly after 1/3 of the breaking strain (equivalent to 10% in this study), and this rearrangement is almost complete at 2/3 of the maximum strain (20% in this study). This is the same trend as that observed in the present study. Furthermore, the curvature of the extracted fibers to estimate the degree of stress on each fiber were analysed. The unstressed fibers had a gentle curve, while the stressed fibers were straight. Therefore, it is possible to estimate whether a fiber carries stress from the curvature. As the strain increased from 10% to 25%, the fraction of fibers with a curvature greater than 0.3 μm^{-1} (radius of curvature less than 3.3 μm) decreased and the fraction of fibers with a curvature less than 0.1 μm^{-1} (radius of curvature greater than 10 μm) increased (Fig. 1-3b, c). The analysis showed that the ratio of stress-bearing fibers in the fiber network was proportional to the magnitude of strain, and this ratio changed significantly at strains above 10%.

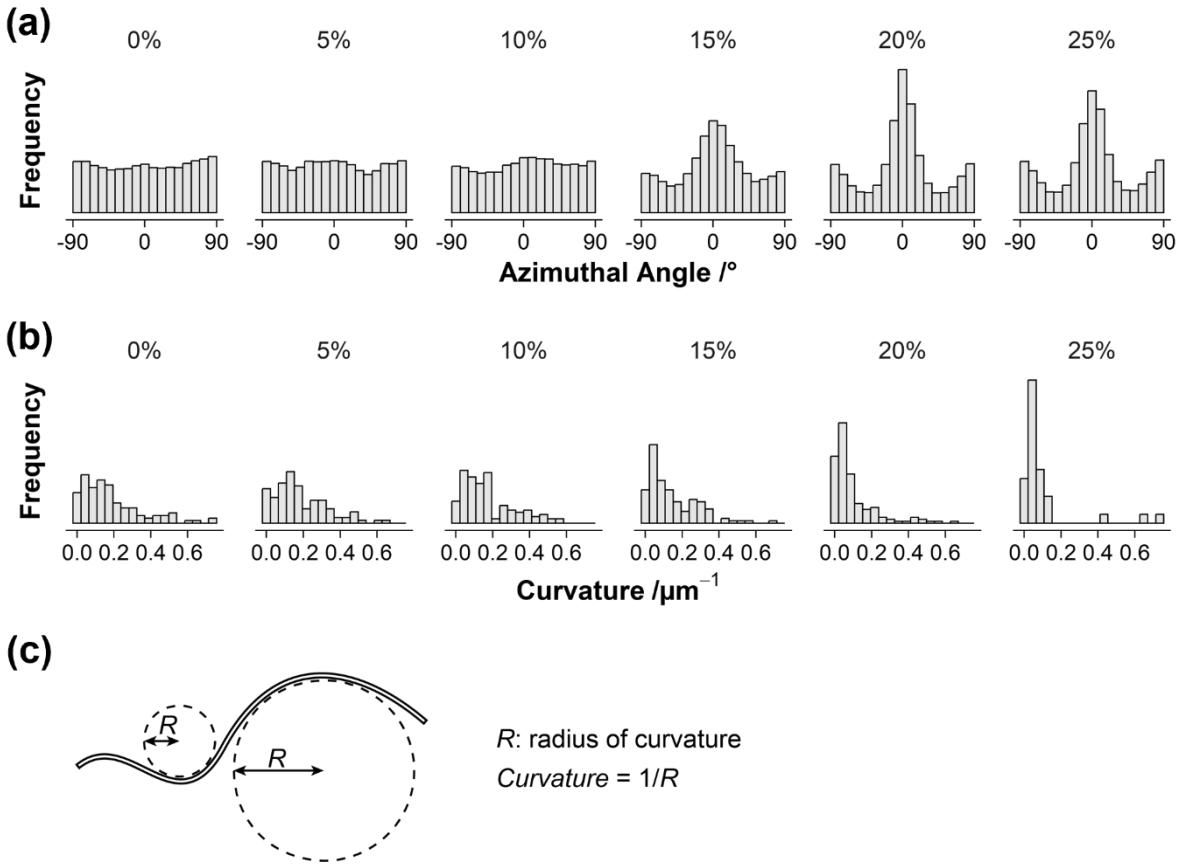

Fig. 1-3 Histograms of the (a) orientation angle and (b) curvature of fibers in hydrated BC pellicles under uniaxial tensile deformation obtained by fiber segmentation analysis. (c) Schematic diagram of the analysis of curvature. In (a), the reference angle for the azimuthal angle (= 0°) coincides with the tensile direction.

Stress relaxation

To investigate the viscoelastic properties of the BC pellicle under tensile deformation, static viscoelasticity was evaluated using stress relaxation measurements. Stress relaxation was observed under all strain conditions, with a large relaxation in the first tens of seconds, followed by a gradual relaxation before finally reaching the equilibrium elastic modulus (Fig. 1-4a) The relaxation time increased as the initial strain increased, and measurements took up to 24 h. The obtained relaxation moduli were fitted to a generalized Maxwell model, and the relaxation

spectra were calculated (Fig. 1-4b). The elastic modulus and relaxation time of typical peaks are listed in Table 1-2. There was an initial strain dependence in the relaxation spectra, and the relaxation mode corresponding to the maximum peak at approximately 1 s was observed under all strain conditions. This suggests that the same relaxation mode occurred first, independent of strain. However, at relaxation times longer than 1 s, a noticeable difference was observed at strains greater than 15%. For initial strains larger than 15%, a superposition of multiple relaxation modes was observed over a wide time range of 10^2–10^5 s. Therefore, with significant deformation, the initial rapid relaxation is followed by a continuous slow relaxation lasting several hours. Although the details of the higher-order relaxation phenomena that are prominent in large deformations are not known, the 1s relaxation phenomena commonly observed for all initial strain conditions can be attributed to the rupture of crosslink points and the rearrangement of segments, which are considered to be responsible for the observed relaxation. The cleavage of crosslink points involves the cleavage of crystalline junction zones between BC ribbons, which is considered to take longer than the cleavage of chemical crosslinks due to covalent bonds.

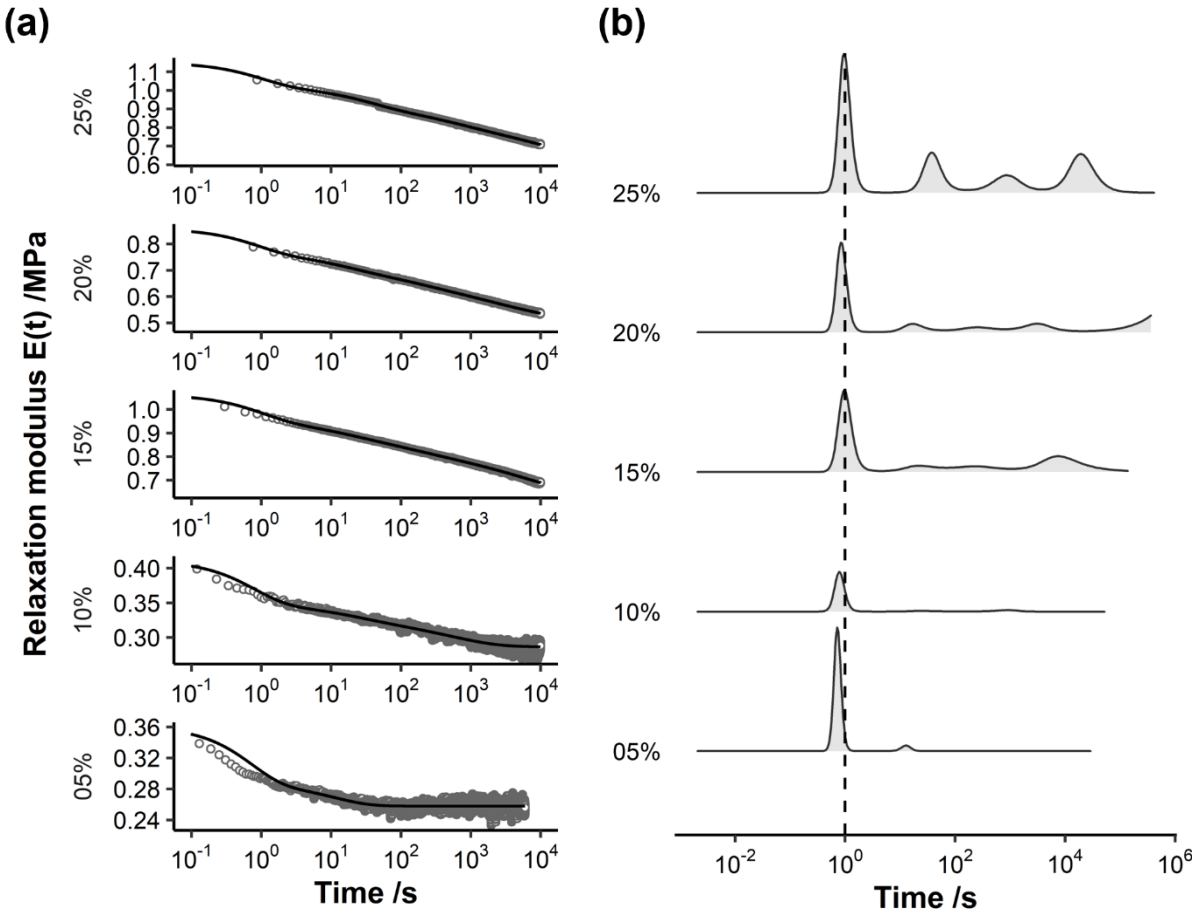

Fig. 1-4 (a) Stress relaxation of hydrated BC pellicles under tensile deformation. The measured relaxation moduli under various initial strains are plotted as points. The solid lines represent the relaxation curves obtained by fitting. Relaxation spectra of BC pellicles at different strains are shown on the logarithmic time scale (b). At all strains, the relaxation mode corresponding to the maximum peak at approximately t = 1 s (dashed line) was observed.

Table 1-2 Elastic moduli and relaxation times of characteristic peaks of the relaxation spectra obtained by fitting the measured relaxation moduli to the generalized Maxwell model.

Initial strain	Mode 1		Mode 2		Mode 3		Mode 4	
	E_1 /MPa	τ_1 /s	E_2 /MPa	τ_2 /s	E_3 /MPa	τ_3 /s	E_3 /MPa	τ_3 /s
5%	7.9×10^{-3}	7.2×10^{-1}	3.6×10^{-4}	1.3×10	-	-	-	-
10%	2.5×10^{-3}	7.8×10^{-1}	3.7×10^{-5}	2.4×10	9.0×10^{-5}	9.4×10^{2}	-	-
15%	5.2×10^{-3}	9.7×10^{-1}	4.0×10^{-4}	2.2×10	3.5×10^{-4}	2.4×10^{2}	-	-
20%	5.7×10^{-3}	8.3×10^{-1}	5.4×10^{-4}	1.7×10	3.2×10^{-4}	2.5×10^{2}	5.6×10^{-4}	3.1×10^{3}
25%	8.9×10^{-3}	9.6×10^{-1}	2.6×10^{-3}	3.8×10	1.1×10^{-3}	8.6×10^{2}	2.5×10^{-3}	1.9×10^{4}

Elongation recovery ratio

To examine the range of strain in which the pellicle behaves elastically, the elongation recovery ratios of the BC pellicle were measured. If the applied strain completely recovers to the pre-deformation state, the elongation recovery ratio is 100%, which is representative of elastic behavior. According to the results of the elongation recovery measurements of the pellicles, the recovery ratio was 70%–80% in the strain range of <10%, with a decrease to 20%–25% in the strain range of >20% (Fig. 1-5). In all strain ranges, the elongation recovery ratio was less than 95%, and complete recovery of strain was not observed. Strain recovery did not occur instantaneously but gradually over a period of 1 h or longer after the strain was released. Therefore, for BC pellicles under tensile deformation, elastic behavior is dominant at strains up to 10%, while plastic deformation without strain recovery becomes dominant as the strain increases.

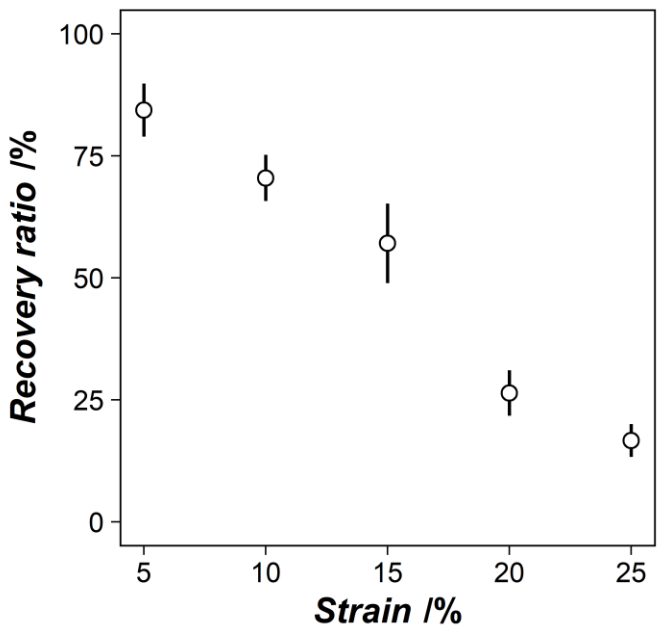

Fig. 1-5 Dependence of the elongation recovery ratio of hydrated BC pellicles on the magnitude of strain. White dots and error bars represent the mean value and standard error, respectively.

Discussion

Tensile deformation model

In this section, some assumptions of the tensile deformation model are discussed first and then a specific tensile deformation model is proposed and its validity is discussed. First, it is assumed that the cross-links are cleaved before the fibers break during deformation. This assumption is based on the following information. Cellulose nanofibrils exhibit a high longitudinal modulus (Young's modulus of 79−88 GPa) along the fiber axial direction, which coincides with the direction of molecular chains consisting of covalently bonded glucopyranose units (Tanpichai et al., 2012). These cellulose nanofibrils form bundles and branches to build the fiber network of BC pellicles. At the cross-linking points, cellulose fibers form crystalline junction zones via hydrogen bonds and van der Waals interactions, which are weaker than the covalent bonds in the molecular chain. Therefore, cross-link cleavage is considered to occur first,

rather than fiber rupture. On this basis, uniaxial tensile deformation of BC pellicles is considered to involve three processes that occur at the microscopic scale: fiber reorientation, fiber stretching, and cross-link cleavage (Fig. 1-6). With an applied strain, the fiber segments anchored in the network via cross-links undergo deformation through rotation and stretching (Fig. 1-6a, b). As a result, the spatial distance between the cross-linking points increases and the strain is resolved. When the applied strain exceeds the limit of elongational deformation via rotation and stretching, cross-link cleavage occurs (Fig. 1-6c). Once the cross-links are cleaved, stresses are concentrated at another cross-linking point on the fiber, creating a new stress loading path. This is similar to the concept of the sacrificial bond and hidden length in network polymers (Smith et al., 1999), which is the mechanism by which fiber segments hidden in the network become functional by cleavage of cross-links in response to deformation. The cycle of fiber rearrangement, fiber elongation, cross-link cleavage, and stress redistribution is considered the deformation mechanism of the fiber network.

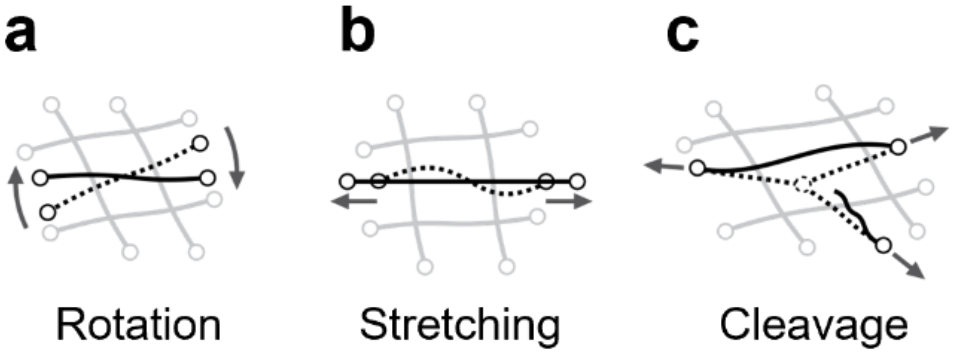

Fig. 1-6 (a−c) Schematic illustration of the processes occurring on the microscopic scale during tensile deformation. The white dots represent cross-linking points, and the lines represent fiber segments. In all cases, the distance between the cross-linking points is longer after the deformation. Fiber rearrangement involves cleavage of one cross-linking point (c), which leads to the formation of a new fiber segment that is longer than the original segment.

Based on the above discussion, the following tensile deformation model to explain the non-linear mechanical response of BC hydrogels are proposed (Fig. 1-7). First, in the range of 0%–2% strain, the tangent modulus is the lowest, which can be explained by the elimination of looseness in the fiber network. The randomly oriented fibers secreted by bacteria is considered to produce loose fiber networks, and the initial small strain stretches this looseness. The elongation recovery ratio indicates that deformation at this stage is reversible, and the fraction of deformation accompanied by the cleavage of cross-links is relatively small. In the range of 2%−12% strain, strain hardening and a linear increase in the tangent modulus is evident, and this can be explained by an increase in the number of stress paths due to axial orientation of the fiber network. The initially isotropic fiber network relieves the applied strain by rearranging the fibers along the tensile direction. However, during the rearrangement, stress is concentrated at relatively short fiber segments, manifested as straight and taut fibers in the CLSM images. The number of these stress paths increases as the strain increases. This is also seen in the analysis of the fiber segment curvature, specifically the curvature decreases with increasing strain. As orientation along the tensile direction continues, the number of stress paths along the tensile direction increases, leading to an increase in the tangent modulus. Next, in the strain region of 12%–25%, the tangent modulus is constant. From the *in situ* observation and segment orientation analysis, rearrangement of the fibers along the tensile direction is almost complete. Therefore, the tangent modulus is constant because the number of stress paths is constant. Because strain relief by angular reorientation does not proceed any further, deformation due to the cleavage of cross-links becomes dominant at this stage. Finally, in the region of 25%–30% strain, the tangent modulus decreases, and rupture of the sample occurs. This can be explained by an increase in fluidity due to a decrease in the number of cross-links and an increase in fibers with free ends.

The rupture occurs when continuity of the fiber network is locally lost in the specimen. Overall, these behaviors of the BC hydrogel under deformation are in good agreement with the simulated tensile response of athermal cross-linked fibrous materials (Broedersz & Mackintosh, 2014; Picu, 2020; Žagar et al., 2015). This indicates that the nanofiber network of BC hydrogels is athermal (enthalpic) rather than thermal (entropy), similar to those of typical semi-flexible fiber networks.

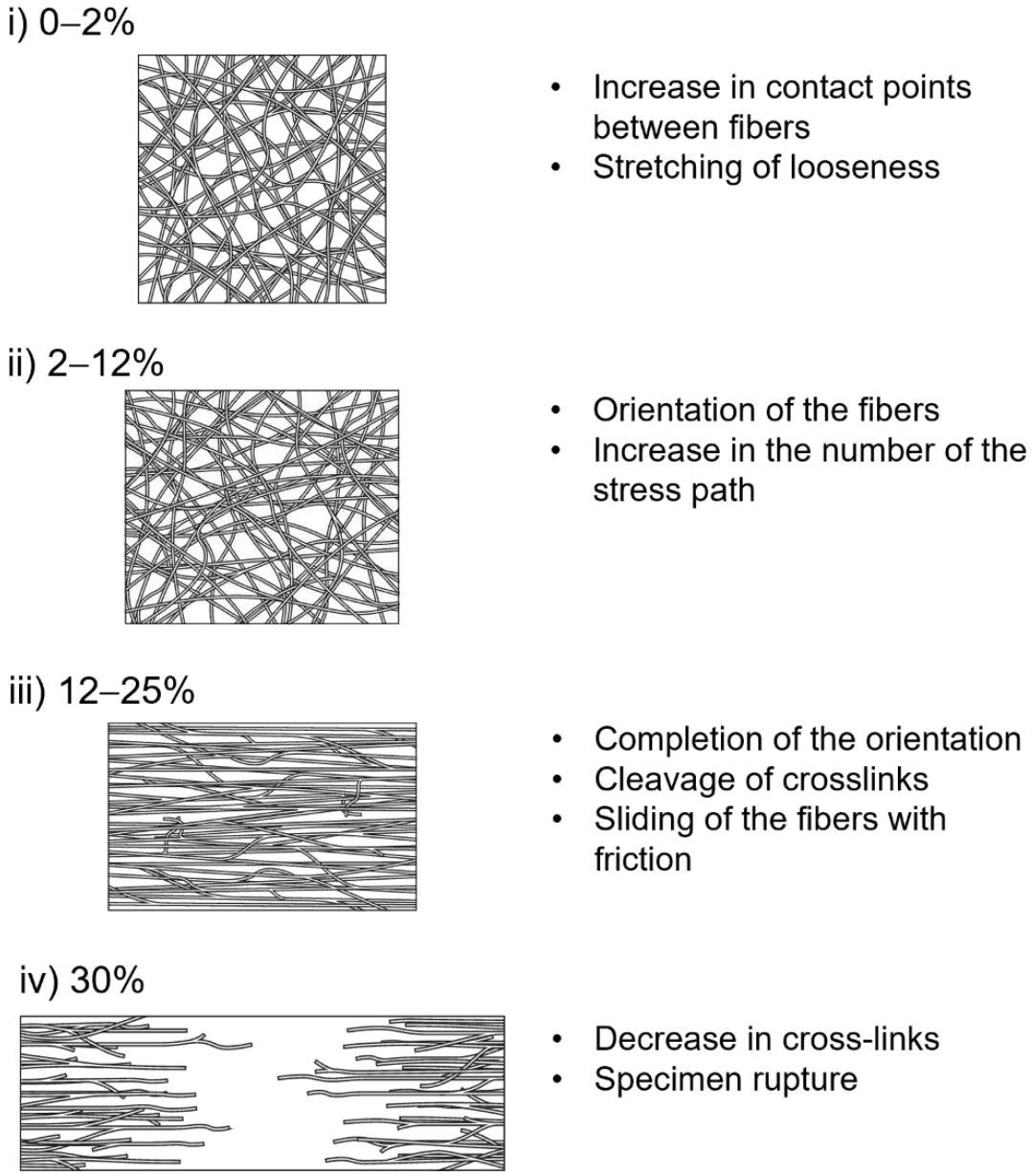

Fig. 1-7 Schematic diagram of the tensile deformation model of the fiber network over a wide range of strains. The tensile direction is horizontal.

Effect of water

During tensile deformation, it is necessary to consider the effect of water as a matrix in addition to the effect of the network. In the strain region of 0%−10%, the hydrated pellicles showed strain hardening, whereas the squeezed pellicles showed strain softening. *In situ*

observations indicated that fiber orientation along the tensile direction occurred in this region. In the hydrated state, the concentration of fiber segments per volume is relatively low (0.39 wt%) and the fibers exist independently. When 95 % of the free water in the network is drained out by squeezing, the distance between fibers shortens and the probability of entanglement during orientation increases. This may result in strain softening in the strain region of 0%−12%. After orientation is complete (strain region of 12%–30%), dehydration due to volume deformation has proceeded in the same manner as the hydrated pellicles and both hydrated and squeezed pellicles have the same stress–strain curve. This suggests that, unlike ordinary hydrogels, the number of water molecules bound to the surface per volume is low and most of the water in the BC pellicle is free water. In contrast, the dried pellicles show typical tensile deformation of nanocellulose films, i.e., the samples yield at a ~1% strain and then plastically deform, reaching rupture at 8% strain. Therefore, interactions between cellulose nanofibrils are dominant in the dehydrated state. The freeze-dried sample behaved similarly to the oven-dried sample up to the yield point around 1%, after which it broke without softening. The freeze-dried samples are considered to maintain the original fiber network structure to some extent. The absence of water is thought to cause friction between cellulose fibers, limiting network rearrangement and leading to premature rupture. This result indicates that the microstructure of the fiber network has a larger effect on the physical properties of the hydrogel in the hydrated state than in the dehydrated state.

Plasticity

There are fewer reports on the plasticity of BC pellicles than on the viscoelasticity. The results of elongation recovery ratio measurements clearly showed the coexistence of plasticity and elasticity in BC pellicles. In fact, the rate of plastic deformation tended to increase in proportion to the magnitude of the strain. This plasticity can be explained by the irreversible

deformation accompanied by the cleavage of cross-links. The elasticity of the network, which allows elongation recovery, is due to the residual stress, observed as E_∞ in the stress relaxation test. Considering that strain recovery was not instantaneous but occurred slowly over several hours, it is likely that the mechanism of strain recovery involves not only the elasticity of the fiber network, but also the swelling of the network caused by water. These results indicate that it is necessary to consider not only the viscoelasticity of the fiber network, but also the plasticity due to the irreversible rupture of cross-links.

Relaxation spectrum

The relaxation spectra obtained from stress-relaxation measurements provide information on the characteristic relaxation modes arising from the tensile deformation of BC pellicles. The relaxation spectra were characterized by a relaxation mode at approximately 1 s, which was common under all strain conditions, and other relaxation modes at 10^2 to 10^5 s, which occurred under strains greater than 15%. These relaxation modes can be explained by first- and higher-order rearrangements during the relaxation of the network. First, in a cross-linked fiber network, relaxation based on rotation, bending, and elongation of individual fiber segments is restricted. Therefore, a possible relaxation mechanism is elongation of the effective segment length (Fig. 1-6c), which occurs when one cross-link is cleaved, leading to the formation of a new longer segment with the next cross-link on the fiber. Rearrangement of the fiber network and cleavage of cross-links occur simultaneously in the first 1 s (first-order relaxation). However, if the initial strain is large (>15%), this rearrangement is insufficient for complete relaxation. In this case, the same relaxation behavior is repeated intermittently (higher-order relaxation). The long relaxation time of higher-order relaxation can be explained by the increase in the effective segment length between cross-linking points. The time required for higher-order relaxation is longer because the

actual segment length is longer due to the cleavage of cross-links during the first-order relaxation. Therefore, the relaxation time increases, resulting in a broad relaxation peak over a long period of time. In addition, the increase in the frictional force between fibers due to the densification of the fiber network by stretching might contribute to the increase in the relaxation time. The nonlinear behavior observed in the tensile deformation of BC pellicles is explained by these relaxation modes of the fiber network.

Conclusion

In this chapter, the response of BC pellicles to tensile deformation on the microscopic scale was elucidated. First, tensile deformation of the pellicle was classified into four characteristic regions on the basis of changes in the tangent modulus from tensile tests. Next, changes in the orientation and curvature were quantitatively evaluated using microscopic images of the fiber network under tensile deformation, and accordingly a tensile deformation model was proposed. In addition, accumulation of stress on fiber segments was directly visualized. Furthermore, characteristic relaxation spectra were obtained from stress-relaxation measurements to understand the rearrangement of fiber segments with the cleavage of cross-links as the main relaxation mode. These results demonstrate that the physical properties of BC pellicles are determined by the cross-link structure of the fiber network rather than by the stiffness of the fibers or the density of the fibers. By adjusting the cross-link density, the physical properties of BC pellicles can be controlled. Therefore, elucidation of the cross-link structure and cross-link formation mechanism is expected to facilitate synthetic biology using BC pellicles.

References

Astley, O. M., Chanliaud, E., Donald, A. M., & Gidley, M. J. (2003). Tensile deformation of bacterial cellulose composites. *International Journal of Biological Macromolecules*, *32*(1–2), 28–35. https://doi.org/10.1016/S0141-8130(03)00022-9

Babi, M., Fatona, A., Li, X., Cerson, C., Jarvis, V. M., Abitbol, T., & Moran-Mirabal, J. M. (2021). Efficient Labeling of Nanocellulose for High-Resolution Fluorescence Microscopy Applications. *Biomacromolecules*, *23*, 1981–1994. https://doi.org/10.1021/acs.biomac.1c01698

Bäckdahl, H., Helenius, G., Bodin, A., Nannmark, U., Johansson, B. R., Risberg, B., & Gatenholm, P. (2006). Mechanical properties of bacterial cellulose and interactions with smooth muscle cells. *Biomaterials*, *27*(9), 2141–2149. https://doi.org/10.1016/j.biomaterials.2005.10.026

Broedersz, C. P., & Mackintosh, F. C. (2014). Modeling semiflexible polymer networks. *Reviews of Modern Physics*, *86*(3), 995–1036. https://doi.org/10.1103/RevModPhys.86.995

Brown, E. E., Laborie, M. P. G., & Zhang, J. (2012). Glutaraldehyde treatment of bacterial cellulose/fibrin composites: Impact on morphology, tensile and viscoelastic properties. *Cellulose*, *19*(1), 127–137. https://doi.org/10.1007/s10570-011-9617-9

Chen, S. Q., Lopez-Sanchez, P., Wang, D., Mikkelsen, D., & Gidley, M. J. (2018). Mechanical properties of bacterial cellulose synthesised by diverse strains of the genus Komagataeibacter. *Food Hydrocolloids*, *81*, 87–95. https://doi.org/10.1016/j.foodhyd.2018.02.031

Frensemeier, M., Koplin, C., Jaeger, R., Kramer, F., & Klemm, D. (2010). Mechanical properties of bacterially synthesized nanocellulose hydrogels. *Macromolecular Symposia*, *294*(2), 38–

44. https://doi.org/10.1002/masy.200900030

Gao, X., Shi, Z., Kušmierczyk, P., Liu, C., Yang, G., Sevostianov, I., & Silberschmidt, V. V. (2016). Time-dependent rheological behaviour of bacterial cellulose hydrogel. *Materials Science and Engineering C*, *58*, 153–159. https://doi.org/10.1016/j.msec.2015.08.019

Gao, X., Shi, Z., Liu, C., Yang, G., Sevostianov, I., & Silberschmidt, V. V. (2015). Inelastic behaviour of bacterial cellulose hydrogel: In aqua cyclic tests. *Polymer Testing*, *44*, 82–92. https://doi.org/10.1016/j.polymertesting.2015.03.021

Guhados, G., Wan, W., & Hutter, J. L. (2005). Measurement of the elastic modulus of single bacterial cellulose fibers using atomic force microscopy. *Langmuir*, *21*(14), 6642–6646. https://doi.org/10.1021/la0504311

Hestrin, S., & Schramm, M. (1954). Synthesis of cellulose by Acetobacter xylinum 2. Preparation of freeze-dried cells capable of polymerizing glucose to cellulose. *The Biochemical Journal*, *58*(2), 345–352. https://doi.org/10.1042/bj0580345

Hsieh, Y. C., Yano, H., Nogi, M., & Eichhorn, S. J. (2008). An estimation of the Young's modulus of bacterial cellulose filaments. *Cellulose*, *15*(4), 507–513. https://doi.org/10.1007/s10570-008-9206-8

McKenna, B. A., Mikkelsen, D., Wehr, J. B., Gidley, M. J., & Menzies, N. W. (2009). Mechanical and structural properties of native and alkali-treated bacterial cellulose produced by Gluconacetobacter xylinus strain ATCC 53524. *Cellulose*, *16*(6), 1047–1055. https://doi.org/10.1007/s10570-009-9340-y

Nishino, T., Takano, K., & Nakamae, K. (1995). Elastic modulus of the crystalline regions of cellulose polymorphs. *Journal of Polymer Science Part B: Polymer Physics*, *33*(11), 1647–1651. https://doi.org/10.1002/polb.1995.090331110

Picu, C. R. (2020). Mechanics of Random Fiber Networks: Structure–Properties Relation. In *CISM International Centre for Mechanical Sciences, Courses and Lectures* (Vol. 596, pp. 1–61). Springer International Publishing. https://doi.org/10.1007/978-3-030-23846-9_1

Schindelin, J., Arganda-Carreras, I., Frise, E., Kaynig, V., Longair, M., Pietzsch, T., Preibisch, S., Rueden, C., Saalfeld, S., Schmid, B., Tinevez, J. Y., White, D. J., Hartenstein, V., Eliceiri, K., Tomancak, P., & Cardona, A. (2012). Fiji: An open-source platform for biological-image analysis. *Nature Methods*, *9*(7), 676–682. https://doi.org/10.1038/nmeth.2019

Shanbhag, S. (2019). pyReSpect: A Computer Program to Extract Discrete and Continuous Spectra from Stress Relaxation Experiments. *Macromolecular Theory and Simulations*, *28*(3), 1–10. https://doi.org/10.1002/mats.201900005

Smith, B. L., Schaffer, T. E., Viani, M., Thonpson, J. B., Frederick, N. A., Kindt, J., Belcher, A., Stucky, G. D., Morse, D. E., & Hansma, P. K. (1999). Molecular mechanistic origin of the toughness of natural adhesives, fibres and composites. *Nature*, *399*, 761–763. www.nature.com

Tanpichai, S., Quero, F., Nogi, M., Yano, H., Young, R. J., Lindström, T., Sampson, W. W., & Eichhorn, S. J. (2012). Effective young's modulus of bacterial and microfibrillated cellulose fibrils in fibrous networks. *Biomacromolecules*, *13*(5), 1340–1349. https://doi.org/10.1021/bm300042t

Xu, T., Vavylonis, D., Tsai, F. C., Koenderink, G. H., Nie, W., Yusuf, E., Lee, I. J., Wu, J. Q., & Huang, X. (2015). SOAX: A software for quantification of 3D biopolymer networks. *Scientific Reports*, *5*(9081), 1–10. https://doi.org/10.1038/srep09081

Žagar, G., Onck, P. R., & Van Der Giessen, E. (2015). Two fundamental mechanisms govern the stiffening of cross-linked networks. *Biophysical Journal*, *108*(6), 1470–1479.

https://doi.org/10.1016/j.bpj.2015.02.015

Chapter 2

Quantitative Evaluation of

Fiber Network Structure–property Relationships

Introduction

Precise control of the material properties is crucial for the material application of BC pellicles, and the development of evaluation methods for the network structure that characterizes these properties is indispensable. Although many studies have been conducted to develop a functional material comprising a BC pellicle, fundamental quality control problems still remain. In many cases, BC pellicles are expected to exhibit suitable mechanical properties when they are used as scaffold materials. In other words, this requires reproducibility and precise control of their physical properties. However, materials produced by living organisms are often subject to variation because of the complex and multifaceted production processes. In fact, cellulose production by *Komagataeibacter* bacteria also depends greatly on the bacterial strain and the culture environment (Chen et al., 2018; Czaja et al., 2004; Kaczmarek et al., 2022; Lee et al., 2015; Machado et al., 2016; Nagashima et al., 2016; Numata et al., 2019; Singhsa et al., 2018). Furthermore, even the same strain of bacteria often differs in its cellulose production depending on the production lot. Consequently, the physical properties of the resulting BC pellicles greatly

vary. Then, the breaking strengths of hydrated pellicles vary from 0.15 to 0.95 MPa (E. E. Brown et al., 2012; Chen et al., 2018). Such variation in mechanical properties is considered a critical problem for the design and quality control of BC pellicles. Therefore, it is necessary to elucidate the structure–property relationship in fiber networks of BC pellicles and develop a method for predicting them.

Considering typical polymer gels, their entropic elasticity is derived from the characteristic thermal fluctuation of molecular chains, and their physical properties are explained by the classical network theory (James & Guth, 1943; Kuhn, 1936). In this theory, the elasticity of the gel is described by the number of crosslinked segments in the network. However, it is unclear whether this molecular theory is applicable to BC hydrogels consisting of nano-sized fiber networks. In the case of semiflexible cellulose nanofibrils, the influence of entropic elasticity derived from thermal fluctuations is expected to be small, whereas the influence of energy elasticity derived from bending and tensile deformation of the fibril is expected to be relatively large. Because of these characteristics, many open questions remain regarding the mechanisms underlying the mechanical properties of BC pellicles. Regarding the physical properties of BC pellicles, Tanpichai et al. reported that the elastic modulus of a single BC ribbon was 79–88 GPa (Guhados et al., 2005; Hsieh et al., 2008; Tanpichai et al., 2012). On the other hand, other researchers have reported that the elastic moduli of BC pellicles in the hydrated state vary greatly from 1.1 to 13 MPa and the breaking strength from 0.15 to 0.93 MPa (E. E. Brown et al., 2012; Chen et al., 2018; McKenna et al., 2009). These data imply that not only the cellulose content but also the way the BC ribbons assemble into the BC pellicle has a significant impact on its physical properties. Therefore, it is necessary to experimentally clarify the

relationship between the number of crosslinks, which is an essential parameter for describing network structures, and the physical properties of BC hydrogels, in addition to cellulose content.

The objective described above requires the establishment of a quantitative evaluation method. In general, investigation of the network structure of BC pellicles is often performed by scanning electron microscopy (SEM). However, such evaluations of 3D fiber networks based on SEM observation are still skeptical for the following reasons: First, quantitative structural evaluation is difficult with the two-dimensional projection images obtained by SEM. Second, observation in the depth direction is limited. Thirdly, dehydration is required for sample preparation, which often causes structural changes to the fiber network (Clasen et al., 2006), thereby hindering a detailed understanding of the network structure.

It may be possible to solve these problems by exploiting techniques used in the field of cell biology, in which the structural analyses of nano-sized biopolymer networks such as cytoskeletons are performed (Özdemir & Reski, 2021). Three-dimensional fiber segmentation analysis has been developed for this purpose. It can be used to extract and analyze fiber structures from 3D fluorescence images (Xu et al., 2015). The technique is also applicable to the structural analysis of BC ribbons of the same order of size as cytoskeletons (Mohan et al., 2017; Takahama et al., 2022). The authors successfully employed this technique to visualize the micro-mechanism underlying the tensile deformation of BC pellicles, as described in chapter 1 (Takayama & Kondo, 2023).

The structural heterogeneity of a BC pellicle due to biological factors is also a disadvantage when attempting to experimentally prove a correlation between its fiber network and its mechanical properties. Unlike polymer gels, BC pellicles secreted by living organisms have intrinsic heterogeneity. For example, there is a gradient in fiber density from bottom to top

in pellicles cultured under normal static conditions (Jacek et al., 2021). This heterogeneity can be attributed to the fact that the bacterial density and nutrient environment changes over time during the long incubation period of 2–4 weeks. Therefore, minimizing changes during culture is likely to ensure a relatively uniform pellicle. For example, the bacteria may be cultured at a high density from the beginning, and/or the pellicle may be harvested within a short period.

This chapter comprises an investigation of the relationships between nanofibril network structures and their physical properties in BC pellicles. Various pellicles with different properties were prepared, and their 3D data were obtained by confocal microscopy to quantitatively evaluate the structure of the fiber network and determine their relationships with the mechanical properties. The measured crosslink density well explained the nonlinear mechanical response of BC pellicles in tensile tests and their breaking strength. These findings will inform the precise design of materials based on BC pellicles, the prediction of their physical properties, and the accompanying quality control strategies.

Materials and methods

Materials

The bacterial strains *Komagataeibacter hansenii* ATCC53582 and *K. hansenii* ATCC23769 were purchased from the American Type Culture Collection (VA, USA). Strains *K. hansenii* NBRC14816, *K. hansenii* NBRC105051, *K. xylinus* NBRC13693, *K. xylinus* NBRC16644, and *K. xylinus* NBRC16682 were purchased from the National Institute of Technology and Evaluation (Tokyo, Japan). Bacto™ peptone and Bacto™ yeast extract were purchased from Difco Laboratories Inc. (Franklin Lakes, New Jersey, USA). Glucose, cellulase (Celluclast® 1.5 L), and Fluorescent Brightener 28 (FB28; also known as Calcofluor White

M2R) were purchased from Sigma Aldrich (St. Louis, Missouri, USA). Disodium hydrogen phosphate heptahydrate ($Na_2HPO_4 \cdot 7H_2O$) was purchased from Nacalai Tesque Inc. (Kyoto, Japan). Citric acid was purchased from Wako Pure Chemical Inc. (Osaka, Japan).

Preparation of the BC pellicles

Seven strains of *Komagataeibacter* bacteria with different cellulose production capabilities were selected and cultured to prepare pellicles of diverse morphology according to our previous report (Takayama & Kondo, 2023). A high-density and short-duration culture method was applied to ensure uniform BC pellicles. First, suspension culture was performed by inoculating a seed culture of the bacteria into a 300 mL baffled flask containing 100 mL of Hestrin & Schramm (HS) medium (Hestrin & Schramm, 1954), then incubating the culture at 30°C while subjecting it to continuous rotary shaking (125 rpm). To prevent cellulose aggregation, 0.1 v/v% cellulase (Celluclast® 1.5 L) was added to the culture medium. The suspension culture was continued until the turbidity (optical density at the wavelength of 600 nm, OD_{600}) of the cell suspension reached 1.0–1.8. The obtained thick cell suspension was then centrifuged (3600 × *g*, 5 min) and the bacteria were collected as a pellet. The collected pellets were resuspended in a small amount of fresh HS medium prior to inoculation. During inoculation, the concentration of the bacteria was adjusted to maintain a constant concentration (OD_{600} = 0.6). Finally, static culture was carried out at 30°C using a 10 cm diameter petri dish containing 20 mL of HS medium to produce BC pellicles. The pellicles were harvested when they were approximately 1 mm thick (12–24 h), purified by washing with ultrapure water and treated with 0.1 w/v% NaOH solution at 80°C for 4 h. Samples of conventional culture conditions (initial OD_{600} = 0.1, culture period = 72 h, ATCC53582) were also prepared for comparison with the

special culture method. To avoid batch-to-batch variation, pellicles were prepared from the same batch of each strain. Specifically, for each strain, cell suspensions pre-cultured in a single flask were inoculated into 10 Petri dishes. From these pellicles, samples were randomly selected to prepare test specimens for subsequent experiments. To minimize any effects from compression during sample preparation, all test specimens were allowed to leave in water for at least one day after cutting before being used for various measurements.

Basic characterization of the BC pellicles

As a basic characterization, the cellulose content of the pellicle was determined (Takayama & Kondo, 2023). Samples for the measurements were prepared by cutting the pellicles into disks (18 mm in diameter) and the wet weight was measured. The dry weight of each sample was measured after heating it in an oven at 100°C for 24 h. The cellulose content of each sample was then calculated as follows: *cellulose content* (%) = *dry weight* (mg) / *wet weight* (mg) × 100. The results from three samples were averaged for each strain.

The morphologies of the BC ribbons were analyzed by atomic force microscopy (AFM). The pellicles were cut into 10 mm squares and placed on a glass slide with the top side (air side) of the pellicle facing up. The samples were then dried at 100°C for 3 h. Finally, the dried samples were investigated by AFM (MFP-3D SA; Asylum Research, Santa Barbara, California, USA). The AFM investigations were performed in tapping mode under ambient conditions. OMCL-AC240TS (spring constant = 2 N/m, resonant frequency = 70 kHz; Olympus Co., Tokyo, Japan) was used as the cantilever. Each sample (area 4.0 μm × 4.0 μm) was scanned at a rate of 1.0 Hz. Considering the flat cross-sectional shape of the BC ribbons, the height, width, and cross-sectional area of each BC ribbon were evaluated based on the height images obtained from

AFM. Gwyddion, an open-source software for scanning probe microscopy data analysis (Nečas & Klapetek, 2012), was used for AFM data analysis and processing. The width and length of each BC ribbon were measured according to the method described previously (Yamanaka & Sugiyama, 2000). Specifically, a line profile perpendicular to the fiber axis was obtained at a point where the fibers overlapped. From the line profile, the height of the upper fiber was obtained by subtracting the height of the lower fiber as a baseline. The width of the fiber was obtained by correcting the tip convolution effect according to a method described previously (Canet-Ferrer et al., 2014; Tsuji et al., 2021). Assuming that the cross-sectional shape of the fiber was rectangular, the cross-sectional area of the fiber was calculated from the height and width values. Three different points in the sample were scanned and ninety-six fibers were averaged for each strain.

Fourier transform infrared (FT-IR) spectra of BC pellicles were measured using FT-IR 6700 (JASCO, Tokyo, Japan). Samples for FT-IR measurements were prepared by drying BC pellicles on polyethylene terephthalate substrates to cast thin films. The measurements were performed in transmission mode at a resolution of 2 cm^{-1} with 16 scans. All the obtained spectra were normalized based on the absorption intensity at 1162 cm^{-1}.

Quantitative analysis of the fiber networks

The 3D data pertaining to the fiber networks in the BC pellicles were obtained using a confocal laser scanning microscope (CLSM). Prior to the investigations, cross-sectional observations were made to evaluate the uniformity of the internal structure of the BC pellicles. For fluorescent imaging, the pellicles were immersed in a 20 μg/mL aqueous solution of Fluorescent Brightener 28 (FB28) and left overnight at 25°C. After dyeing, the samples were

washed thoroughly with ultrapure water. The stained samples were embedded in a 4% agar solution and allowed to soak for 3 hours before being solidified. Subsequently, transverse sections were prepared by sectioning the agar-embedded samples with a razor blade (Fig.1 and Fig. S2a-c). The sections were examined under a TCS SP8 CLSM (Leica Microsystems, Wetzlar, Germany) equipped with a ×100 objective lens (HCX PL APO ×100/1.40, Leica Microsystems, Wetzlar, Germany). The pinhole size for confocal imaging was set at 1.0 Airy Unit (110 μm). The excitation and emission wavelengths for the fluorescence investigations were set to 405 nm and 415–470 nm, respectively. To evaluate the uniformity of the internal structure, sections were scanned in the height direction of the pellicle and the position dependence of fluorescence intensity was analyzed (Fig. 2-1, right). For each bacterial strain, three sections were prepared, and data were obtained from at least three different regions.

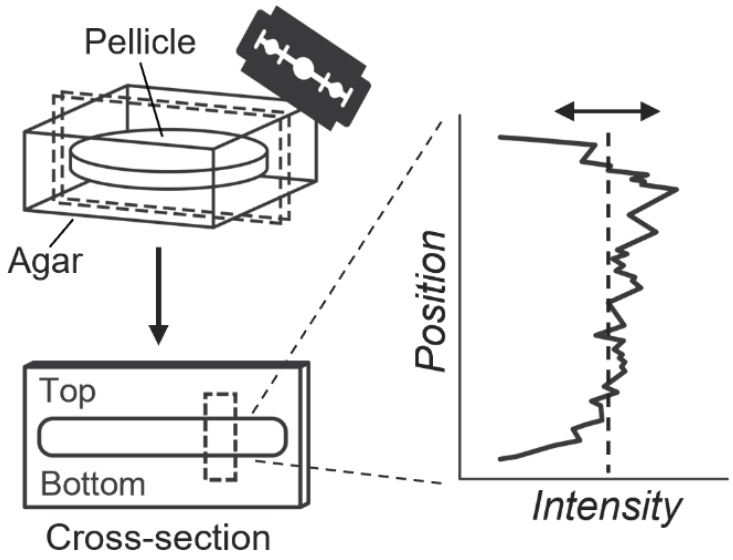

Fig. 2-1. Schematic illustration for the preparation of transverse sections of pellicles (left), followed by the analysis of fluorescence intensity distribution along the height direction (right).

To observe the fiber networks, samples were stained using the same procedure described above, but without agar embedding. At a depth of 5–10 μm from the top surface of the pellicle, a 15 μm × 15 μm × 5 μm region was scanned at a resolution of 512 pixels × 512 pixels × 47 frames (28 nm × 28 nm ×110 nm in voxel size). For each bacterial strain, three samples were prepared, and data were collected from at least 12 different regions. Fiber segmentation analyses of the 3D fluorescence images of the pellicles were carried out to quantitatively evaluate the fiber networks as follows (Mohan et al., 2017): The images were deconvoluted using Huygens Professional (Scientific Volume Imaging, Hilversum, Netherlands). A theoretical point spread function was applied as a deconvolution parameter. Further processing, i.e., luminance normalization, smoothing with a Gaussian blur filter, and resizing to 256 pixels × 256 pixels, was conducted using ImageJ Fiji software (Schindelin et al., 2012). The preprocessed images were submitted to SOAX, which is software for the quantification of 3D fiber networks (Xu et al., 2015). SOAX extracts the fiber structure from the 3D brightness distribution. As hyperparameters for SOAX analysis, the ridge threshold and stretch factor were set to 0.01 and 0.1, respectively. Under the above conditions, the fiber segmentation analysis was performed, and the 3D coordinates of the fiber segments were obtained. Using these coordinates, the crosslinking point was detected as a point where the fibers became closer than a certain distance from each other. The value of the crosslink density (crosslinking points per volume) was obtained by counting the number of such crosslinking points.

Determination of the mechanical properties of the BC pellicles

The mechanical properties of the samples were evaluated by tensile testing, as reported previously (Takayama & Kondo, 2023). The samples were prepared by cutting the BC pellicles

into dumbbell-shaped test pieces (ISO 37-4) using a dumbbell cutter (Super-Dumbbell Co., Ltd, Saitama, Japan). The thickness of each sample was measured using digital calipers (OMV-25MX; Mitutoyo, Kanagawa, Japan). For each strain, the thicknesses of at least five samples were measured and the average thickness was used.

The prepared test pieces were subjected to a tensile testing machine (STA-1250, A&D, Tokyo, Japan) equipped with a 50N load cell and manual tensile grips (J-UF2-50N, A&D, Tokyo, Japan). To prevent the sample from slipping, sandpaper was glued to the clamps. The sample was set by sandwiching both ends of the specimen between small pieces of wet filter paper. The distance between the clamps was set at 12 mm. To eliminate any sagging of the sample, a tension of 5 mN was applied to the sample before starting the measurement. The value of the crosshead displacement was adopted as the strain, The error between the actual strain of the specimen and the crosshead displacement was less than a few percent (< 3%). Ten measurements were performed on each of the seven BC pellicles. From the obtained stress–strain curves, the apparent elastic moduli, breaking strength, and extensibility are calculated. Previous research on tensile testing of BC pellicles has indicated that their stress–strain curves display non-linearity (McKenna et al., 2009). In stress–strain curves with non-linearity, the elastic modulus depends on the magnitude of the strain. In the present study, the apparent elastic modulus is calculated as the slope in the region of 60–90% of the maximum stress, avoiding the region of small strain where the nonlinearity is significant.

Statistical analysis

Statistical analyses and data visualizations were performed using R statistical analysis software (R Core Team, 2021). To examine the relationships among the various parameters,

correlation analysis was carried out by calculating the Pearson product-moment correlation coefficients. Multiple comparisons were made using the Steel-Dwass test for the AFM analysis results and the Tukey-Kramer test for the other experimental results. The significance level is set at 5%.

Results

Tensile properties of BC pellicles

BC pellicles with various properties were prepared by culturing seven different strains of *Komagataeibacter* bacteria. Tensile tests were carried out to evaluate the mechanical properties of the BC pellicles. Pellicles, which are composed of nanofiber networks, show a nonlinear tensile deformation behavior including plastic deformation due to rearrangement of its fiber networks (Astley et al., 2003; Takayama & Kondo, 2023). The stress–strain curves of various pellicles obtained by tensile testing are shown in Fig. 2-2a. The values of tensile mechanical properties were within the range of the previously reported values, and the variation is observed among the strains (Table 2-1). In terms of stress–strain curves, some samples showed significant strain hardening (e.g., ATCC23769, ATCC53582), whereas others did not (e.g., NBRC16644, NBRC16682). The log–log plots of stress–strain curves showed linear relationships and obeyed the power law ($\sigma = C \times \varepsilon^{\alpha}$, α: scaling exponent, C: intercept), as shown in Fig. 2-2b. The scaling exponents α obtained by fitting the power function were in the range of 0.93–1.87 (Table 2-1), indicating that the exponents were dependent on bacterial strains. A scaling exponent of 1 indicates a perfectly linear response ($\sigma = C \times \varepsilon^{1}$), while a power exponent greater than 1 is nonlinear and implies strain hardening.

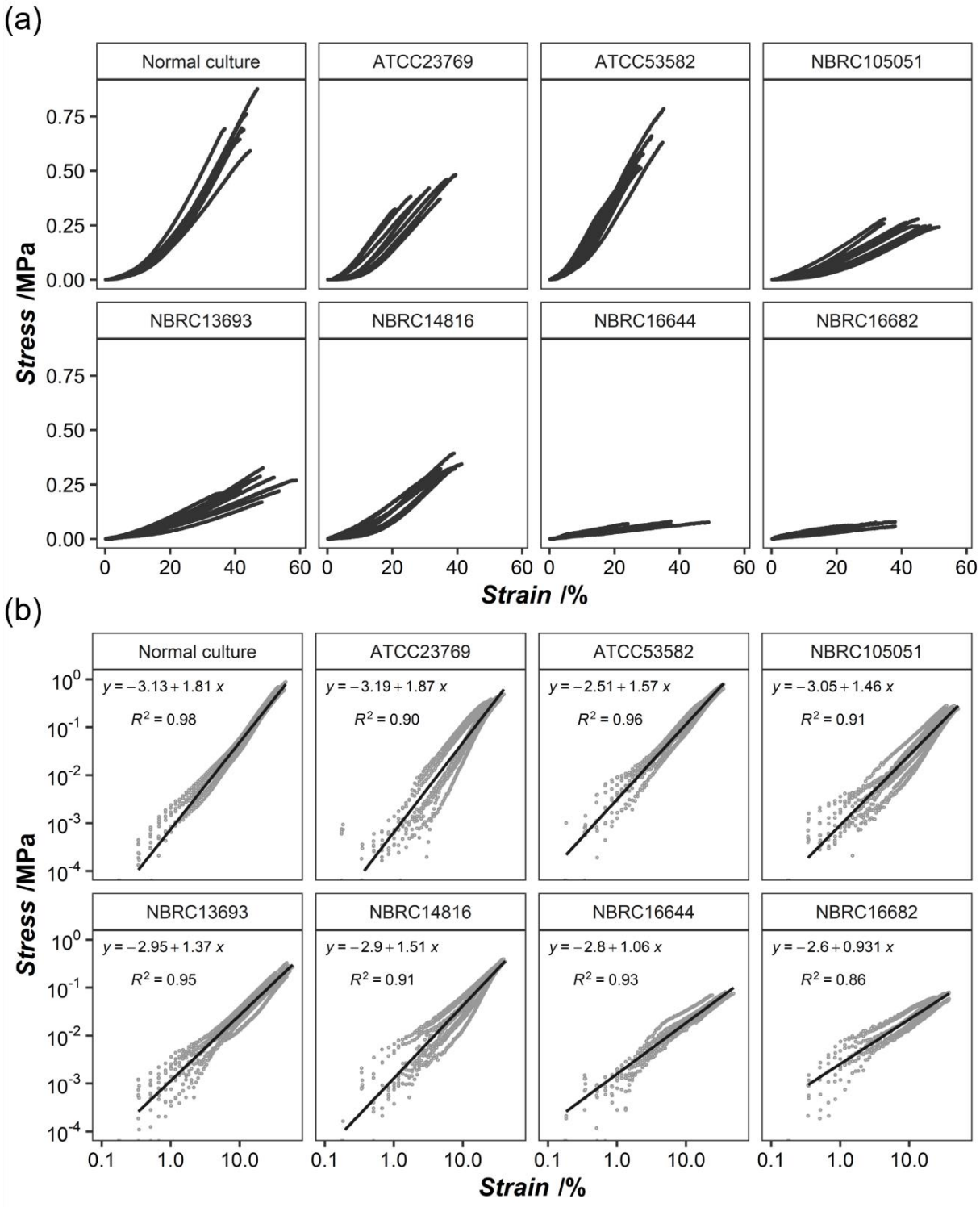

Fig. 2-2 (a) Stress–strain curves of pellicles produced by various bacterial strains and (b) their log–log plots. The lines in (b) represent the regression lines. The regression equations and R^2 values are shown in the plots.

Table 2-1 Results of tensile testing and basic characterization of bacterial cellulose pellicle produced by different strains (Mean values ± standard errors). Superscripts attached to the values indicate significant differences in multiple comparison tests at a significance level of 0.05%.

Bacterial strain	Cellulose content (w/w%)	Fiber height (nm)	Fiber width (nm)	Fiber cross-sectional area (nm^2)	Crosslink density ($10^8/m^3$)	Elastic modulus (MPa)	Strength (MPa)	Breaking strain (%)	Scaling exponent
K. hansenii ATCC23769	0.44 ± 0.02^{ab}	11.3 ± 0.5^{c}	64.6 ± 2.3^{c}	781 ± 50^{bc}	12.0 ± 0.6^{a}	1.79 ± 0.08^{b}	0.39 ± 0.02^{c}	29.5 ± 2.2^{cd}	1.87
K. hansenii ATCC53582	0.30 ± 0.03^{bc}	14.4 ± 0.7^{ab}	92.6 ± 4.0^{a}	1411 ± 109^{a}	10.2 ± 0.2^{ab}	2.66 ± 0.08^{a}	0.60 ± 0.03^{b}	28.4 ± 1.3^{d}	1.57
K. hansenii NBRC105051	0.38 ± 0.02^{b}	11.4 ± 0.5^{c}	62.4 ± 2.1^{c}	773 ± 63^{c}	9.1 ± 0.5^{bc}	0.84 ± 0.03^{d}	0.24 ± 0.04^{d}	37.0 ± 1.8^{abc}	1.46
K. xylinus NBRC13693	0.60 ± 0.06^{a}	14.8 ± 0.6^{a}	65.2 ± 2.0^{c}	1049 ± 73^{abc}	7.9 ± 0.7^{cd}	0.71 ± 0.05^{d}	0.25 ± 0.05^{d}	44.2 ± 1.9^{a}	1.37
K. hansenii NBRC14816	0.45 ± 0.02^{ab}	12.8 ± 0.6^{abc}	76.9 ± 2.1^{ab}	1041 ± 60^{ab}	7.1 ± 0.3^{d}	1.27 ± 0.06^{c}	0.32 ± 0.02^{cd}	32.0 ± 1.2^{bc}	1.51
K. xylinus NBRC16664	0.39 ± 0.09^{b}	11.6 ± 0.7^{c}	76.3 ± 2.2^{ab}	965 ± 70^{bc}	7.1 ± 0.2^{d}	0.22 ± 0.02^{e}	0.07 ± 0.00^{e}	30.0 ± 2.4^{bd}	1.06
K. xylinus NBRC16682	0.17 ± 0.02^{c}	11.7 ± 0.6^{bc}	73.9 ± 3.1^{bc}	944 ± 69^{bc}	6.2 ± 0.3^{d}	0.20 ± 0.01^{e}	0.06 ± 0.00^{e}	26.2 ± 2.1^{d}	0.93
K. hansenii ATCC53582 *Normal culture	—	—	—	—	10.9 ± 0.3^{a}	2.73 ± 0.11^{a}	0.69 ± 0.03^{a}	37.8 ± 1.1^{ab}	1.81

Basic characterization of the prepared BC pellicles

The cellulose content in the pellicle and the fiber morphology of the BC ribbon were evaluated as basic characteristics of the samples. The measured cellulose content of each BC pellicle is shown in Tabl2 2-1. The mean values of the cellulose contents were in the range of 0.17–0.60 w/v%, depending on the bacterial strain. The values of cellulose contents reported so far are within the range of 0.2%–3% (Chen et al., 2018; Kaczmarek et al., 2022). Therefore, the cellulose contents of the samples employed in the present study were relatively small.

Next, the fiber morphologies, including the heights and widths of the BC ribbons constituting the fiber networks, were evaluated by AFM images. Depending on the bacterial strain, the mean values of fiber width, fiber height, and fiber cross-sectional areas were in the ranges 11–15 nm, 62–93 nm, and 770–1400 nm^2, respectively (Table 2-1). Comparing the bacterial strains, ATCC23769 and NBRC105051 produced fibers with smaller widths, heights, and cross-sectional areas, whereas ATCC53582 produced fibers with larger values.

Additionally, Fourier transform infrared spectroscopy (FT-IR) was performed to evaluate the molecular scale differences of BC pellicles derived from various strains (Fig. 2-3). The FT-IR spectra showed a typical BC spectrum. Focusing on the absorption bands at 3240cm^{-1}, which is the absorption band due to cellulose Iα, and 3270cm^{-1}, which is the absorption band due to Iβ (Persson et al., 1991), no significant difference in the ratio of absorption intensity was observed among the samples. Namely, all samples were apparently Iα-rich in their crystalline phases.

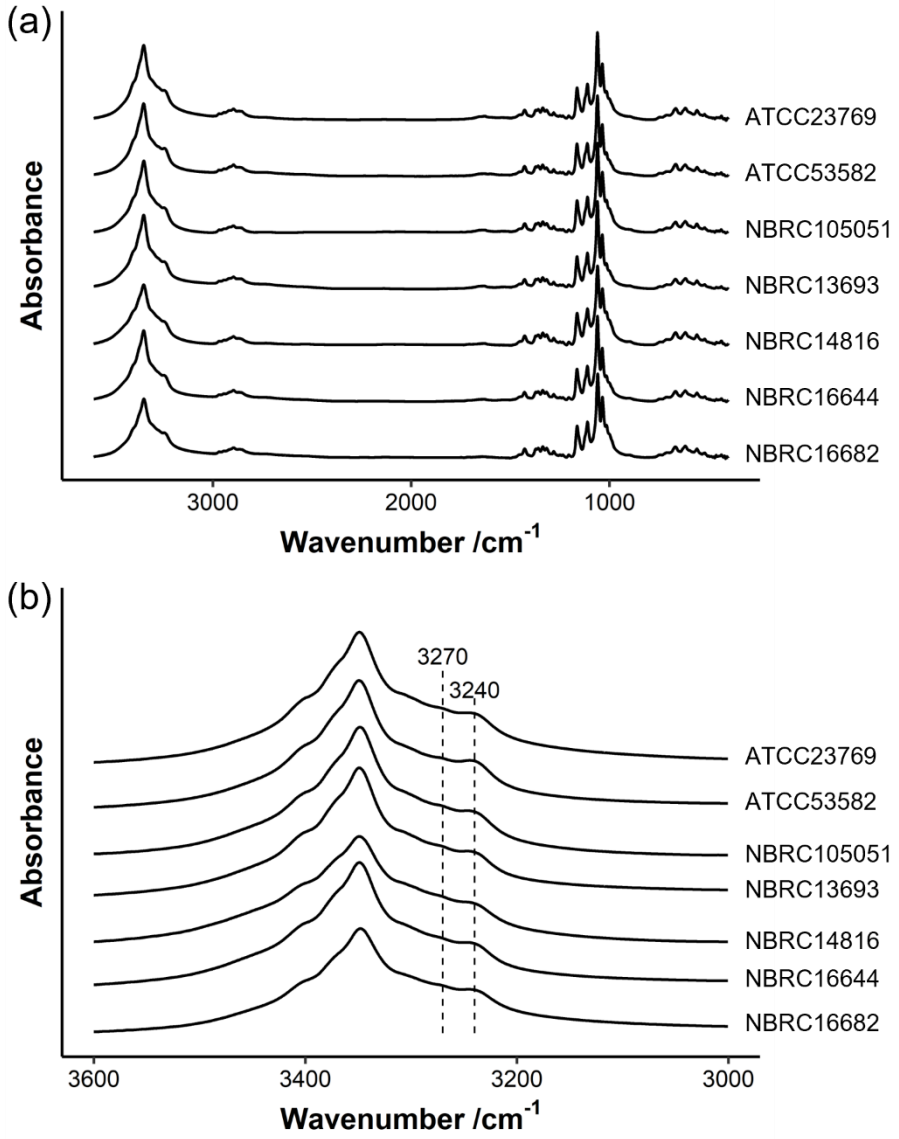

Fig. 2-3 FT-IR spectra of BC pellicles obtained by various bacterial strains in the range of (a) 3600–400 cm^{-1} and (b) 3600–3000 cm^{-1}. Dashed lines in (b) indicates the absorption bands due to cellulose Iα and Iβ crystalline phases at 3240 cm^{-1} and 3270 cm^{-1}, respectively.

Cross-sectional observation of the BC pellicles

Fluorescence microscopic observations of transverse sections of the pellicles were performed to evaluate the uniformity of the internal structure. Cellulose fibers were fluorescently stained, and the internal structure of the pellicle was analyzed from the fluorescence intensity.

First, no compressive deformation was observed in the transverse sections of the BC pellicles, and the effects of cutting were limited to the surface of the cut section by a few micrometers. It is hypothesized that the agar penetrated the BC network, forming a double network structure at the boundary, which prevented interface delamination and mitigated stress concentration during cutting. The fluorescence intensity profile along the height direction of the pellicle is shown in Fig. 2-4. The fluorescence intensities were averaged over three or more observation points and normalized by the average fluorescence intensity. For all pellicles, the variation from the mean, indicated by the standard deviation, was in the range of 0.21−0.45 (21%–45%). The present incubation method reduced the evident heterogeneity in height direction (Jacek et al., 2021; Klemm et al., 2001) that is occasionally observed in pellicles in the normal incubation method. Comparing the bacterial strains, the pellicles of ATCC53582 and NBRC16682 were more homogeneous, while those of NBRC105051 were less homogeneous.

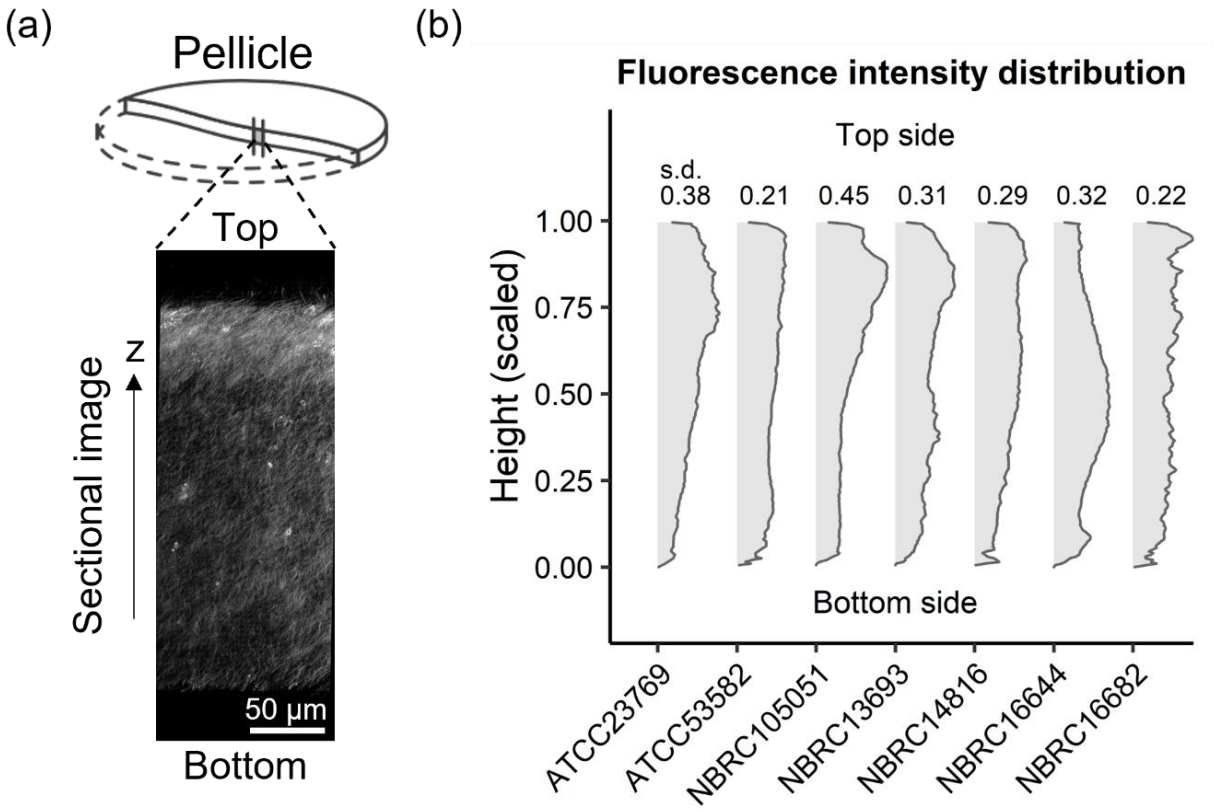

Fig. 2-4 (a) A representative confocal laser scanning microscope (CLSM) image of a transverse section of a pellicle and (b) fluorescence intensity distribution in the height direction for various pellicles. Fluorescence intensity and height are normalized by the mean value and the maximum value, respectively. Height 1 and 0 correspond to the top and bottom surfaces, respectively. The numbers in the plots indicate the standard deviation of fluorescence intensity along the height position.

Three-dimensional fiber network in the BC pellicles

The CLSM observation revealed the diversity of the fiber network structure among the bacterial strains (Fig. 2-5). Although CLSM is inferior to SEM observation in terms of resolution, it provides the three-dimensional spatial information essential for the analysis of higher-order structures. Furthermore, the CLSM images did not show any structural changes caused by electron beam damage or dehydration, allowing the observation of an intact network structure.

To quantitatively evaluate the obtained fiber networks, fiber segmentation analyses were performed on the acquired 3D fluorescence data, and the densities of the crosslink points were calculated. During fiber segmentation analysis by SOAX, which is based on active contour model (Kass et al., 1988), the 3D coordinates of the fiber structure were extracted from the fluorescence image, as shown in Fig. 2-5a, b. Segmentation analysis detects ridge structures in the fluorescence intensity distribution as fibers. In addition, SOAX analysis can detect the crosslinking points where fibers are closer than a certain distance from each other. By applying this analysis to the BC pellicles, the crosslink density was obtained for each bacterial strain, as listed in Table 2-1. The mean values of the crosslink density, i.e., $6.2–12.0 \times 10^8$ counts/mm^3, were dependent on the bacterial strain (Fig. 2-5d). The obtained crosslink density reflected the density of the fibers in the fluorescence images. For example, the pellicles produced by NBRC16644 and NBRC16682 had sparse fiber networks according to the fluorescence images, and the SOAX results of the images also indicated a sparse fiber network and low crosslink density (Fig. 2-5c). This agreement validates the segmentation process used in the current study.

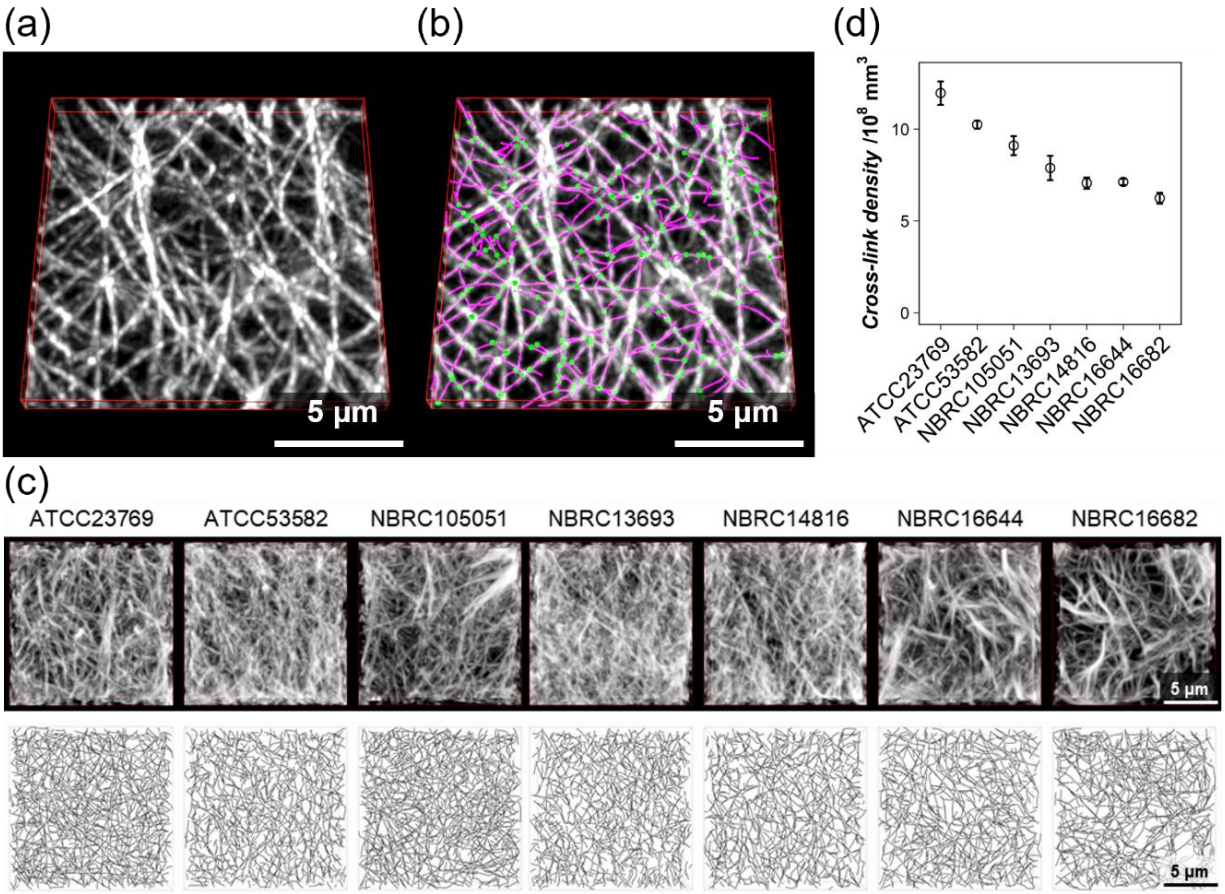

Fig. 2-5 (a) Three-dimensional fluorescence image of a bacterial cellulose (BC) pellicle, and (b) the corresponding SOAX-analyzed image. The magenta lines represent segmented fibers, and the green dots represent crosslink points. (c) Three-dimensional fluorescence images of the various BC pellicles obtained by confocal laser microscopy and the corresponding fiber networks analyzed using SOAX. (d) Crosslink density for various pellicles. Each image in (a) and (b) covers a volume of 15 μm × 15 μm × 1 μm, and the image in (c) covers a volume of 15 μm × 15 μm × 5 μm.

Correlation analysis

Correlation analysis was performed to evaluate the effects of parameters such as crosslink density, cellulose content, and fiber morphology on the tensile mechanical properties. The obtained correlation coefficients are shown in Table 2-2 (Full data are shown in Fig. 2-6). First, the crosslink density shows a strong positive correlation with the scaling exponent (correlation

coefficient = 0.87, p-value = 0.012). In addition to the scaling exponent, the apparent elastic modulus and breaking strength showed a strong positive correlation with the density (correlation coefficient = 0.75, p-value = 0.05 for elastic modulus, correlation coefficient = 0.73, p-value = 0.06 for breaking strength). Other correlations between structural parameters and physical properties were not as apparent as these three. Although a positive correlation between cellulose content and tensile strength was reported in a previous study (Chen et al., 2018), no clear correlation was found in the present study. These results suggest that the tensile properties of BC pellicles are more affected by the number of crosslinking points in the fiber network than by the cellulose content or ribbon thickness.

Table 2-2. Correlation analysis of the relationships between the physical properties and structural factors (i.e., crosslink density, cellulose content, and Fiber cross-sectional area). Pearson's correlation coefficients are shown.

Parameter	**Elastic modulus**	**Strength**	**Scaling exponent**
Crosslink density	0.75	0.73	0.87
Cellulose content	0.03	0.14	0.43
Fiber cross-sectional area	0.56	0.57	0.09

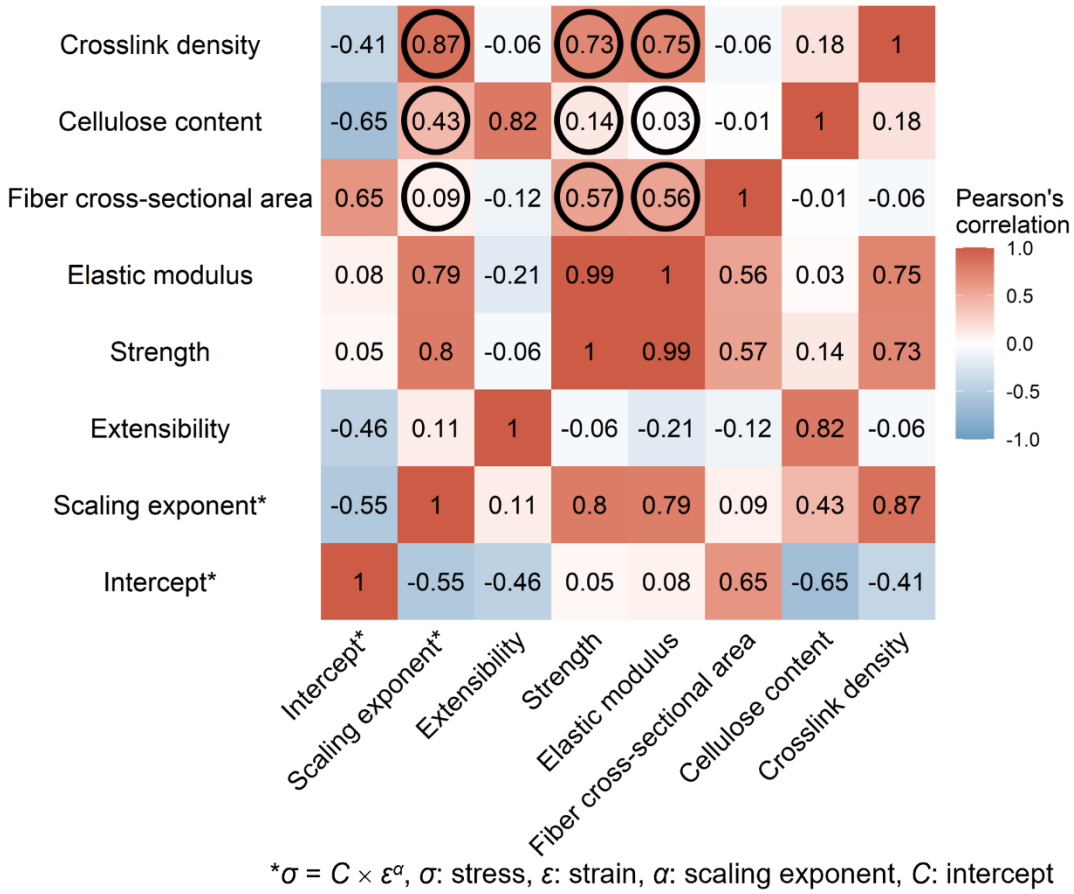

Fig. 2-6 Correlation plot for all the structural parameters and tensile mechanical properties. Positive correlations are colored in red, negative correlations are colored in blue, and uncorrelated correlations are colored in white, according to the values of correlation coefficients. This shows the prediction of tensile properties by measuring crosslink density is expected to be a robust method applicable to BC samples. The circled correlation coefficients in the correlation plots are listed in Table 2-2.

Discussion

Stress–strain curves in tensile testing of BC pellicles

Stress–strain curves in tensile testing of pellicles typically show strain hardening, although slight strain softening has been reported in some cases, and there is no unified view on this trend (Astley et al., 2003; Chen et al., 2018; Gao et 2015; McKenna et al.). The log–log plots

of stress–strain curves revealed that they follow a power law; $\log \sigma = \alpha \times \log \varepsilon + C$ (σ: stress, ε: strain, α: scaling exponent, C: constant). Furthermore, a linear relationship was found between the scaling exponent α and the crosslink density (Fig. 2-7a). This suggests that the crosslink density can explain the strain hardening phenomenon. In chapter 1, *in situ* observation of the fiber network during tensile deformation was performed and the formation of stress transfer paths due to the rearrangement of the fiber network was visualized (Takayama & Kondo, 2023). These observations suggest that strain hardening is proportional to the number of stress transfer paths formed during deformation. The number of stress paths is considered to be determined by the crosslink density. Therefore, the present results show the possibility of predicting the tensile properties of various pellicles simply by measuring the crosslink density. From the viewpoint of quality control of pellicles, it is advantageous to be able to roughly predict physical properties with simple microscopic measurements. Improving prediction accuracy by increasing data points is the next challenge.

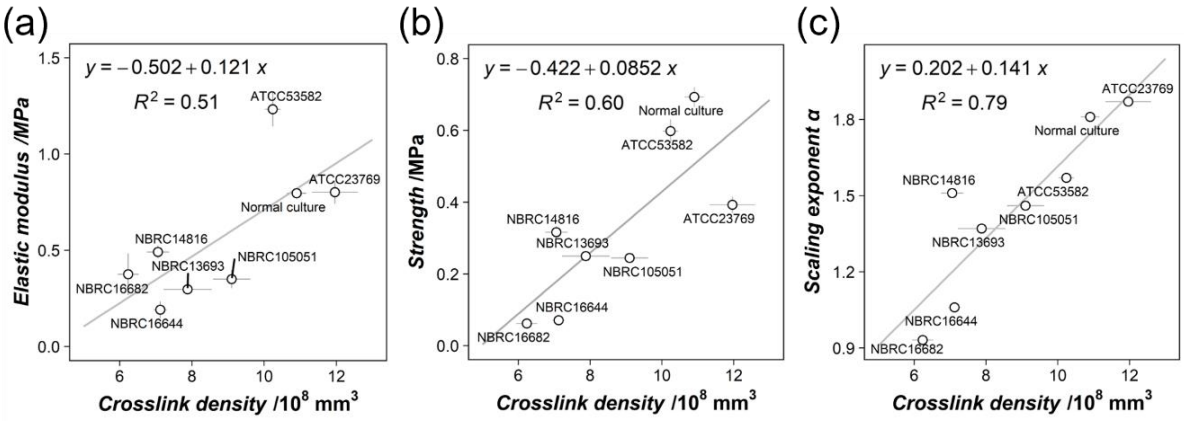

Fig. 2-7. (a) Elastic modulus, (b) breaking strength, and (c) scaling exponent versus crosslink density. The mean ± standard error (SE) of each strain is plotted. The gray lines represent the regression lines. The regression equations and R^2 values are shown in the plots.

Prediction of physical properties by crosslink density measurements

For application, it is important that the method proposed in this study should be universally applicable to pellicles. The pellicles prepared in this study were thinner than typical pellicles, with a thickness of less than 1 mm. This is due to the special culture method of inoculating at high density and harvesting in a short time to prepare a uniform pellicle. In practical use, pellicles thicker than 1 mm are often used. The issue is whether the relationship between crosslink density and tensile properties obtained in this study can be applied to pellicles several mm thick. In this regard, the pellicle obtained by the normal culture method also shows reasonable agreement with the linear relationship between crosslink density, scaling exponent, apparent elastic modulus, and breaking strength obtained with the pellicles prepared by the special culture method (Fig. 2-7). Therefore, the prediction of tensile properties by measuring crosslink density is expected to be a robust method applicable to thicker specimens.

Effect of cellulose content and fiber morphology on physical properties

Cellulose content and fiber width are also considered structural factors that are commonly measured as basic properties of BC pellicles. However, the results in the current study show that the correlation between these structural factors and mechanical properties was relatively weak, and rather, the network structure of the fibers has a relatively strong impact on the tensile properties. This indicates that the network structure of the fibers determines the shape of the stress−strain curve and that a complex of factors such as network structure, amount, and thickness of cellulose fibers determine the magnitude of the stress. This result supports the theory that the crosslink density, rather than the fiber content, determines the physical properties of the fiber network (Amjad & Picu, 2022; Deogekar et al., 2019; Münster et al., 2013). Thus, it

is not enough to measure cellulose content and fiber morphology as in the conventional approach to predict the physical properties of pellicles; it is also important to analyze the network structure.

Crosslink structure

In the present study, the crosslink density was used as a quantitative index of the fiber network. Crosslink points, which are defined as points close to each other, have two types of bonding based on the nature of the crosslinks: those with branching points and those with contact points (Fig. 6b). At a branching point, one fiber branches into two or more fibers. This is a characteristic of BC pellicles, and results in strong and permanent physical crosslinking due to crystalline junction zones. This branching structure can also be clearly seen in the AFM image shown in Fig. 6a. A contact point occurs when there is literal contact between fibers, and is considered to be a transient crosslink based on the weak interaction due to hydrogen bonding and/or van der Waals forces. SOAX analysis is supposed to detect both branching and contact points. The branching points are thought to contribute to the solid-like behavior of a BC pellicle (Whitney et al., 1999). For example, dilute dispersions of nanocelluloses, which do not have branching points but only contact points, behave as liquids. Furthermore, differences in the interactions that form the network may also affect its deformation behavior, i.e., a cellulose molecular gel can be stretched several times more than a pellicle (Kondo et al., 2001; Togawa & Kondo, 1999). This is due to the reversible nature of molecular scale interactions, which is in contrast to the irreversible cleavage of branching points of nanofiber networks in pellicles (Takayama & Kondo, 2023). Taking these into account, the elastic modulus of the BC pellicle can be expressed as $E = E_{\mathrm{branch}} + E_{\mathrm{contact}}$. The elastic modulus derived from the branching point (E_{bracnch}) has a linear relationship with the fiber content, and the proportionality constant is considered to depend on the bacterial strain and the cultivation method. The elastic modulus

derived from the contact point ($E_{contact}$) depends on the cellulose content (Tatsumi et al., 2002). The development of an analysis algorithm that can distinguish these types of cross-linking points will lead to more accurate prediction of physical properties of pellicles.

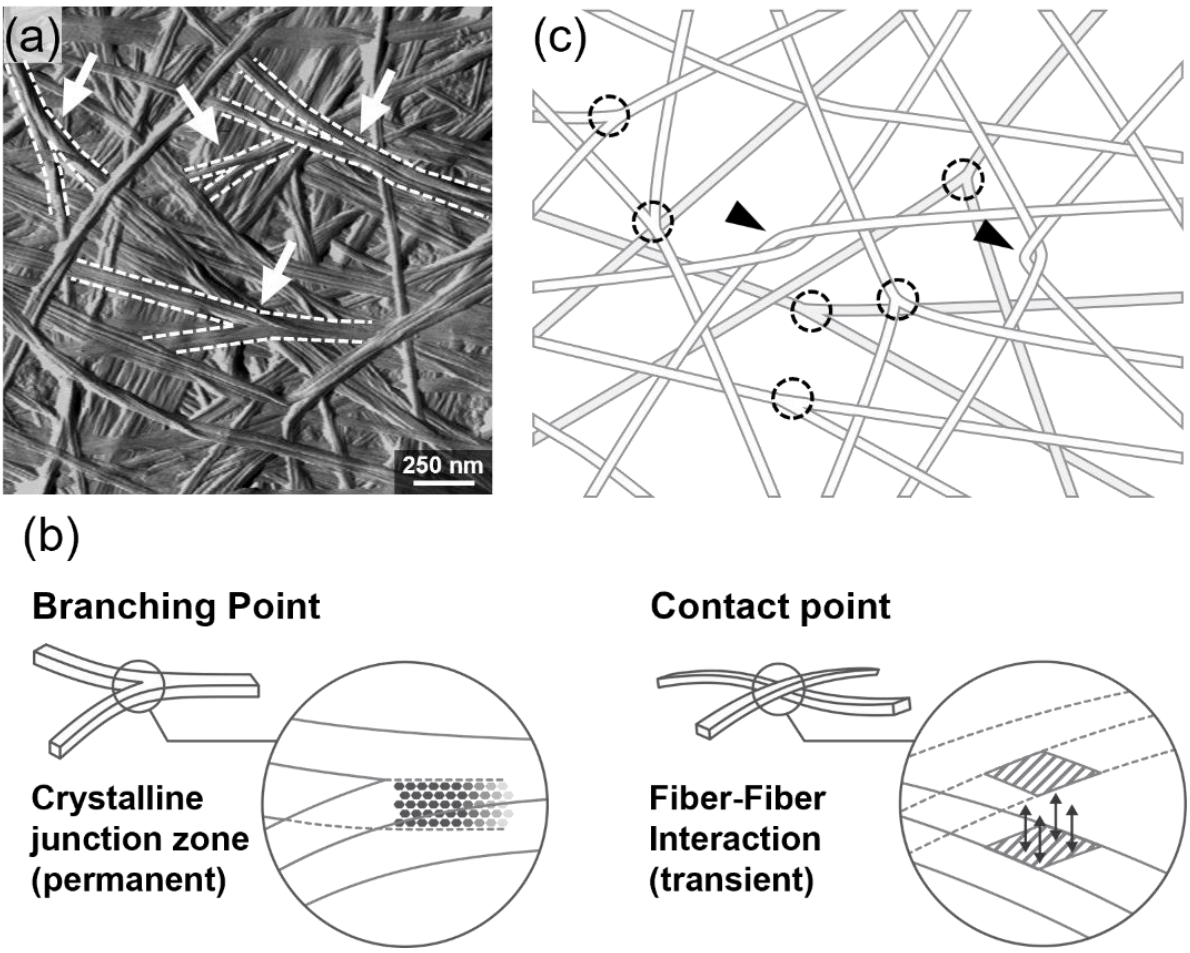

Fig. 2-8. (a) Branching points found in an atomic force microscopy (AFM) error signal image of the fiber network, and (b, c) schematic images of a branching point and a contact point. The white arrows in (a) indicate Y-shaped branching points. The dashed circles and arrowheads in (c) indicate branching points and entanglements, respectively.

The differences in the fiber networks among the bacterial strains were presumably related to the secretory behavior of the BC ribbons from the bacteria. The formation of a fiber network is

closely related to the collective behavior of the bacteria. The unique behavior of bacteria with regard to the secretion of cellulose fibers has been reported in detail (R. M. Brown et al., 1976; Hesse & Kondo, 2005; Tomita & Kondo, 2009). Although the mechanism by which bacteria form pellicles has not been fully elucidated, factors such as the production rate of the cellulose fibers by the bacteria and their habit of movement are thought to lead to differences in the fiber network. Bacteria deposit new BC ribbons while moving over previously secreted ribbons; this behavior resembles tracing (Tomita & Kondo, 2009). This leads to the bundling of the ribbons and the formation of thicker ribbons. In addition, ribbon-secreting bacteria sometimes move from one fiber to another. This transfer behavior creates branching points and connects the ribbons together to form a strong fiber network. Therefore, control of bacterial fiber secretion behavior is expected to facilitate the precise design of the network structure, leading to the control of elastic modulus, extensibility, and toughness.

Conclusions

In summary, the current study experimentally demonstrates that the network structure of BC pellicles has a significant influence on their tensile mechanical properties. The measured crosslink density indices adequately explained the strain hardening of the BC pellicles and the elastic modulus. Although the relationship between cellulose content, crosslink point density, and mechanical properties in BC pellicles is an ongoing area of scientific debate, this study provides basic experimental data and analytical methods that will lead to the elucidation of the fundamentals and material applications.

The properties of BC pellicles are greatly influenced by the bacterial strains and culture conditions used to produce the pellicles. Therefore, the determination of the optimum conditions for pellicle production is required for material development. However, the determination of the

physical properties of BC pellicles is time-consuming and labor-intensive. The method proposed in this study, which uses only a general-purpose confocal microscope and open-source analysis software, is expected to be applied to a simple, non-destructive evaluation method of BC hydrogels.

References

Amjad, S. N., & Picu, R. C. (2022). Stress relaxation in network materials: The contribution of the network. *Soft Matter*, *18*(2), 446–454. https://doi.org/10.1039/d1sm01546j

Astley, O. M., Chanliaud, E., Donald, A. M., & Gidley, M. J. (2003). Tensile deformation of bacterial cellulose composites. *International Journal of Biological Macromolecules*, *32*(1–2), 28–35. https://doi.org/10.1016/S0141-8130(03)00022-9

Brown, E. E., Laborie, M. P. G., & Zhang, J. (2012). Glutaraldehyde treatment of bacterial cellulose/fibrin composites: Impact on morphology, tensile and viscoelastic properties. *Cellulose*, *19*(1), 127–137. https://doi.org/10.1007/s10570-011-9617-9

Brown, R. M., Willison, J. H., & Richardson, C. L. (1976). Cellulose biosynthesis in Acetobacter xylinum: visualization of the site of synthesis and direct measurement of the in vivo process. *Proceedings of the National Academy of Sciences*, *73*(12), 4565–4569. https://doi.org/10.1073/pnas.73.12.4565

Canet-Ferrer, J., Coronado, E., Forment-Aliaga, A., & Pinilla-Cienfuegos, E. (2014). Correction of the tip convolution effects in the imaging of nanostructures studied through scanning force microscopy. *Nanotechnology*, *25*(39), 395703. https://doi.org/10.1088/0957-4484/25/39/395703

Chen, S. Q., Lopez-Sanchez, P., Wang, D., Mikkelsen, D., & Gidley, M. J. (2018). Mechanical properties of bacterial cellulose synthesised by diverse strains of the genus Komagataeibacter. *Food Hydrocolloids*, *81*, 87–95. https://doi.org/10.1016/j.foodhyd.2018.02.031

Clasen, C., Sultanova, B., Wilhelms, T., Heisig, P., & Kulicke, W. M. (2006). Effects of

different drying processes on the material properties of bacterial cellulose membranes. *Macromolecular Symposia*, *244*, 48–58. https://doi.org/10.1002/masy.200651204

Czaja, W., Romanovicz, D., & Brown, R. malcolm. (2004). Structural investigations of microbial cellulose produced in stationary and agitated culture. *Cellulose*, *11*(3/4), 403–411. https://doi.org/10.1023/b:cell.0000046412.11983.61

Deogekar, S., Islam, M. R., & Picu, R. C. (2019). Parameters controlling the strength of stochastic fibrous materials. *International Journal of Solids and Structures*, *168*, 194–202. https://doi.org/10.1016/j.ijsolstr.2019.03.033

Guhados, G., Wan, W., & Hutter, J. L. (2005). Measurement of the elastic modulus of single bacterial cellulose fibers using atomic force microscopy. *Langmuir*, *21*(14), 6642–6646. https://doi.org/10.1021/la0504311

Hesse, S., & Kondo, T. (2005). Behavior of cellulose production of Acetobacter xylinum in 13C-enriched cultivation media including movements on nematic ordered cellulose templates. *Carbohydrate Polymers*, *60*(4), 457–465. https://doi.org/10.1016/j.carbpol.2005.02.018

Hestrin, S., & Schramm, M. (1954). Synthesis of cellulose by Acetobacter xylinum 2. Preparation of freeze-dried cells capable of polymerizing glucose to cellulose. *The Biochemical Journal*, *58*(2), 345–352. https://doi.org/10.1042/bj0580345

Hsieh, Y. C., Yano, H., Nogi, M., & Eichhorn, S. J. (2008). An estimation of the Young's modulus of bacterial cellulose filaments. *Cellulose*, *15*(4), 507–513. https://doi.org/10.1007/s10570-008-9206-8

Jacek, P., Silva, F. A. G. S. da, Dourado, F., Bielecki, S., & Gama, M. (2021). Optimization and characterization of bacterial nanocellulose produced by Komagataeibacter rhaeticus K3. *Carbohydrate Polymer Technologies and Applications*, *2*, 100022.

https://doi.org/10.1016/j.carpta.2020.100022

James, H. M., & Guth, E. (1943). Theory of the elastic properties of rubber. *The Journal of Chemical Physics*, *11*(10), 455–481. https://doi.org/10.1063/1.1723785

Kaczmarek, M., Jędrzejczak-Krzepkowska, M., & Ludwicka, K. (2022). Comparative Analysis of Bacterial Cellulose Membranes Synthesized by Chosen Komagataeibacter Strains and Their Application Potential. *International Journal of Molecular Sciences*, *23*(6). https://doi.org/10.3390/ijms23063391

Kass, M., Witkin, A., Ave., H., & Alto, P. (1988). Snakes: Active Contour Models. *Int. J. Comput. Vis.*, *32*, 321–331. https://doi.org/10.1016/j.procs.2018.10.231

Klemm, D., Schumann, D., Udhardt, U., & Marsch, S. (2001). Bacterial synthesized cellulose - Artificial blood vessels for microsurgery. *Progress in Polymer Science (Oxford)*, *26*(9), 1561–1603. https://doi.org/10.1016/S0079-6700(01)00021-1

Kondo, T., Togawa, E., & Brown, R. M. (2001). "Nematic ordered cellulose": A concept of glucan chain association. *Biomacromolecules*, *2*(4), 1324–1330. https://doi.org/10.1021/bm0101318

Kuhn, W. (1936). Beziehungen zwischen Molekülgröße, statistischer Molekülgestalt und elastischen Eigenschaften hochpolymerer Stoffe. *Kolloid-Zeitschrift*, *76*(3), 258–271. https://doi.org/10.1007/BF01451143

Lee, C. M., Gu, J., Kafle, K., Catchmark, J., & Kim, S. H. (2015). Cellulose produced by Gluconacetobacter xylinus strains ATCC 53524 and ATCC 23768: Pellicle formation, post-synthesis aggregation and fiber density. *Carbohydrate Polymers*, *133*, 270–276. https://doi.org/10.1016/j.carbpol.2015.06.091

Machado, R. T. A., Gutierrez, J., Tercjak, A., Trovatti, E., Uahib, F. G. M., Moreno, G. de P.,

Nascimento, A. P., Berreta, A. A., Ribeiro, S. J. L., & Barud, H. S. (2016). Komagataeibacter rhaeticus as an alternative bacteria for cellulose production. *Carbohydrate Polymers*, *152*, 841–849. https://doi.org/10.1016/j.carbpol.2016.06.049

McKenna, B. A., Mikkelsen, D., Wehr, J. B., Gidley, M. J., & Menzies, N. W. (2009). Mechanical and structural properties of native and alkali-treated bacterial cellulose produced by Gluconacetobacter xylinus strain ATCC 53524. *Cellulose*, *16*(6), 1047–1055. https://doi.org/10.1007/s10570-009-9340-y

Mohan, S., Jose, J., Kuijk, A., Veen, S. J., Van Blaaderen, A., & Velikov, K. P. (2017). Revealing and Quantifying the Three-Dimensional Nano- and Microscale Structures in Self-Assembled Cellulose Microfibrils in Dispersions. *ACS Omega*, *2*(8), 5019–5024. https://doi.org/10.1021/acsomega.7b00536

Münster, S., Jawerth, L. M., Leslie, B. A., Weitz, J. I., Fabry, B., & Weitz, D. A. (2013). Strain history dependence of the nonlinear stress response of fibrin and collagen networks. *Proceedings of the National Academy of Sciences of the United States of America*, *110*(30), 12197–12202. https://doi.org/10.1073/pnas.1222787110

Nagashima, A., Tsuji, T., & Kondo, T. (2016). A uniaxially oriented nanofibrous cellulose scaffold from pellicles produced by Gluconacetobacter xylinus in dissolved oxygen culture. *Carbohydrate Polymers*, *135*, 215–224. https://doi.org/10.1016/j.carbpol.2015.08.077

Nečas, D., & Klapetek, P. (2012). Gwyddion: An open-source software for SPM data analysis. *Central European Journal of Physics*, *10*(1), 181–188. https://doi.org/10.2478/s11534-011-0096-2

Numata, Y., Kono, H., Mori, A., Kishimoto, R., & Tajima, K. (2019). Structural and rheological characterization of bacterial cellulose gels obtained from Gluconacetobacter genus. *Food*

Hydrocolloids, *92*(January), 233–239. https://doi.org/10.1016/j.foodhyd.2019.01.060

Özdemir, B., & Reski, R. (2021). Automated and semi-automated enhancement, segmentation and tracing of cytoskeletal networks in microscopic images: A review. *Computational and Structural Biotechnology Journal*, *19*, 2106–2120. https://doi.org/10.1016/j.csbj.2021.04.019

Persson, J., Chanzy, H., & Sugiyama, J. (1991). Combined Infrared and Electron Diffraction Study of the Polymorphism of Native Celluloses. *Macromolecules*, *24*(9), 2461–2466. https://doi.org/10.1021/ma00009a050

R Core Team. (2021). *R: A language and environment for statistical computing*. R Foundation for Statistical Computing, Vienna, Austria. https://www.r-project.org/

Singhsa, P., Narain, R., & Manuspiya, H. (2018). Physical structure variations of bacterial cellulose produced by different Komagataeibacter xylinus strains and carbon sources in static and agitated conditions. *Cellulose*, *25*(3), 1571–1581. https://doi.org/10.1007/s10570-018-1699-1

Takahama, R., Kato, H., Takayama, G., Tajima, K., & Kondo, T. (2022). Physical characteristics and cell-adhesive properties of in vivo fabricated bacterial cellulose/hyaluronan nanocomposites. *Cellulose*, *29*(6), 3239–3251. https://doi.org/10.1007/s10570-022-04480-2

Takayama, G., & Kondo, T. (2023). In situ visualization of the tensile deformation mechanism of bacterial cellulose network. *Carbohydrate Polymers*, *313*(March), 1–9. https://doi.org/10.1016/j.carbpol.2023.120883

Tanpichai, S., Quero, F., Nogi, M., Yano, H., Young, R. J., Lindström, T., Sampson, W. W., & Eichhorn, S. J. (2012). Effective young's modulus of bacterial and microfibrillated cellulose fibrils in fibrous networks. *Biomacromolecules*, *13*(5), 1340–1349.

https://doi.org/10.1021/bm300042t

Tatsumi, D., Ishioka, S., & Matsumoto, T. (2002). Effect of Fiber Concentration and Axial Ratio on the Rheological Properties of Cellulose Fiber Suspensions. *Journal of Society of Rheology, Japan*, *30*(1). http://dx.doi.org/10.1678/rheology.30.27

Togawa, E., & Kondo, T. (1999). Change of Morphological Properties in Drawing Water-Swollen Cellulose Films Prepared from Organic Solutions. A Viwe of Molecular Orientation in the Drawing Process. *Journal of Polymer Science: Part B: Polymer Physics*, *37*, 451–459.

Tomita, Y., & Kondo, T. (2009). Influential factors to enhance the moving rate of Acetobacter xylinum due to its nanofiber secretion on oriented templates. *Carbohydrate Polymers*, *77*(4), 754–759. https://doi.org/10.1016/j.carbpol.2009.02.022

Tsuji, T., Tsuboi, K., Yokota, S., Tagawa, S., & Kondo, T. (2021). Characterization of an Amphiphilic Janus-Type Surface in the Cellulose Nanofibril Prepared by Aqueous Counter Collision. *Biomacromolecules*, *22*(2), 620–628. https://doi.org/10.1021/acs.biomac.0c01464

Whitney, S. E. C., Gothard, M. G. E., Mitchell, J. T., & Gidley, M. J. (1999). Roles of cellulose and xyloglucan in determining the mechanical properties of primary plant cell walls. *Plant Physiology*, *121*(2), 657–663. https://doi.org/10.1104/pp.121.2.657

Xu, T., Vavylonis, D., Tsai, F. C., Koenderink, G. H., Nie, W., Yusuf, E., Lee, I. J., Wu, J. Q., & Huang, X. (2015). SOAX: A software for quantification of 3D biopolymer networks. *Scientific Reports*, *5*(9081), 1–10. https://doi.org/10.1038/srep09081

Yamanaka, S., & Sugiyama, J. (2000). Structural modification of bacterial cellulose. *Cellulose*, *7*(3), 213–225. https://doi.org/10.1023/A:1009208022957

Chapter 3

Three-dimensional Structural Formation Process of Bacterial Cellulose Pellicles Revealed by Trajectory Analysis

Introduction

The previous sections have proposed that the fibrous network structure in BC pellicle plays a crucial role in precise material design using *Komagataeibacter* bacteria in relation to the physical properties. To date, BC production has been often optimized based on its yield, and there is a limited number of detailed reports on its properties. The production of BC pellicles can vary depending on the strains of bacteria, culture media compositions, and cultivation methods used (Chen et al., 2018; Kaczmarek et al., 2022; Lee et al., 2015; Lu et al., 2011; McKenna et al., 2009; Numata et al., 2019). However, there is still a lack of understanding regarding how these factors specifically influence the structure and properties of the formed pellicles.

Although limited in number, some research has been conducted to produce structurally controlled BC pellicles by controlling bacterial movements using template techniques; for instance, precise control of cellulose fiber secretion patterns has been achieved by manipulating bacterial movements using patterned substrates such as uniaxial alignment or honeycomb templates through cellulose/template interaction (Hesse & Kondo, 2005; Kondo et al., 2002,

2012; Kondo & Kasai, 2014; Putra et al., 2008; Tomita & Kondo, 2009; Uraki et al., 2007). These studies have provided valuable insights into the design of novel structures by controlling bacterial movements. Due to the two-dimensional nature of the substrate, there are limitations to expanding the structures into three dimensions.

Technique that can control bacterial movements without relying on template is another way to create BC network materials with high design flexibility. To achieve this, a detailed understanding of the structural formation process by bacteria is essential. Elucidating the nature of *Komagataeibacter* bacteria as "self-propelled particles" makes it feasible to achieve a spontaneous pattern formation. The spontaneous structure formation by self-propelled particles (Czirók & Vicsek, 2000), which is universally observed in nature, is a field of study known as active matter physics. It is related to understanding of the mechanisms of pattern formation in collective behavior of various particles at different scales, including anisotropic particles, microorganisms and animals (Deutsch et al., 2012; Gompper et al., 2020; Vernerey et al., 2019; Vicsek & Zafeiris, 2012). In the case of *Komagataeibacter* bacteria, such an analysis of collective motion mechanisms resulting in formation of BC networks provides a significance not only from a scientific perspective like active matter physics, but also from a technological standpoint for material design. Understanding the collective motion of *Komagataeibacter* bacteria can lead to the elucidation of network structure formation and contribute to precise material design using *Komagataeibacter* bacteria.

Previous studies have reported the movement of bacterial cells on substrates using time-lapse microscopy (Brown et al., 1976; Hesse & Kondo, 2005; Kondo et al., 2002, 2012; Kondo & Kasai, 2014; Tomita & Kondo, 2009). These observations have provided important insights into the patterns of bacterial movements. However, the studies were limited to the two-

dimensional environment of the solid substrates, which differs from the actual three-dimensional cultivation environment. By extending these observations to the process of three-dimensional network formation in liquid culture media, a new insight may arise. The primary aim of this chapter is, therefore, to unravel the formation mechanisms of network structures by *Komagataeibacter* bacteria. To achieve this, tracking and analysis techniques to investigate the collective motion of bacteria during BC pellicle formation were performed. The ultimate goal is to advance precise material design and develop innovative BC materials.

Materials and methods

CLSM Observation of BC Pellicles

The BC pellicles were subjected to fluorescent staining with FB28 or 6FAM (Details of staining protocols are described in Chapters 1 and 2). CLSM (TCS, Leica Microsystems, Wetzlar, Germany) equipped with a 100× objective lens was used to observe the fluorescently labeled BC pellicles. The TileScan function of the LAS X software (Leica Microsystems, Wetzlar, Germany) was utilized to acquire wide field-of-view images.

AFM Observation of BC Network

To reveal the nano-scale structure of the fibrous network that cannot be observed with the resolution of confocal microscopy, AFM observations were conducted. Poly-L-lysine-coated glass substrates were employed for AFM sample preparation, enhancing the adhesion of cellulose nanofibers and bacteria. *Komagataeibacer* bacteria dispersed in HS medium (Hestrin & Schramm, 1954) were drop-cast onto the substrates and incubated for 30 minutes to allow cellulose fiber production. The substrates were rinsed with water and dried to prepare samples for observation. AFM observations were performed using an MFP-3D-SA (Oxford Instruments,

Santa Barbara, CA, USA) equipped with a cantilever OMCL-AC240TS (spring constant = 2 N/m; Olympus Co., Tokyo, Japan). From the height images based on AFM observations, the height and width of the fibers were estimated (N=75). Unless otherwise specified, all data are presented as mean ± standard deviation.

Time-Lapse Imaging of Network Formation Process

To capture the bacterial movements in liquid culture, time-lapse observations were conducted using a phase-contrast microscope (CK40, Olympus, Tokyo). An observation chamber was created using polydimethylsiloxane (PDMS), with a height of approximately 200 μm and an outer diameter of 6 mm, featuring a cylindrical protrusion. The chamber was filled with 40 μL suspension of the bacterial cells. Then the chamber was inverted and mounted on a 35 mm glass-bottom dish to encapsulate the bacterial suspension (Fig. 3-1). The chamber was statically cultured until a network of cellulose nanofibers formed within it. After confirming the subsiding of bacterial Brownian motion and the initiation of bacterial movement along the BC ribbons, time-lapse observations using a phase-contrast microscope were started. A 40× objective lens (Phase contrast) and a CCD camera (Spot insight, SPOT Imaging, Michigan, USA) with a resolution of 1600 × 1200 px were employed. TIFF images were captured at 2-second intervals, resulting in a time-lapse dataset comprising a total of 1800 frames over the course of 1 hour.

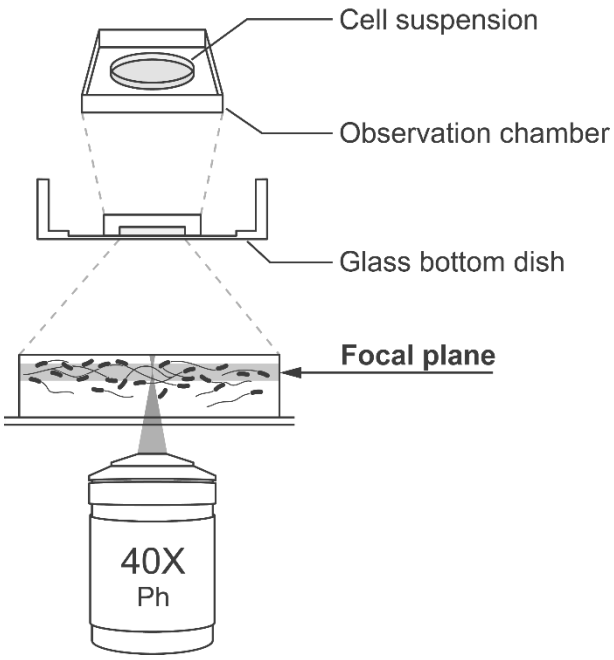

Fig. 3-1 Schematic illustration of experimental setup for time-lapse microscopy. A PDMS observation chamber was employed to provide a stable and clear visualization of the movement of bacteria in the liquid medium.

Image Analysis

Image analysis was performed to study the movement of bacteria in the time-lapse video images. The analysis utilized ImageJ FIJI (Schindelin et al., 2012) and its plugin, TrackMate (Tinevez et al., 2017). Average velocity of the bacteria, contour length ($l_{contour}$) and end-to-end distance ($l_{end\text{-}to\text{-}end}$) of the trajectories were calculated from the obtained data. Average velocity represented the mean moving rate of bacteria within a single trajectory, contour length indicated the cumulative distance covered in a single trajectory, and end-to-end distance indicated the straight-line distance between the starting and ending points of a trajectory.

Results

Structural patterns in BC pellicle visualized by CLSM

CLSM observation of BC pellicles revealed occasional presence of distinctive patterned structures, deviating from the commonly observed isotropic fiber network architecture (Fig. 3-2). Firstly, a pattern characterized by interconnected domains with aligned fibers was observed (Fig. 3-2b). Secondly, a vortex structure where fibers exhibited a helical arrangement was identified (Fig. 3-2c). Although these unique patterns appeared infrequently, these structures are expected to contribute novel properties distinct from those exhibited by the isotropic fiber network.

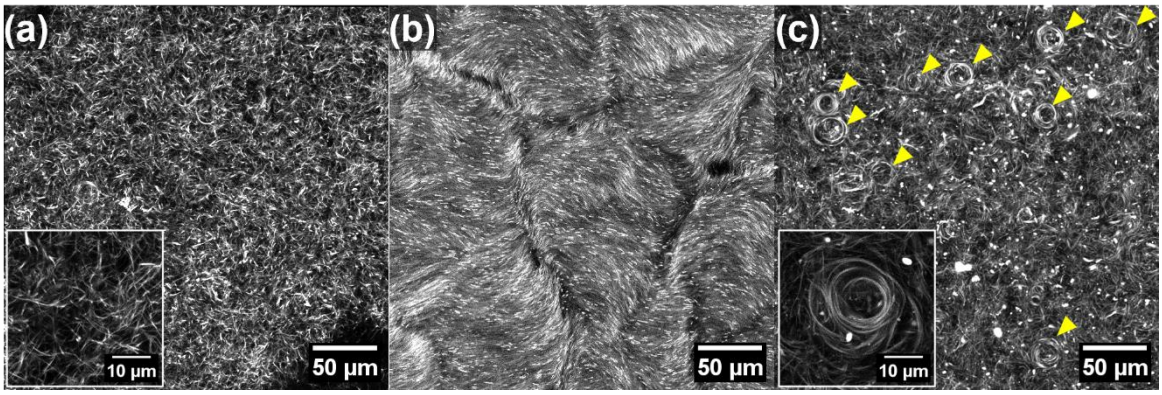

Fig. 3-2 CLSM images of various BC pellicles as represent for (a) an isotropic fiber network, (b) anisotropic domains, and (c) shows vortex structures. Arrowheads in the (c) indicates the vortex patterns.

i) Chiral nematic-like structure

The characterization of the three-dimensional structure of aligned-fiber domains produced by ATCC53582 strain and the determination of their sizes were performed. Three-dimensional scanning using CLSM was performed to analyze the spatial distribution of the fiber-aligned domains. Fig. 3-3a exhibits images obtained by systematically varying the vertical height at the same XY region, along with their corresponding Fast Fourier transformed (FFT) images.

These results indicate the presence of a chiral nematic-like structure where BC fibers exhibited rotational orientation. The rotation followed a right-handed helical pattern with a pitch of approximately 36 μm per revolution. Wide field scanning across a 1.2 mm square area revealed discontinuous boundaries where the orientation abruptly changed. Based on these boundaries, the domains were segmented, and their sizes were calculated (Fig. 3-3b, c). The average domain area was determined to be 14700 ± 8500 μm^2 (Fig. 3-3d), indicating the presence of structures at a size scale of approximately 100 μm.

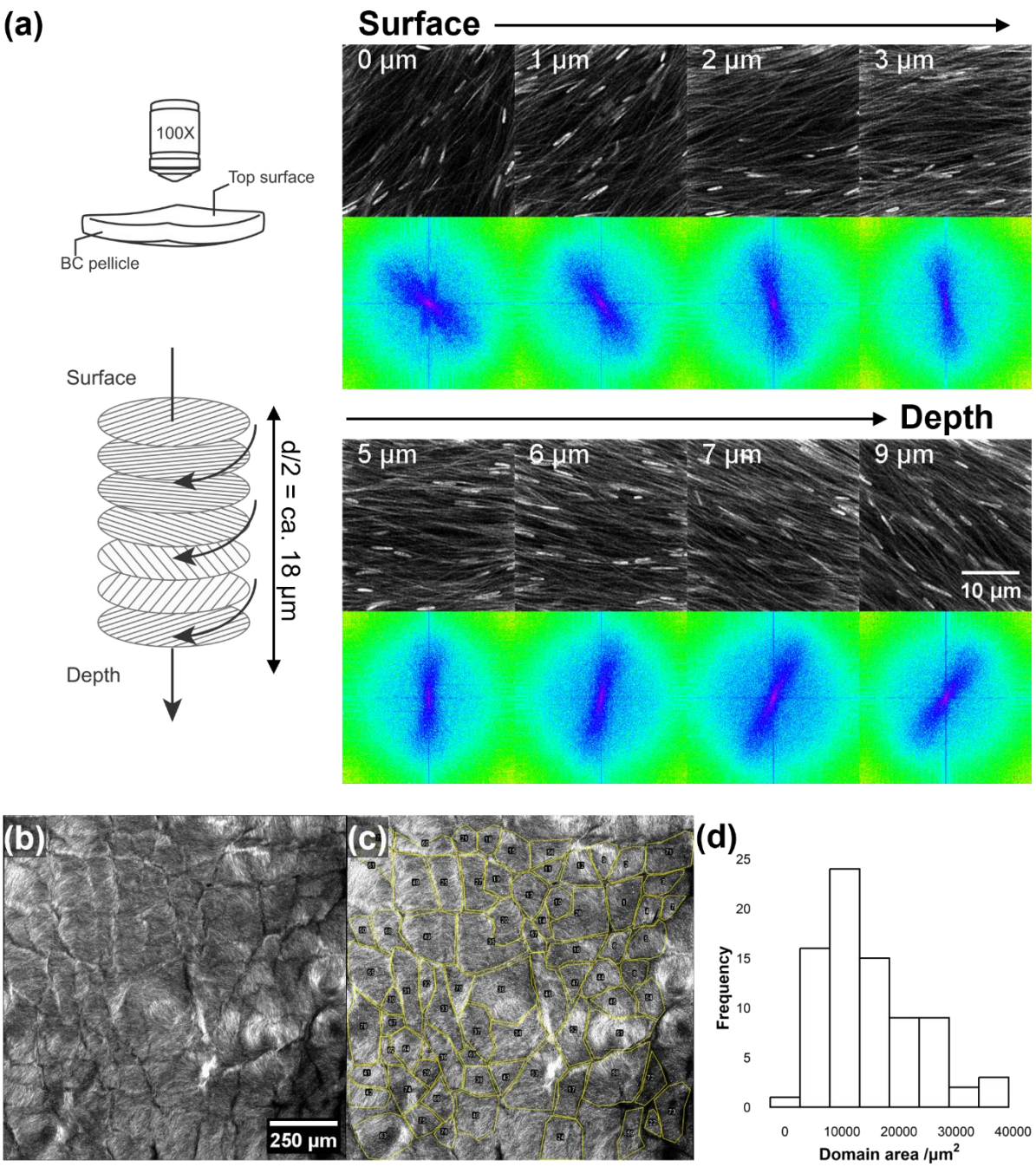

Fig. 3-3 (a) CLSM images of chiral nematic-like domains in BC pellicle produced by ATCC53582 and their corresponding FFT images, (b, c) an overview images and its segmented version, and (d) a histogram of segmented domain area.

ii) Vortex Pattern

The vortex structure was observed sporadically in BC pellicle produced by strains NBRC14816, ATCC23769, and ATCC700178. The loop structures exhibited a robust configuration formed by multiple bundles of BC ribbons (Fig. 3-4a). The loop diameters were found to be 19 ± 4 μm (Fig. 3-4b), which is several times larger than the length of individual bacteria. This result is consistent with the previous report about the circling behavior of bacteria (Hesse & Kondo, 2005; Tomita & Kondo, 2009).

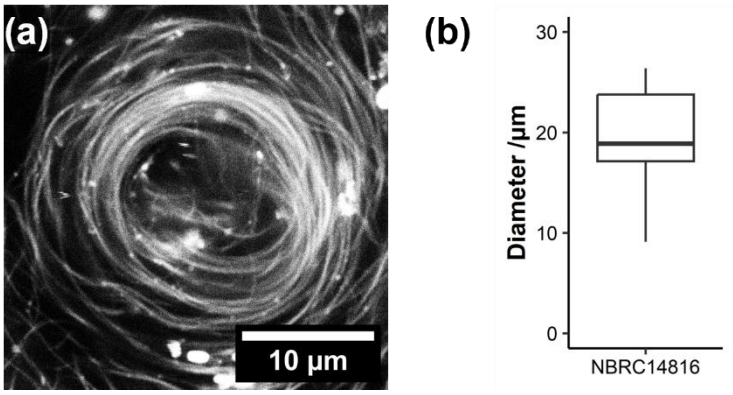

Fig. 3-4 (a) Vortex pattern in BC pellicle visualized by CLSM and (b) a boxplot showing the diameter of vortex.

Trajectories of Bacterial movements

The movement of *Komagataeibacter* bacteria plays a crucial role in the formation of the fibrous network structure in BC. *Komagataeibacter* bacteria, which is an obligate aerobe, in liquid culture, vigorously proliferates in oxygen-rich regions near the gas-liquid interface. Simultaneously, it produces BC ribbons while moving, and stacks 2-dimensional layers to form a BC pellicle. To understand this process in detail, time-lapse observation of bacterial collective movements during pellicle formation was conducted. The use of a custom-designed observation chamber allowed stable observation of bacterial movements in the liquid medium (Fig. 3-5a).

From the recorded time-lapse images, bacteria were segmented for each frame, colorized according to time, and then all the frames were superimposed to create a time-projection image, as shown in Fig. 3-5b. By connecting the bacterial cells in the time-lapse images, the trajectories of cellulose fibers, which are not visible in the phase-contrast images, were visualized (Fig. 3-5c). It should be noted that bacteria, which did not secrete BC ribbons, exhibited Brownian motion and diffused in the medium, making them distinguishable from the bacteria involved in fiber secretion.

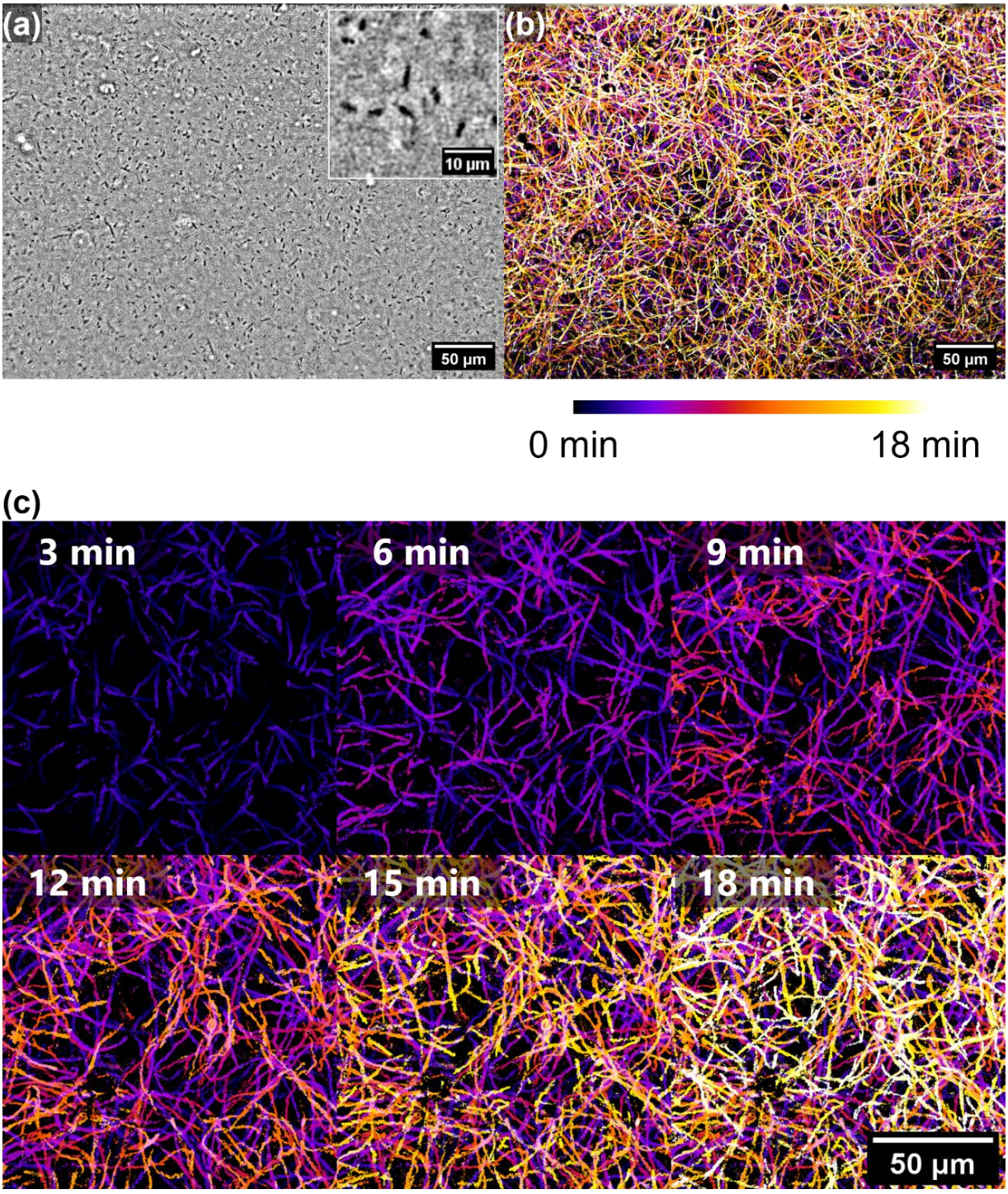

Fig. 3-5 (a) Phase-contrast microscopic image of bacteria during BC pellicle formation and (b) their time-projected trajectories colorized based on time, (c) time-lapse composite images showing the process of BC ribbon network formation, providing insights into the network formation process. The color bar indicates the corresponding time period.

Quantitative Analysis of Bacterial Trajectories

To quantitatively evaluate bacterial movements, trajectory analysis of the bacterial cells in the time-lapse data was performed. From the trajectories of bacterial movements, average velocity, contour length, as well as end-to-end distance were calculated as illustrated in Fig. 3-6a. A total of 11,450 tracks were analyzed, and the average velocity was determined to be 6.1 ± 1.7 μm/min (Fig. 3-6b), which is higher than the previously reported moving rates of *Komagataeibacter* bacteria on solid substrates (Brown et al., 1976; Hesse & Kondo, 2005; Kondo et al., 2002; Tomita & Kondo, 2009). Detailed analysis of the velocity distribution shows that in addition to the largest peak at 6.8 μm/min, there is a smaller peak at 4.4 μm/min (Fig. 3-6b). In previous studies, it has been reported that the moving rate of the bacteria changes depending on the state of the interaction between the secreted BC ribbons and the substrate and the secretion rate of the BC ribbons (Hesse & Kondo, 2005; Tomita & Kondo, 2009). Considering this, it is possible that the difference between tracing the existing BC ribbons or secreting new BC ribbons off the existing ribbons is the cause of the appearance of the two peaks. The contour length ($l_{contour}$) is 9.0 ± 0.1 μm (mean ± SD, Fig. 3-6c) and the longest $l_{contour}$ is 107 μm. The scatter plot in Fig. 3-6d illustrates the relationship between $l_{end\text{-}to\text{-}end}$ and $l_{contour}$, indicating the linearity of bacterial movements. When the $l_{end\text{-}to\text{-}end}$ and $l_{contour}$ coincide, it indicates that the bacteria are moving in an ideal straight-line manner without deviating from their path. However, in the density plot overlaid on the scatter plot, it can be observed that as the $l_{contour}$ increases, the $l_{end\text{-}to\text{-}end}$ decreases. This suggests a decrease in trajectory linearity, indicating that the bacteria are deviating from straight-line movement and exhibiting more random or curved trajectories. The straightness of bacterial trajectories can be evaluated by the ratio of the end-to-end distance to the contour length (Fig. 3-6e). The histogram of $l_{end\text{-}to\text{-}end}/l_{contour}$ displays a

peak around 1, with a value of 0.74 ± 0.28 (mean ± SD). Supposed that the trajectory of the bacteria coincides with the shape of the secreted cellulose fibers, the $l_{end\text{-}to\text{-}end}/l_{contour}$ corresponds to the curvature of the fibers in the network. Therefore, while the BC ribbons possess some flexibility, their movement is predominantly linear.

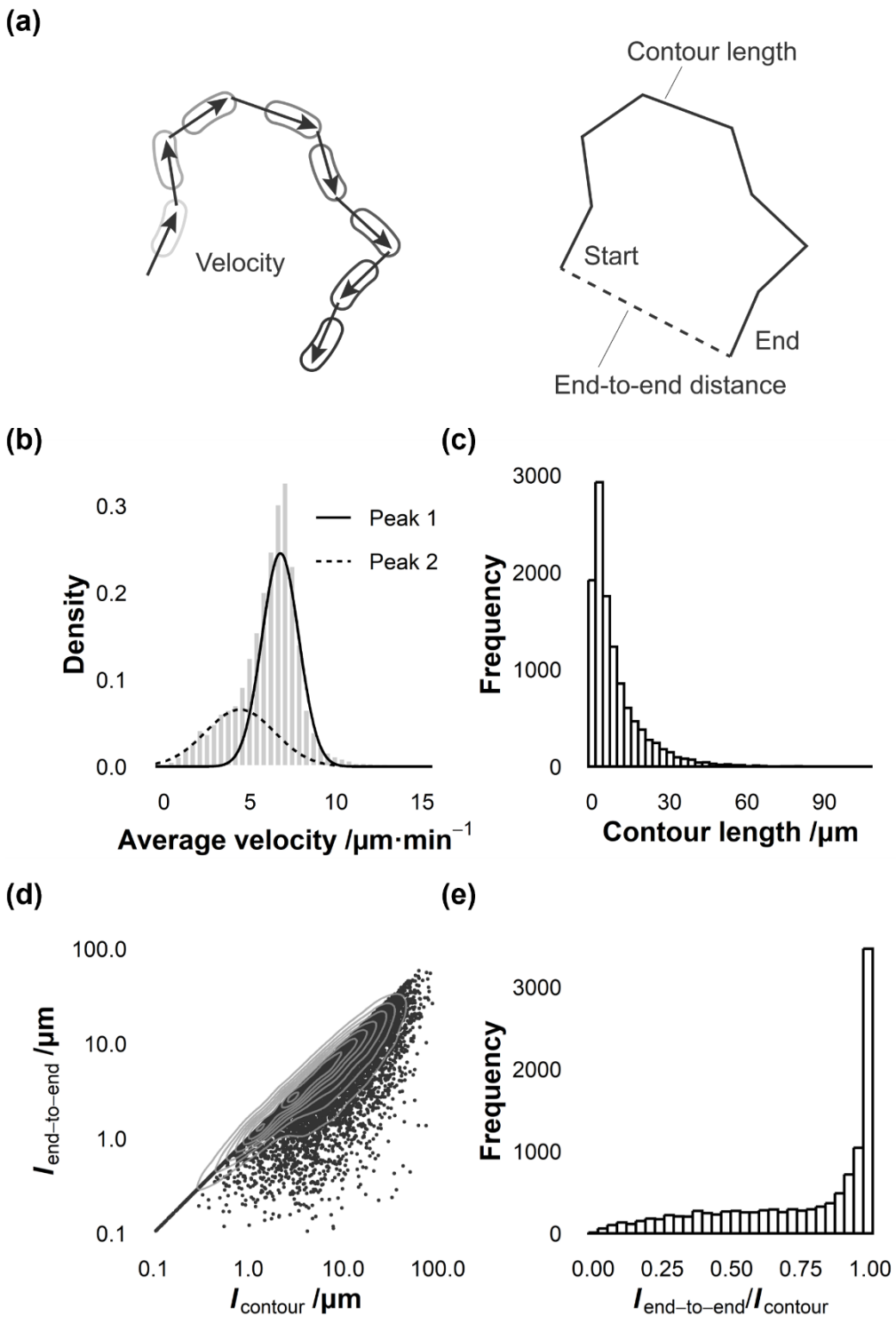

Fig. 3-6 (a) Schematic diagram illustrating the analysis of bacterial cell trajectories. (b) Histogram of average velocity of bacterial cells, (c) Histogram of contour length ($l_{contour}$) of the trajectories, (d) Scatter plot of end-to-end distance ($l_{end\text{-}to\text{-}end}$) plotted against $l_{contour}$, (e) Histogram of the ratio of end-to-end distance to contour length ($l_{end\text{-}to\text{-}end}$/ $l_{contour}$).

Formation of Branching Structures

By focusing on the individual trajectories of bacteria, the process of network formation by *Komagataeibacter* bacteria was qualitatively evaluated. Fig. 3-7 demonstrates the formation of branching structures by two tentative mechanisms, i.e., deviation from the original track and bacterial cell division. A bacterium secreting BC ribbons made a U-turn in the opposite direction of its movement (5 min), and after moving forward, it deviated from the initial track, forming the first branching point (7 min). Subsequently, as the bacterium underwent cell division, a second branching point was formed (9 min).

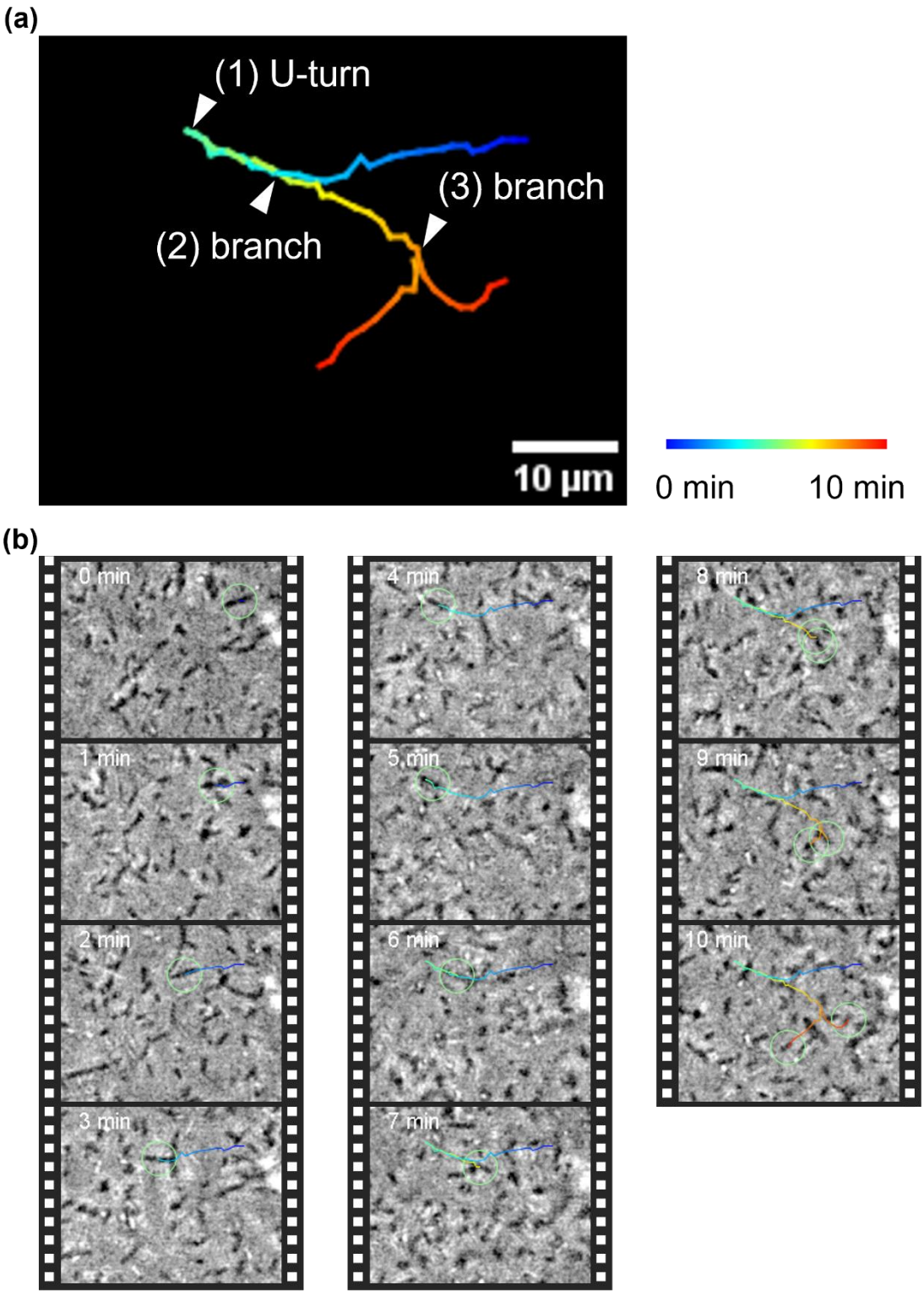

Fig. 3-7 (a) A trajectory of a bacterium obtained from tracking analysis and (b) corresponding time-lapse images: Directional changes, branching formation due to deviation from the original path, and branching formation due to bacterial cell division are shown.

Loop Formation

The loop structure formation leading to the vortex pattern was observed multiple times within the 60-minute observation period. Fig. 3-8 shows the typical trajectory and time-lapse images capturing the formation of the vortex pattern. Once bacterial cells formed a closed loop (16 min), they repeated the circular movement over multiple rounds. It should be noted that bacterial cells forming loop structures tended to be longer than normal cells. While the average bacterial cell length for the entire population was 3.2 ± 1.5 μm, bacterial cells forming loop structures had an average length of 12.6 ± 3.7 μm (Fig. 3-8c).

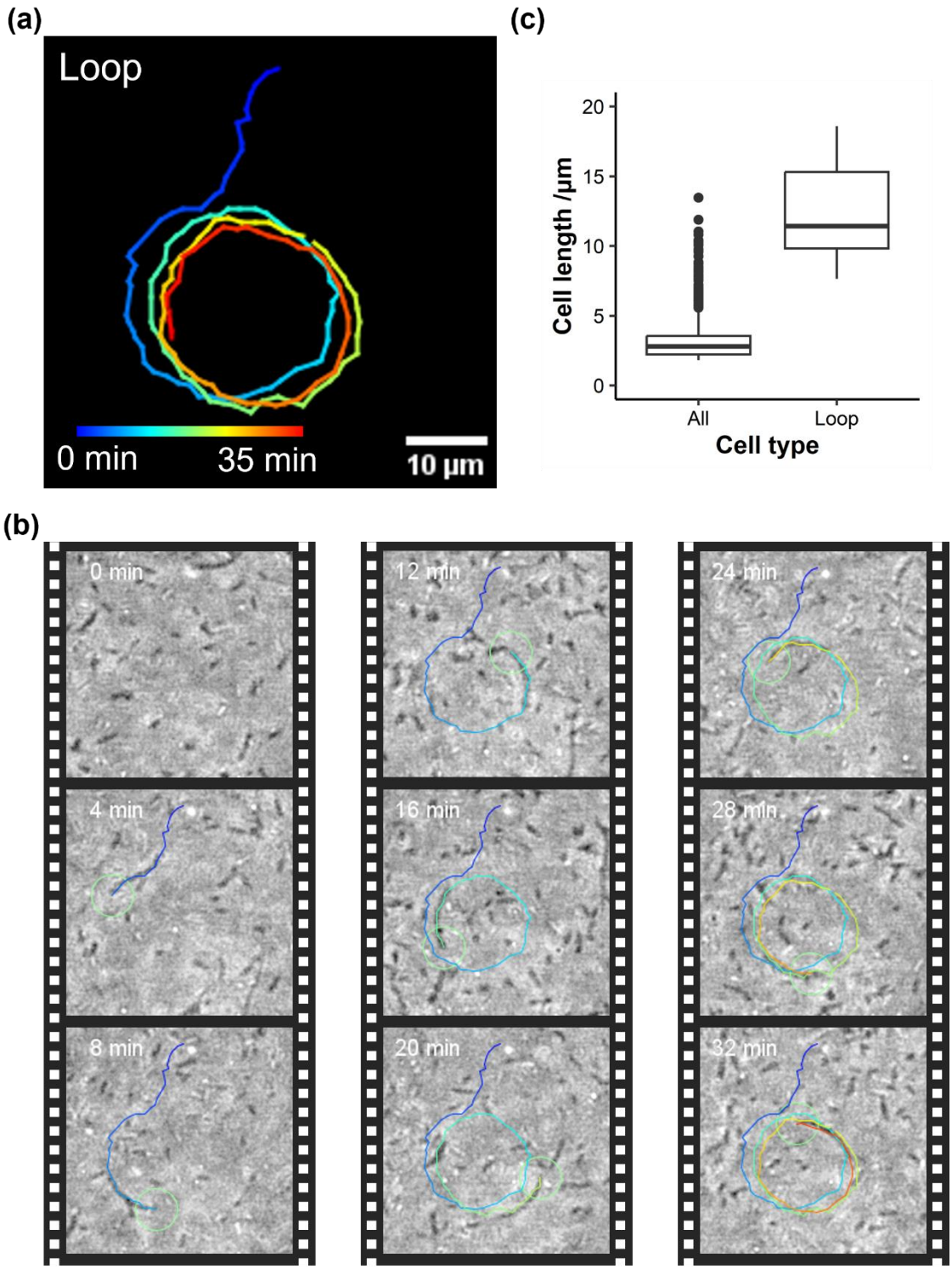

Fig. 3-8 (a) Tracking analysis results of bacterial cells forming loop structures and (b) corresponding time-lapse images. (c) Boxplot illustrating the difference in cell lengths between the overall bacterial population and the bacterial cells forming loops.

Merge/Split through Secreted BC Ribbons

Some interactions between bacterial cells or between a bacterial cell and a BC ribbon were also observed at the loop structures shown in Fig. 3-8 (Fig. 3-9a). Specifically, in Fig. 3-9b, a bacterial cell changed its direction upon encountering another cell. In Fig. 3-9c, bacterial cells collided with pre-formed BC tracks and then changed their direction. In Fig. 3-9d, a bacterial cell merged with the loop-forming cell, traveled together for a few minutes, and then separated. These results indicate that the higher-order structure of the network is formed through two types of interactions: i) interactions between bacterial cells and ii) interactions mediated by the trajectories of cellulose nanofibers.

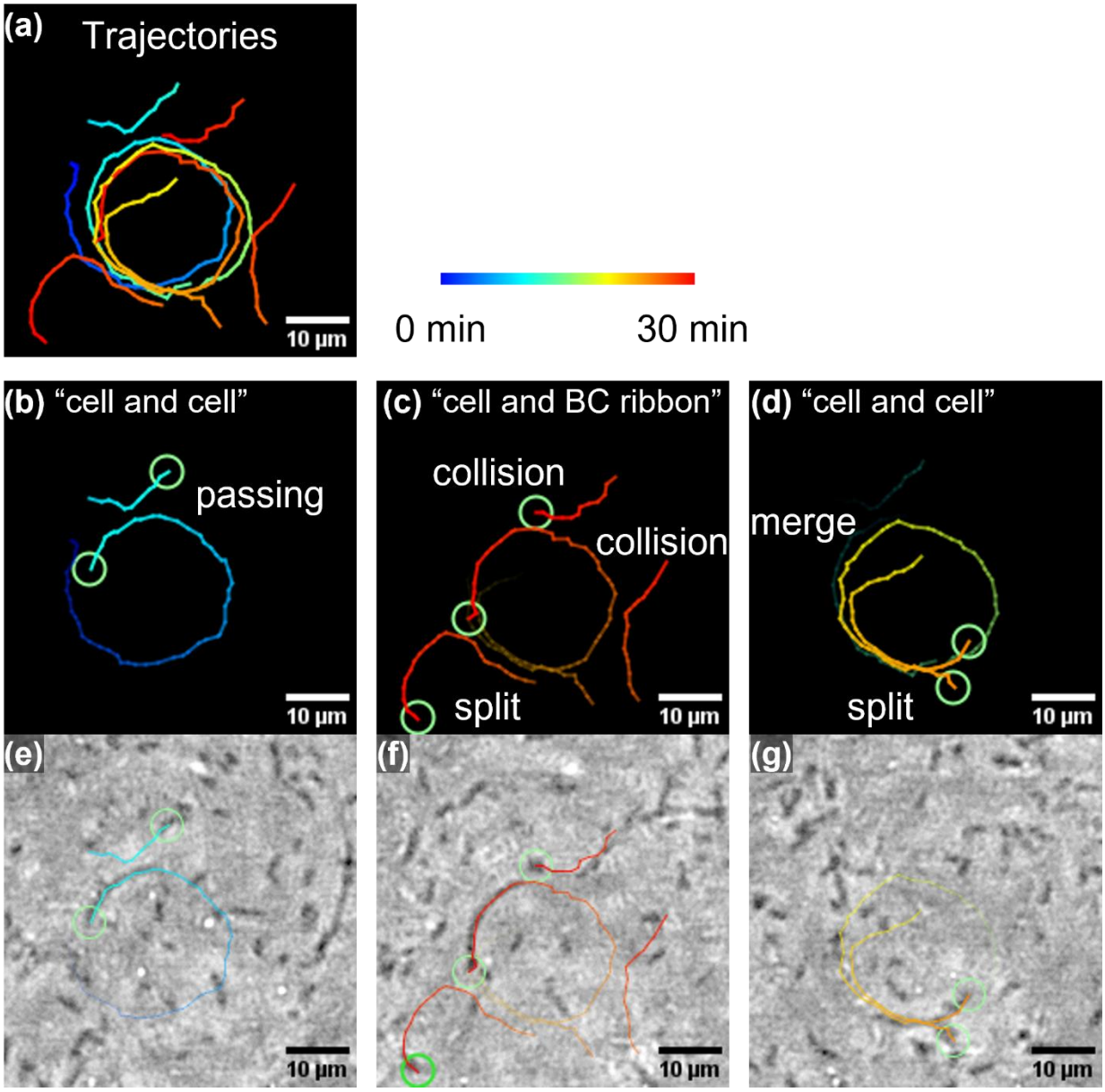

Fig. 3-9 Trajectories visualizing the interactions between bacteria and the interactions between bacteria and BC ribbons. Bacteria can be observed colliding, merging, and separating with the accumulated loop-shaped BC trajectories.

Observation of morphology of the BC network

To elucidate the fine structure of nanofiber networks that cannot be observed by fluorescence microscopy, AFM observations were conducted. BC ribbon exhibits a bundled

structure twisted in a right-handed direction (Fig. 3-10a, b) as previously reported (Brown et al., 1976; Colvin & Biology, 1961; Hanley et al., 1997). The width of single BC ribbons was measured to be 9.3 ± 4.2 nm in height and 104 ± 44 nm in width (Fig. 3-10c, d). These BC ribbons often form thicker fibers by bundling together with several BC ribbons. The AFM observation reveals that the bundled BC ribbons exhibit branching/merging structures at certain locations (Fig. 3-10b).

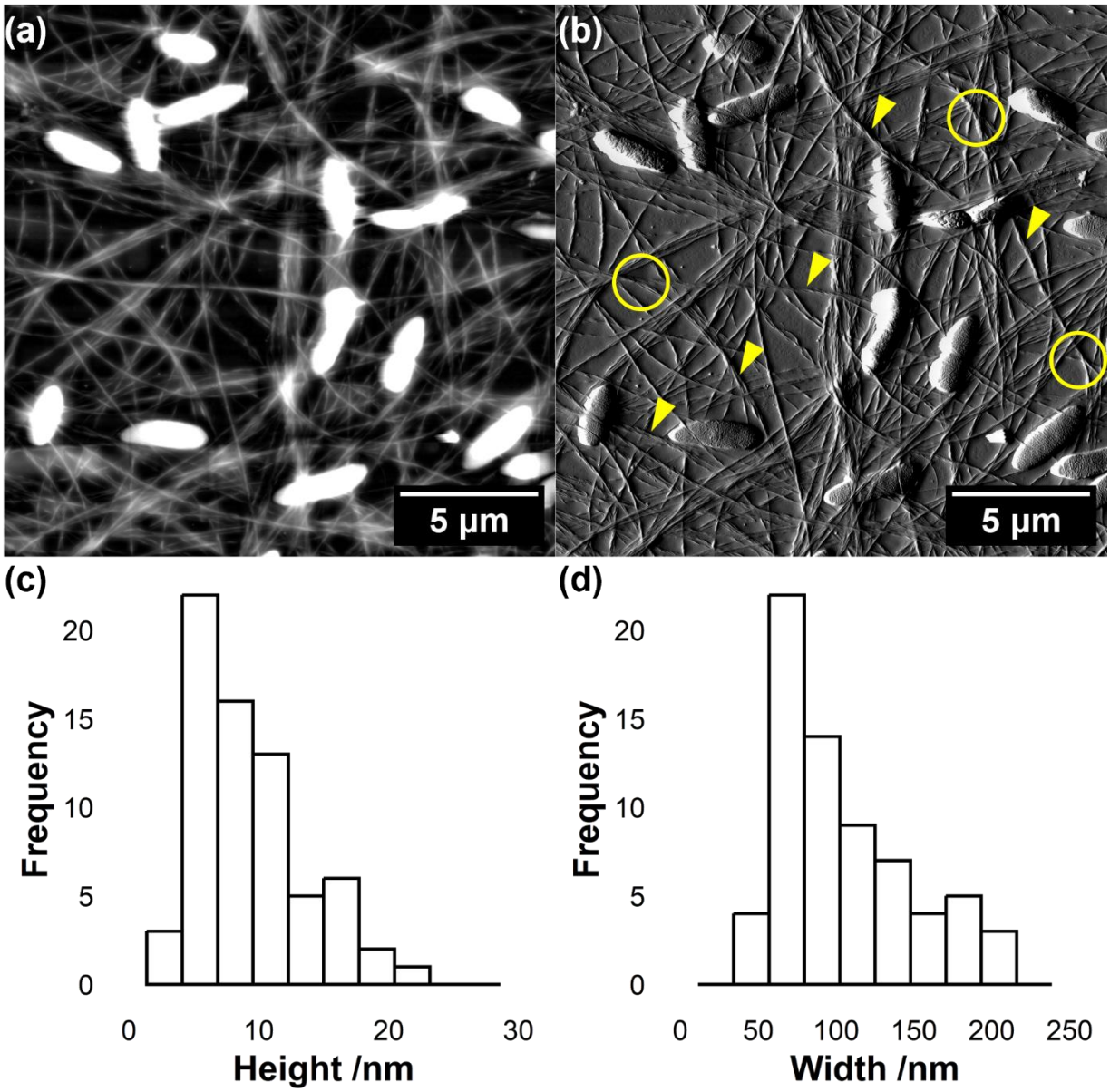

Fig. 3-10 AFM images of BC ribbons during the initial stage of network formation. (a) represents the height image, and (b) the amplitude image. Arrowheads and circles indicate bundled ribbons and branching points, respectively. Histograms of the height and width of BC ribbons are shown in (c) and (d), respectively.

Discussion

Material design strategy for BC pellicles

The collective motion of *Komagataeibacter* bacteria and the resulting unique structural patterns, as revealed in this chapter, are expected to be utilized in the creation and precise control of novel properties in BC pellicles. Fig. 3-11 summarizes the various structural formation based on the bioassembly process by *Komagataeibacter* bacteria and the expected mechanical properties. For instance, by controlling the frequency of branching formation by *Komagataeibacter* bacteria, it becomes possible to control the crosslinking density, leading to enhancements in tensile properties. The nematic structure and the chiral nematic-like domain structure, formed by the aligned movement of *Komagataeibacter* bacteria, are expected to contribute to increased rigidity. In addition, the uniaxially aligned nematic structure is anticipated to exhibit anisotropic mechanical properties in both the alignment direction and the perpendicular direction. By introducing the vortex pattern into the BC pellicle, elastic properties can potentially be imparted to the BC pellicles. To achieve such material design, it is crucial to thoroughly understand these patterns and the structural formation process driven by *Komagataeibacter* bacteria. In the following sections, the mechanisms behind these pattern formations are discussed.

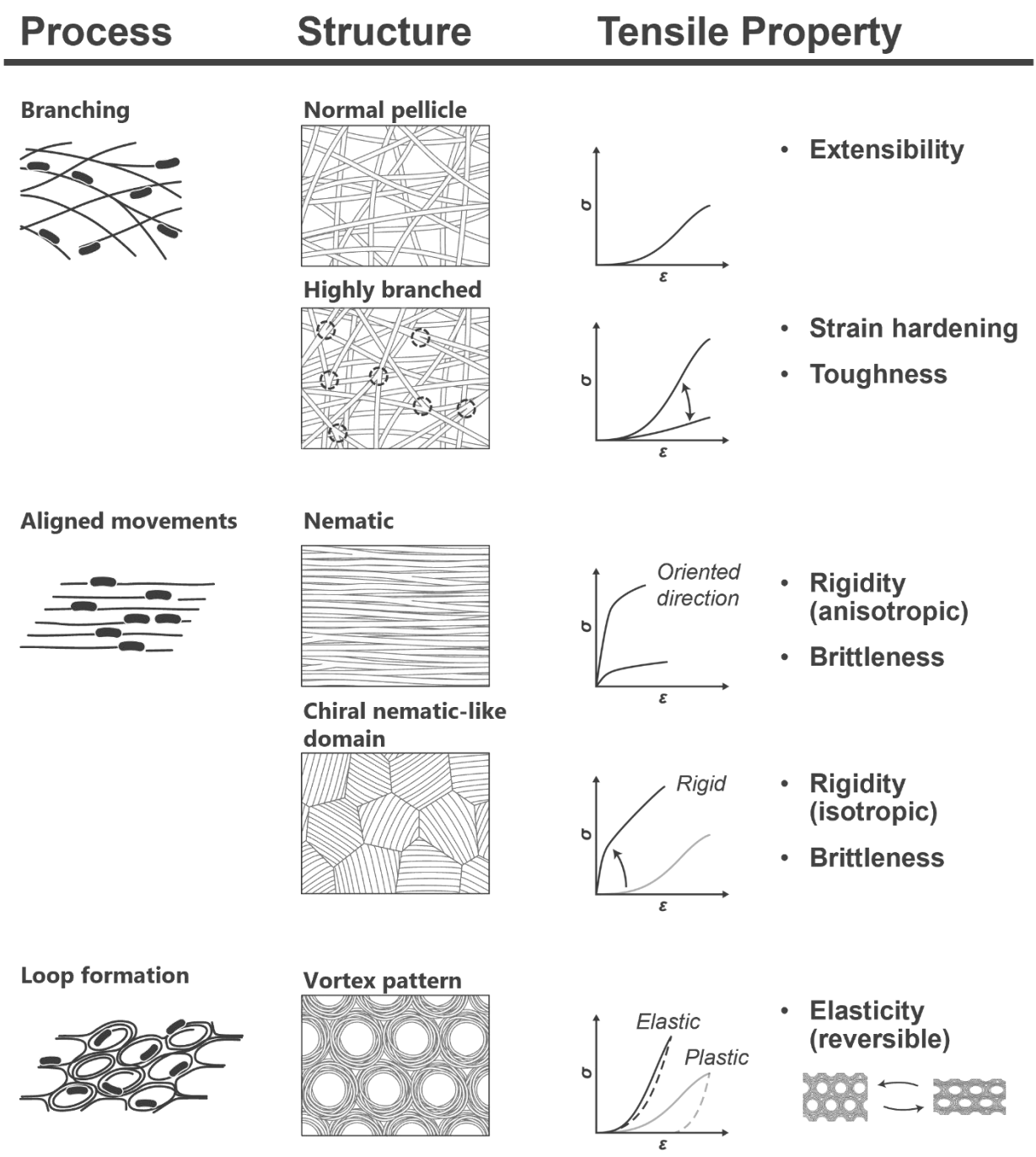

Fig. 3-11 Schematic illustration of the structure formation process by *Komagataeibacter* bacteria, the resulting structural patterns, and the expected mechanical properties of BC pellicle.

Branching structure in BC networks and its origin

Branching structure is critical parameter to determine the physical property of BC pellicle as demonstrated in chapter 2. The property of native cellulose I crystals, which is considered to be stabilized in a twisted state (Bu et al., 2015; Ogawa, 2021; Zhao et al., 2013), is likely to have a significant influence on the formation of higher-order structures in the BC networks. Similar to other cellulose nanofibrils, BC ribbons also are twisted along the fiber axis (Colvin & Biology, 1961). As observed by AFM, the bridging structure of the fiber network in BC pellicles is formed through the bundling and unbundling of BC ribbons (Fig. 10b). Therefore, the twisting derived from the geometric shape of BC ribbons may contributes to the formation of bridging structures in addition to the interactions between cellulose fibers. In other words, not only chemical interactions but also topological effects are synergetically involved in the formation of cross-linked structures of BC ribbons. Thus, rupture of the bridging structure requires not only breaking the chemical bonds but also to geometrically untangling the fibers that are intertwined while being twisted. Then, bundle structures mediated by twisting are thermodynamically challenging to re-bundle once they have been untangled. Therefore, the robustly bridged fiber network structure can be dependent on the unique secreting behavior of *Komagataeibacter* bacteria, which is totally different from thermodynamical formation of nanocellulose networks.

Mechanism of branching point formation

Despite the influence on the mechanical properties, there have been limited experimental studies investigating the mechanism of branching structure formation in BC ribbons. Previously, it was proposed that branching structures are formed when cells in the process of fiber secretion undergo division (Gromovykh et al., 2020; Yamanaka & Sugiyama, 2000). However, this study using trajectory analyses of bacterial movements revealed that the formation of junction

structures does not necessarily require bacterial division. Firstly, trajectory analysis has shown that junction structures are formed by derailment due to physical obstacles, for example, collisions between bacteria or interference with other BC ribbons. Secondly, experimental evidence has demonstrated that merging structures, which are the opposite of branching structure formation, appear when the bacteria switch to another scaffolds of BC ribbons, and then merge with them.

Mechanism of vortex structure formation

The key in the mechanism of loop structure formation is considered to be the cell length of the bacteria. Bacteria, which are forming loop structures, showed a tendency to be approximately four times longer than other bacteria. It has been reported that as bacteria become longer, TC length and ribbon width also increase (Yamanaka & Sugiyama, 2000). Considering that cellulose nanofibrils stabilize due to twisting, it is assumed that stronger twisting occurs when the fiber cross-section becomes flatter (Bu et al., 2015; Ogawa, 2021; Zhao et al., 2013). The twisting behavior has been found to contribute to the higher curvature of BC ribbons. Then, the formation of closed loop structures becomes more favorable. In this way, the formation of the loop structure is likely to be induced depending on the length of the bacteria.

Mechanism of chiral nematic-like domain formation

The formation of chiral nematic-like structures, not only in cellulose derivative solutions (Giasson et al., 1988; Gilbert & Patton, 1983) and nanocellulose dispersions (Parker et al., 2018; Parton et al., 2022; Revol et al., 1992) but also in BC pellicles, is an important insight for controlling higher-order structures in materials design. In particular, unlike cellulose derivative solutions and nanocellulose dispersions, the translational and rotational movements of fibers in

BC pellicles are significantly restricted by the cross-linking structure. Therefore, although the chiral nematic-like structure in BC pellicles ultimately originates from the twisting of molecular chains, the mechanism of structure formation is thought to involve different processes than those of conventional liquid crystal formation. Although the formation of chiral nematic-like domains was not observed under the time-lapse observation conditions in this study, the density of bacterial colonies is considered a key factor in the formation of ordered domains. When the spatial density of bacterial cells and BC ribbons is low, the frequency of fiber collisions is low, allowing isotropic network formation. However, as the spatial density of bacterial cells and BC ribbons increases, rod-shaped bacteria and semi-rigid BC ribbons are expected to align for stability. This is partly supported by experimental reports using optical tweezers, which indicate that *Komagataeibacter* bacteria in oriented BC hydrogels tend to move in the direction of its orientation (Repula et al., 2022). Indeed, bacterial strain ATCC53582, where chiral nematic-like structure was observed, is known as a bacterial strain that actively produces cellulose fibers over an extended period compared to other strains. Therefore, it is expected that the spontaneous formation of orientational domain structures can be achieved by using bacterial strains with high cellulose production capacity and cultivating them under optimal conditions for cellulose production.

Conclusion

In this chapter, the movement of bacteria were investigated to characterize the formation process of the network structure that determines the properties of BC pellicles. As a result, the insights into the mechanisms of branching/merging structure formation, loop structure formation, orientational structure formation were obtained. The introduction of these structures is expected to enable control of multifaceted mechanical properties such as strength, elasticity, and

toughness, leading to precise material design of BC pellicles. The knowledge of the structural formation process by bacterial cells obtained in this study is expected to make it possible to fabricate BC pellicles with desired characteristics by controlling the movement of bacterial cells. In addition, the quantitative analysis of bacterial movements can also be applied to purposes such as comparing strain characteristics and optimizing cultivation conditions in BC pellicle production.

References

Brown, R. M., Willison, J. H., & Richardson, C. L. (1976). Cellulose biosynthesis in Acetobacter xylinum: visualization of the site of synthesis and direct measurement of the in vivo process. *Proceedings of the National Academy of Sciences*, *73*(12), 4565–4569. https://doi.org/10.1073/pnas.73.12.4565

Bu, L., Himmel, M. E., & Crowley, M. F. (2015). The molecular origins of twist in cellulose I-beta. *Carbohydrate Polymers*, *125*, 146–152. https://doi.org/10.1016/j.carbpol.2015.02.023

Chen, P., Ogawa, Y., Nishiyama, Y., Ismail, A. E., & Mazeau, K. (2018). Iα to Iβ mechano-conversion and amorphization in native cellulose simulated by crystal bending. *Cellulose*, *25*(8), 4345–4355. https://doi.org/10.1007/s10570-018-1860-x

Colvin, J. R., & Biology, A. (1961). Twisting of bundles of bacterial cellulose microfibrils. *Journal of Polymer Science*, *49*(152), 473–477. https://doi.org/10.1002/pol.1961.1204915227

Czirók, A., & Vicsek, T. (2000). Collective behavior of interacting self-propelled particles. *Physica A: Statistical Mechanics and Its Applications*, *281*(1), 17–29. https://doi.org/10.1016/S0378-4371(00)00013-3

Deutsch, A., Theraulaz, G., & Vicsek, T. (2012). Collective motion in biological systems. *Interface Focus*, *2*(6), 689–692. https://doi.org/10.1098/rsfs.2012.0048

Giasson, J., Revol, J. -F, Ritcey, A. M., & Gray, D. G. (1988). Electron microscopic evidence for cholesteric structure in films of cellulose and cellulose acetate. *Biopolymers*, *27*(12), 1999–2004. https://doi.org/10.1002/bip.360271210

Gilbert, R. D., & Patton, P. A. (1983). Liquid crystal formation in cellulose and cellulose derivatives. *Progress in Polymer Science*, *9*(2–3), 115–131. https://doi.org/10.1016/0079-

6700(83)90001-1

Gompper, G., Winkler, R. G., Speck, T., Solon, A., Nardini, C., Peruani, F., Löwen, H., Golestanian, R., Kaupp, U. B., Alvarez, L., Ki rboe, T., Lauga, E., Poon, W. C. K., Desimone, A., Muiños-Landin, S., Fischer, A., Söker, N. A., Cichos, F., Kapral, R., … Kale, S. (2020). The 2020 motile active matter roadmap. *Journal of Physics Condensed Matter*, *32*(19). https://doi.org/10.1088/1361-648X/ab6348

Gromovykh, T. I., Pigaleva, M. A., Gallyamov, M. O., Ivanenko, I. P., Ozerova, K. E., Kharitonova, E. P., Bahman, M., Feldman, N. B., Lutsenko, S. V., & Kiselyova, O. I. (2020). Structural organization of bacterial cellulose: The origin of anisotropy and layered structures. *Carbohydrate Polymers*, *237*(February), 116140. https://doi.org/10.1016/j.carbpol.2020.116140

Hanley, S. J., Revol, J. F., Godbout, L., & Gray, D. G. (1997). Atomic force microscopy and transmission electron microscopy of cellulose from Micrasterias denticulata; evidence for a chiral helical microfibril twist. *Cellulose*, *4*(3), 209–220. https://doi.org/10.1023/A:1018483722417

Hesse, S., & Kondo, T. (2005). Behavior of cellulose production of Acetobacter xylinum in 13C-enriched cultivation media including movements on nematic ordered cellulose templates. *Carbohydrate Polymers*, *60*(4), 457–465. https://doi.org/10.1016/j.carbpol.2005.02.018

Hestrin, S., & Schramm, M. (1954). Synthesis of cellulose by Acetobacter xylinum 2. Preparation of freeze-dried cells capable of polymerizing glucose to cellulose. *The Biochemical Journal*, *58*(2), 345–352. https://doi.org/10.1042/bj0580345

Kaczmarek, M., Jędrzejczak-Krzepkowska, M., & Ludwicka, K. (2022). Comparative Analysis of Bacterial Cellulose Membranes Synthesized by Chosen Komagataeibacter Strains and

Their Application Potential. *International Journal of Molecular Sciences*, *23*(6). https://doi.org/10.3390/ijms23063391

Kondo, T., & Kasai, W. (2014). Autonomous bottom-up fabrication of three-dimensional nano/microcellulose honeycomb structures, directed by bacterial nanobuilder. *Journal of Bioscience and Bioengineering*, *118*(4), 482–487. https://doi.org/10.1016/j.jbiosc.2014.04.002

Kondo, T., Kasai, W., Nojiri, M., Hishikawa, Y., Togawa, E., Romanovicz, D., & Brown, R. M. (2012). Regulated patterns of bacterial movements based on their secreted cellulose nanofibers interacting interfacially with ordered chitin templates. *Journal of Bioscience and Bioengineering*, *114*(1), 113–120. https://doi.org/10.1016/j.jbiosc.2012.02.020

Kondo, T., Nojiri, M., Hishikawa, Y., Togawa, E., Romanovicz, D., & Brown, R. M. (2002). Biodirected epitaxial nanodeposition of polymers on oriented macromolecular templates. *Proceedings of the National Academy of Sciences of the United States of America*, *99*(22), 14008–14013. https://doi.org/10.1073/pnas.212238399

Lee, C. M., Gu, J., Kafle, K., Catchmark, J., & Kim, S. H. (2015). Cellulose produced by Gluconacetobacter xylinus strains ATCC 53524 and ATCC 23768: Pellicle formation, post-synthesis aggregation and fiber density. *Carbohydrate Polymers*, *133*, 270–276. https://doi.org/10.1016/j.carbpol.2015.06.091

Lu, Z., Zhang, Y., Chi, Y., Xu, N., Yao, W., & Sun, B. (2011). Effects of alcohols on bacterial cellulose production by Acetobacter xylinum 186. *World Journal of Microbiology and Biotechnology*, *27*(10), 2281–2285. https://doi.org/10.1007/s11274-011-0692-8

McKenna, B. A., Mikkelsen, D., Wehr, J. B., Gidley, M. J., & Menzies, N. W. (2009). Mechanical and structural properties of native and alkali-treated bacterial cellulose

produced by Gluconacetobacter xylinus strain ATCC 53524. *Cellulose*, *16*(6), 1047–1055. https://doi.org/10.1007/s10570-009-9340-y

Numata, Y., Kono, H., Mori, A., Kishimoto, R., & Tajima, K. (2019). Structural and rheological characterization of bacterial cellulose gels obtained from Gluconacetobacter genus. *Food Hydrocolloids*, *92*(January), 233–239. https://doi.org/10.1016/j.foodhyd.2019.01.060

Ogawa, Y. (2021). Release of internal molecular torque results in twists of Glaucocystis cellulose nanofibers. *Carbohydrate Polymers*, *251*(July 2020), 117102. https://doi.org/10.1016/j.carbpol.2020.117102

Parker, R. M., Guidetti, G., Williams, C. A., Zhao, T., Narkevicius, A., Vignolini, S., & Frka-Petesic, B. (2018). The Self-Assembly of Cellulose Nanocrystals: Hierarchical Design of Visual Appearance. *Advanced Materials*, *30*(19). https://doi.org/10.1002/adma.201704477

Parton, T. G., Parker, R. M., van de Kerkhof, G. T., Narkevicius, A., Haataja, J. S., Frka-Petesic, B., & Vignolini, S. (2022). Chiral self-assembly of cellulose nanocrystals is driven by crystallite bundles. *Nature Communications*, *13*(1), 1–9. https://doi.org/10.1038/s41467-022-30226-6

Putra, A., Kakugo, A., Furukawa, H., Gong, J. P., Osada, Y., Uemura, T., & Yamamoto, M. (2008). Production of bacterial cellulose with well oriented fibril on PDMS substrate. *Polymer Journal*, *40*(2), 137–142. https://doi.org/10.1295/polymj.PJ2007180

Repula, A., Abraham, E., Cherpak, V., & Smalyukh, I. I. (2022). Biotropic liquid crystal phase transformations in cellulose-producing bacterial communities. *Proceedings of the National Academy of Sciences of the United States of America*, *119*(24), 1–11. https://doi.org/10.1073/pnas.2200930119

Revol, J. F., Bradford, H., Giasson, J., Marchessault, R. H., & Gray, D. G. (1992). Helicoidal

self-ordering of cellulose microfibrils in aqueous suspension. *International Journal of Biological Macromolecules, 14*(3), 170–172. https://doi.org/10.1016/S0141-8130(05)80008-X

Schindelin, J., Arganda-Carreras, I., Frise, E., Kaynig, V., Longair, M., Pietzsch, T., Preibisch, S., Rueden, C., Saalfeld, S., Schmid, B., Tinevez, J. Y., White, D. J., Hartenstein, V., Eliceiri, K., Tomancak, P., & Cardona, A. (2012). Fiji: An open-source platform for biological-image analysis. *Nature Methods*, *9*(7), 676–682. https://doi.org/10.1038/nmeth.2019

Tinevez, J. Y., Perry, N., Schindelin, J., Hoopes, G. M., Reynolds, G. D., Laplantine, E., Bednarek, S. Y., Shorte, S. L., & Eliceiri, K. W. (2017). TrackMate: An open and extensible platform for single-particle tracking. *Methods*, *115*, 80–90. https://doi.org/10.1016/j.ymeth.2016.09.016

Tomita, Y., & Kondo, T. (2009). Influential factors to enhance the moving rate of Acetobacter xylinum due to its nanofiber secretion on oriented templates. *Carbohydrate Polymers*, *77*(4), 754–759. https://doi.org/10.1016/j.carbpol.2009.02.022

Uraki, Y., Nemoto, J., Otsuka, H., Tamai, Y., Sugiyama, J., Kishimoto, T., Ubukata, M., Yabu, H., Tanaka, M., & Shimomura, M. (2007). Honeycomb-like architecture produced by living bacteria, Gluconacetobacter xylinus. *Carbohydrate Polymers*, *69*(1), 1–6. https://doi.org/10.1016/j.carbpol.2006.08.021

Vernerey, F. J., Benet, E., Blue, L., Fajrial, A. K., Lalitha Sridhar, S., Lum, J. S., Shakya, G., Song, K. H., Thomas, A. N., & Borden, M. A. (2019). Biological active matter aggregates: Inspiration for smart colloidal materials. *Advances in Colloid and Interface Science, 263*, 38–51. https://doi.org/10.1016/j.cis.2018.11.006

Vicsek, T., & Zafeiris, A. (2012). Collective motion. *Physics Reports*, *517*(3–4), 71–140.

https://doi.org/10.1016/j.physrep.2012.03.004

Yamanaka, S., & Sugiyama, J. (2000). Structural modification of bacterial cellulose. *Cellulose*, *7*(3), 213–225. https://doi.org/10.1023/A:1009208022957

Zhao, Z., Shklyaev, O. E., Nili, A., Mohamed, M. N. A., Kubicki, J. D., Crespi, V. H., & Zhong, L. (2013). Cellulose microfibril twist, mechanics, and implication for cellulose biosynthesis. *Journal of Physical Chemistry A*, *117*(12), 2580–2589. https://doi.org/10.1021/jp3089929

Summary

Chapter 1 elucidates the fundamentals of the mechanical properties of the BC pellicle in tensile deformation, where the characteristics of the fiber network are prominently expressed. In order to understand the microscopic deformation mechanism, in situ fluorescence microscopy observations of the fiber network during tensile deformation were conducted. As a result, it was visualized that the fiber segments rearrange themselves as the strain progresses, forming stress transfer pathways. Moreover, it was revealed that the deformation of BC hydrogels involves non-affine deformation, where the entire fiber network deforms non-uniformly, contradicting the assumption of affine deformation underlying the theory of polymer rubber elasticity. Additionally, relaxation time measurements during tensile deformation demonstrated that after an initial rapid relaxation (1 second), secondary relaxation continues over a long duration. Based on these findings, a novel tensile deformation model for BC hydrogels was proposed, which is based on the microscopic mechanism involving stress concentration at crosslinking points and subsequent rearrangement accompanied by their cleavage.

Chapter 2 deals with establishment of a methodology to quantitatively analyze the network structure of various BC hydrogels with different mesh structures and also to evaluate their influence on mechanical properties. Seven BC hydrogels with different properties were prepared, and their tensile characteristics were characterized in correlation with the fiber network

structure. As expected, an increase in crosslinking point density resulted in improved strength. Notably, the crosslinking point density exhibited a linear relationship with strength, and moreover accurately explained the nonlinear strain-hardening behavior over a wide range of strains from small to large deformations. These findings are expected to contribute to predicting the properties of BC hydrogels and quality assurance.

Chapter 3 attempts to analyze the unique nano-fiber assembly structure and the structural formation process by *Komagataeibacter* bacteria, leading to novel material design. Although BC hydrogels has been believed to exhibit an isotropic mesh structure, it has been discovered that chiral nematic-like structures and vortex structures distinct from the typical isotropic network structure co-exist. By inducing the spontaneous formation of such special patterns, it is expected to modify the properties of BC hydrogels without composite materialization or chemical modification. As a basis for artificially controlling such structural formation, the bacterial movements during the structural formation process of BC hydrogels were analyzed in detail, demonstrating the possibility of structural control through the manipulation of bacterial motility.

To expand the range of material applications of BCs, the following two improvements are imperative. The first is to design the material to exhibit properties tailored to the application, and the second is to improve its mechanical properties. First, for medical materials such as drug delivery systems and cell culture scaffolds, it is important to precisely control their mechanical properties, surface morphology, and pore size. To facilitate such applications, it is necessary to manufacture BC pellicles according to their purpose. In Chapters 1 & 2, it was demonstrated that the nanofiber network structure significantly influences the physical properties of BC pellicles. By accumulating data on the process–structure–property relationship in various strains and cultivation methods and by constructing a database, tailored BC material is expected to be

realized. In particular, the permanent branching/merging structure unique to BC pellicles is expected to contribute to elastic properties, and the transient entanglement structure between nanofibers determined by cellulose content is expected to contribute to viscous properties. Thus, it is expected that not only control of elastic properties but also control of viscoelastic properties will become possible.

Next, regarding the enhancement of mechanical properties, it has been demonstrated that BC pellicles with novel structures can be created by inducing spontaneous structure formation of the bacteria and nanofibers. Currently, the mechanical properties of BC pellicles have an elastic modulus on the order of MPa, similar to those of ordinary hydrogels, but if an elastic modulus exceeding 1 GPa can be achieved in the hydrated state, it is expected that the range of applications for BC pellicles will be greatly expanded. In particular, the chiral nematic-like structure shown in Chapter 3 is expected to increase the cellulose content and cross-link density, and is thought to exhibit unprecedentedly high elastic modulus and high strength mechanical properties. The elucidation of the structural formation mechanism and its application to materials eagerly await further exploration.

In conclusion, this dissertation aimed to establish a foundation for the precise material design of BC hydrogels, which are fibrous network materials created by microorganisms. Throughout this study, the relationship between the network structure and properties of BC hydrogels, as well as the process of structural formation by *Komagataeibacter* bacteria, was investigated. The obtained insights into the fiber network structure−property relationship are expected to contribute to challenges related to the uncontrollable properties of bacterial cellulose in material design and quality management. Furthermore, the knowledge obtained regarding the process of structural formation by bacteria can provide guidance for material design based on

synthetic biology. Therefore, the outcomes of this dissertation are expected to unlock the potential of BC hydrogels and contribute to the advancement of materials design science using microorganisms, ultimately leading to the realization of a sustainable society.

List of Publications

1) In situ visualization of the tensile deformation mechanism of bacterial cellulose network

Go Takayama and Kondo Tetsuo

Carbohydrate Polymers, 313, 120883 (2023)

(https://doi.org/10.1016/j.carbpol.2023.120883)

(Chapter 1)

2) Quantitative evaluation of fiber network structure–property relationships in bacterial cellulose hydrogels

Go Takayama and Tetsuo Kondo

Carbohydrate Polymers, 321, 121311 (2023)

(https://doi.org/10.1016/j.carbpol.2023.121311)

(Chapter 2)

3) Physical characteristics and cell-adhesive properties of in vivo fabricated bacterial cellulose/hyaluronan nanocomposites

Ryo Takahama, Honami Kato, Go Takayama, Kenji Tajima and Tetsuo Kondo

Cellulose, 29, 3239-3251 (2022)

(https://doi.org/10.1007/s10570-022-04480-2)

Acknowledgements

This dissertation is the outcomes of doctoral research conducted at the Graduate School of Bioresource and Bioenvironmental Sciences, Kyushu University, during 2018–2023 under supervision of Professor Tetsuo Kondo.

The First and foremost, the author would like to express the utmost gratitude to Professor Tetsuo Kondo, Tokyo University of Agriculture and Technology (former professor, Graduate school of Bioresource and Bioenvironmental Sciences, Kyushu University). Without Professor Kondo's guidance, discussions, and supervision, the achievement of this research would not have been possible.

The author would like to extend their sincere appreciation to Associate Professor Daisuke Tatsumi, Graduate School of Bioresource and Bioenvironmental Sciences, Kyushu University, who graciously agreed to serve as the chief examiner for the dissertation. Associate professor Daisuke Tatsumi has consistently engaged in open and insightful discussions, providing inspiration for the research.

Special thanks are extended to Associate Professor Shingo Yokota, Graduate School of Bioresource and Bioenvironmental Sciences, Kyushu University, for the invaluable support and meaningful discussions. Without the collaboration of Associate Professor Shingo Yokota, the completion of this study would not have been feasible.

The author would also like to express the profound gratitude to Professor Kiyohiko Igarashi, Graduate School of Agricultural and Life Sciences, the University of Tokyo and

Professor Takuya Kitaoka, Graduate School of Bioresource and Bioenvironmental Sciences, Kyushu University, for reviewing this dissertation.

The author wishes to express thanks to the Center for Advanced Instrumental and Educational Supports, Faculty of Agriculture, Kyushu University, for the assistance with the CLSM (TCS SP8).

The author is thankful to Mrs. Runa Watanabe for her generous and precise support in practical aspects of the research work.

Acknowledgments are extended to Dr. Koichiro Ishida, with whom the author has strived and grown together as a fellow student.

The author would like to express their gratitude to Dr. Ryo Takahama for numerous discussions on the research.

Appreciation is also extended to all the members and associates of the Biomaterial Design Laboratory and Biomacromolecular Materials Laboratory, Graduate School of Bioresource and Bioenvironmental Sciences, Kyushu University.

Last but not least, I would like to express the gratitude to my partner and parents for their warmest support and encouragement throughout this research journey.

July, 8, 2023

At Hokkaido

Go Takayama